AD A

Technical Path Evaluation for High Efficiency, Low Emission Natural Gas Engine

INTERIM REPORT
TFLRF No. 363

by

Timothy J. Callahan
Lee G. Dodge
Charles E. Roberts
Chad H. Stovell
Gary D. Bourn
Magdi K. Khair
Gordon J. Bartley

Southwest Research Institute
San Antonio, TX 78228

Under Contract to

Department of the U.S. Army
Tank-Automotive and Armaments Command
Warren, MI 48397-5000

for

U.S. Department of Energy
626 Cochrans Mill Road
Pittsburgh, PA 15236-0940

Approved for Public Release; Distribution Unlimited

TARDEC Contract Nos. DAAE07-99-C-L053 (WD06)
SwRI Project No. 03-03227

May 2002

Technical Path Evaluation for High Efficiency, Low Emission Natural Gas Engine

INTERIM REPORT
TFLRF No. 363

by

Timothy J. Callahan
Lee G. Dodge
Charles E. Roberts
Chad H. Stovell
Gary D. Bourn
Magdi K. Khair
Gordon J. Bartley

Southwest Research Institute
San Antonio, TX 78228

Under Contract to
Department of the U.S. Army
Tank-Automotive and Armaments Command
Warren, MI 48397-5000

for
U.S. Department of Energy-FETC
626 Cochrans Mill Road
Pittsburgh, PA 15236-0940

Approved for Public Release; Distribution Unlimited

TARDEC Contract Nos. DAAE07-99-C-L053 (WD06)
SwRI Project No. 03-03227

May 2002

Approved by:

Daniel W. Stewart, Director
Engine Research Department
Engine & Vehicle Research Division

Approved by:

Ed Owens, Director
Fuels & Lubricants Technology Dept.
Engine & Vehicle Research Division

REPORT DOCUMENTATION PAGE

Form Approved
OMB No. 0704-0188

1. AGENCY USE ONLY	2. REPORT DATE May 2002	3. REPORT TYPE AND DATES COVERED Interim, September 1998 – May 2002

4. TITLE AND SUBTITLE
Technical Path Evaluation for High Efficiency, Low Emission Natural Gas Engine

5. FUNDING NUMBERS
DAAE07-99-C-L053; WD 06

6. AUTHOR(S)
Callahan, Timothy J.

7. PERFORMING ORGANIZATION NAME(S) AND ADDRESS(ES)
Engine & Vehicle Research Division
Southwest Research Institute
P.O. Drawer 28510
San Antonio, Texas 78228-0510

8. PERFORMING ORGANIZATION REPORT NUMBER
TFLRF No. 363

9. SPONSORING/MONITORING AGENCY NAME(S) AND ADDRESS(ES)
U.S. Army TACOM
TARDEC Petroleum and Water Business Area
Warren, MI 48397-5000

10. SPONSORING/MONITORING AGENCY REPORT NUMBER

11. SUPPLEMENTARY NOTES

12a. DISTRIBUTION/AVAILABILITY STATEMENT
Limited distribution; not approved for public release

12b. DISTRIBUTION CODE

13. ABSTRACT (Maximum 200 words)
The work presented in this report was partially funded by DOE, Office of Power Technology (OPT), National Energy Technology Laboratory (NETL), through TACOM under the **Advanced Reciprocating Engine Systems (ARES)** cooperative research program for stationary, natural gas engines used for power generation. The program goal was to identify engine technology to achieve 50 percent break thermal efficiency and 5 ppm NO_x for stationary engines. Members of the program were Caterpillar, Cooper Energy Services, Cummins Engine Company, Waukesha Engine Division, Southern California Gas, Woodward Governor, Altronic, Federal Mogul, Gas Research Institute, and the Department of Energy. Research concentrated on developing technical solutions to combustion barriers (knock and misfire), exhaust aftertreatment, and power density limitations. The research results are organized under the following topics:

A. Evaluation of Technical Paths to Achieve High Efficiency and Low Emissions Natural Gas Engines
B. Knock Modeling and Mitigation for Large Bore Natural Gas Engines
C. Evaluation of Technologies for Achieving High BMEP Levels in Natural Gas Engines
D. Microfine Water Spray Injection for Knock and NO_x Control in Natural Gas Engines
E. Micro-Pilot Ignition - Technology Survey
F. Evaluation of NO_x Catalysts for Lean-Burn Natural Gas Engines

Research efforts are documented in this report for each of the above projects. This report covers the ARES project from, September 1998 through May 2002.

Major findings of this work were the identification of technology required for high efficiency, low emission, natural gas engines, including: requirements for exhaust aftertreatment, exhaust energy recovery, use of over expanded cycle, and need for combustion improvements. Structural limitations, as well as knock, impact the maximum achievable engine efficiency. Modeling results indicated that greater than 50 percent thermal efficiency is attainable.

The continued development of high efficiency, low emission, natural gas engines is recommended. Given the technologies required, barriers to overcome, this development requires a 5 to 7 year effort.

14. SUBJECT TERMS
Natural Gas, Large Bore, NO_x Catalyst(s), Caterpillar 3501
Water Injection, High Efficiency, Miller Cycle, Pilot Injection
Low NO_x Emission(s)

15. NUMBER OF PAGES
149

16. PRICE CODE

17. SECURITY CLASSIFICATION OF REPORT	18. SECURITY CLASSIFICATION OF THIS PAGE	19. SECURITY CLASSIFICATION OF ABSTRACT	20. LIMITATION OF ABSTRACT
Unclassified	Unclassified	Unclassified	

NSN 7540-01-280-5500

Standard Form 298 (Rev. 2-89)
Prescribed by ANSI Std. Z39-18
298-102

ABSTRACT

The work presented in this report was partially funded by the Department of Energy, Office of Power Technology and National Energy Technology Laboratory (NETL), through TACOM under the **Advanced Reciprocating Engine Systems (ARES)** cooperative research program for stationary, natural gas engines used for power generation. The program goal was to identify engine technology to achieve 50 percent break thermal efficiency and 5 ppm NO_x for stationary engines. Members of the program were Caterpillar, Cooper Energy Services, Cummins Engine Company, Waukesha Engine Division, Southern California Gas, Woodward Governor, Altronic, Federal Mogul, Gas Research Institute, and the Department of Energy. Research concentrated on developing technical solutions to combustion barriers (knock and misfire), exhaust aftertreatment, and power density limitations. The research results are organized under the following topics:

A. Evaluation of Technical Paths to Achieve High Efficiency and Low Emissions Natural Gas Engines
B. Knock Modeling and Mitigation for Large Bore Natural Gas Engines
C. Evaluation of Technologies for Achieving High BMEP Levels in Natural Gas Engines
D. Microfine Water Spray Injection for Knock and NO_x Control in Natural Gas Engines
E. Micro-Pilot Ignition Technology Evaluation
F. Evaluation of Aftertreatment Technology for Lean-Burn Natural Gas Engines

Research efforts are documented in this report for each of the above areas. This report covers the ARES project from, September 1998 through May 2002.

Major findings of this work were the identification of technology required for high efficiency, low emission, natural gas engines, including: requirements for exhaust aftertreatment, exhaust energy recovery, use of over expanded cycle, and need for combustion improvements. Structural limitations, as well as knock, impact the maximum achievable engine efficiency. Modeling results indicated that greater than 50 percent thermal efficiency is attainable.

The continued development of high efficiency, low emission, natural gas engines is recommended. Given the technologies required and barriers to overcome, this development requires a 5 to 7 year effort.

NOMENCLATURE LIST

A	area
A_f	flame front area
A_T	turbulent flame front area
A_L	laminar flame front area
cyl	cylinder
D	cylinder bore
D_f	fractal dimension
EVC	exhaust valve closing crank angle
EVO	exhaust valve opening crank angle
F	flame
f	flame
h	enthalpy
H_{cyl}	cylinder height
i	iteration number, zone number
ign	ignition
INT	intake
Ign	ignition crank angle
IVC	intake valve closing crank angle
IVO	intake valve opening crank angle
K	turbulence kinetic energy
L_i	integral length scale
L_{max}	maximum length scale for turbulence
L_{min}	minimum length scale for turbulence
LPP	location (crank angle) of peak pressure
m	mass
n	total number (moles, species,iterations)
N_{in}	test points inside of chamber
N_{out}	test points outside of chamber
P	pressure
P_{intake}	turbulence production term
$P_{exhaust}$	turbulence production term
P_{tumble}	turbulence production term
P_{swirl}	turbulence production term
P_{squish}	turbulence production term
Q	energy term
R	gas constant
S_L	stretched laminar flame speed
t	time
T	temperature
u	unburned
u'	turbulence intensity
u_T	turbulent flame speed
u_L	laminar flame speed
V	volume
vppm	volume parts per million

Greek Symbols

ε	turbulence dissipation
ρ	mass density
v	eddy diffusivity

BMEP	Brake mean effective pressure
CAD	Crankangle degree
CDF	Conventional dual-fuel
COV	Coefficient of Variation
IMEP	Indicated Mean Effective Pressure
kPa	kilopascals
LaCHIP	Late-cycle, high injection pressure
ϕ	Fuel-air equivalence ratio
Lambda	$1/\phi$
MPa	Megapascals
MPI	Micro-pilot ignition
MPOC	Micro-pilot open chamber
MPPC	Micro-pilot pre-chamber
OP	Opposed-piston
SIOC	Spark-ignited open chamber
SIPC	Spark-ignited pre-chamber

TABLE OF CONTENTS

TABLE OF FIGURES

LIST OF TABLES

TITLE **PAGE**

A. EVALUATION OF TECHNICAL PATHS TO ACHIEVE HIGH EFFICIENCY, LOW EMISSION, NATURAL GAS ENGINES

EXECUTIVE SUMMARY

An analytical investigation was performed using SwRI's proprietary ALAMO_ENGINE simulation software. The intent was to provide guidance for the overall ARES program by estimating gains possible through the application of each new technology. Technologies were investigated both analytically and through examination of current and expected technology limitations. Parametric investigations led to an optimum engine design and conclusions regarding the application of many of the technologies investigated.

The predicted performance for the optimized engine design was 50.7-percent brake thermal efficiency (BTE) with 0.7 g/bhp-hr NO_x. The NO_x target for the ARES program was not met with this engine design. However, exhaust aftertreatment was examined as part of the ARES program to further reduce NO_x emissions. The 50-percent BTE engine utilizes two-stage turbocharging with interstage and aftercooling. The Miller cycle is applied with an optimized expansion factor. A fully insulated exhaust system retains heat for use by the turbocharger and turbocompounder turbines.

A1.0 OBJECTIVE

The objective of the technical path evaluation phase was to investigate possible technical approaches for achieving the goals of the ARES program. The intent was to provide guidance for the overall ARES program by estimating gains possible through the application of each new technology. In addition, because significant interactions were expected between some of the potential technologies, the technical path evaluation phase was tasked with determining the optimum combination of technologies for achieving the overall goals.

A2.0 APPROACH

A2.1 Methodology

Given the broad scope of the technical path evaluation objective, a rapid method for investigating each approach for achieving the ARES program goals was required. It was determined that an analytical approach would allow the maximum number of options to be investigated in the least possible time. The software option selected was SwRI engine simulation code ALAMO_ENGINE. ALAMO_ENGINE uses a set of in-cylinder models coupled with valve flow and turbocharger models. ALAMO_ENGINE however, does not incorporate models of the working fluid outside the cylinder.

A2.2 Description of ALAMO_ENGINE

The ALAMO_ENGINE (A_E) code is a PC-based code that is used to compute power, efficiency, and NO_x emissions for diesel, spark-ignited, stoichiometric and lean-burn gasoline engines, lean-burn natural gas engines, and homogeneous-charge compression-ignition engines. The A_E code is a zero-dimensional cycle simulation code that includes detailed gas composition data to accurately include the effects of exhaust gas recirculation (EGR), residual gases, fuel composition, water from humidity in intake air, water in fuel-water emulsions, and water injected in-manifold or in-cylinder on NO_x emissions. The model also includes a complete chemical equilibrium code to compute chemical species in the combustion gases, and kinetics for the formation of nitric oxides. The model includes different heat transfer correlations selectable from the input menu.

The code includes a submodel to predict nitric oxides, one of the most tightly regulated emissions of both diesel and spark-ignition engines. ALAMO_ENGINE has the built-in capability of computing the effects of many different types of NO_x control strategies on engine performance and NO_x emissions, including EGR, intake charge chilling, water-fuel mixtures, water injection, and timing retard.

The code predicts knock tendency in spark-ignited engines through calculation of a knock parameter. Correlation of a knock parameter value with the onset of knock must be determined from experimental data for specific engine designs.

A2.3 ALAMO_ENGINE Code Validation

Validation of the ALAMO_ENGINE code was confirmed through comparison of predictions with measurements taken from the Caterpillar 3501 single-cylinder test engine. Comparisons were made at 1170, 1240, and 1310 kPa (170, 180, and 190 psi) Brake Mean Effective Pressure (BMEP) over a range of air-fuel ratios and ignition timing values. BMEP represents the power density of the engine and is computed by the work per cycle divided by the engine displacement per cycle. The correlation between measurements and predictions was similar for all three BMEP levels.

A3.0 PARAMETRIC INVESTIGATIONS

The parametric studies were done in a stepwise manner, working from a baseline engine, representative of the technology most frequently seen today, to a fully optimized design intended to meet the ARES program goals. By moving towards the final design in discrete steps, the relative contribution of each set of changes could be gauged. In addition, interactions between variables were easier to assess. Because initial studies indicated that the NO_x target could only be met through the use of aftertreatment, the primary goal for the parametric investigations was the achievement of the BTE goal. Where possible, design values were selected to aid in the achievement of low NO_x provided BTE was not sacrificed.

A3.1 Baseline Engine

The parametric studies were started from a modern baseline engine design. Details of the design are shown in Table A3-1 along with the predicted performance. The baseline engine has a rated brake thermal efficiency of 39.1-percent and 0.9 g/bhp-hr NO_x. Table A3-2 shows the distribution of fuel energy within the engine. Note that exhaust and heat rejection losses account for a large fraction of the total. Both areas represent significant opportunities for improving the brake thermal efficiency.

Table A3-1. Baseline Engine Design and Performance Details

Description	Value
Arrangement	6 cylinder 4-stroke 4 valve turbocharger aftercooled spark-ignited open chamber natural gas engine with wet exhaust manifolds
Bore	170 mm
Stroke	180 mm
Connecting rod length	349 mm
Geometric compression ratio	12.0:1
Expansion factor	1.0
Intake valve diameter	53.6 mm
Exhaust valve diameter	53.6 mm
Engine speed	1800 rpm
Air-fuel ratio	32.0:1
Back pressure (on turbine)	10.0 mbar
Brake Mean Effective Pressure (BMEP)	12.05 bar
Indicated Mean Effective Pressure (IMEP)	14.42 bar
Friction Mean Effective Pressure (FMEP)	2.37 bar
Mechanical efficiency	85%
Intake manifold pressure	2.36 bar
Exhaust manifold pressure	2.00 bar

Intake manifold temperature	327 K
Turbocharger compressor efficiency	80%
Turbocharger turbine efficiency	80%
Brake thermal efficiency (BTE)	39.1%
Engine-Out NO_x Emission	0.90 g/bhp-hr
Peak cylinder pressure	112 bar
Spark timing	33.0° BTDC
Start of combustion	13.6° BTDC
10% burn	3.8° BTDC
90% burn	16.2° ATDC
ALAMO_ENGINE flow multiplier	1.0
Combustion efficiency	98%

Table A3-2. Baseline Engine Energy Distribution

	Energy per cylinder (J)	Percent of Total Fuel Energy (%)
Fuel Low Heating Valve (LHV)	12,598	100
Brake Power	4,922	39.1
Friction	969	7.7
Heat Rejection (aftercooler + cylinder + exhaust system)	2582	20.5
Aftercooler Heat Rejection	908	7.2
Incomplete Combustion	252	2.0
Turbocharger Friction *	19	0.1
Exhaust Gases	2946	23.4

* Assumed 98% mechanical efficiency of turbocharger bearings

A3.2 Modification of the Baseline Engine

Initial investigations for the effect of BMEP, expansion factor, compression ratio, in-cylinder heat loss, engine speed, and turbocompounder restriction were intended to determine the brake thermal efficiency (BTE) possible with currently available technology and to fix values for some of the variables whenever possible. By selecting the variables expected to show the least dependence on each other, and then investigating through simulation the actual level of dependence, it was hoped that some variables could be fixed and hence removed from further studies.

A3.2.1 BMEP

BMEP was swept over a wide range by varying boost pressure. The turbocharger model recalculated the exhaust manifold pressure for each boost setting. Maximum brake torque (MBT) ignition timing and baseline friction and heat transfer were used. The results are shown in Figures A3-1 and A3-2 for a range of compression ratios. Figure

A3-1 shows that brake thermal efficiency continually increases with BMEP and compression ratio. Brake specific NO_x, ($BSNO_x$) shown in Figure A3-2, increases with BMEP and compression ratio and thus with BTE.

Increasing the BMEP of an engine will improve the mechanical efficiency and hence, the brake thermal efficiency. However, knock, peak cylinder pressure, and NO_x will limit the extent by which BMEP can be increased.

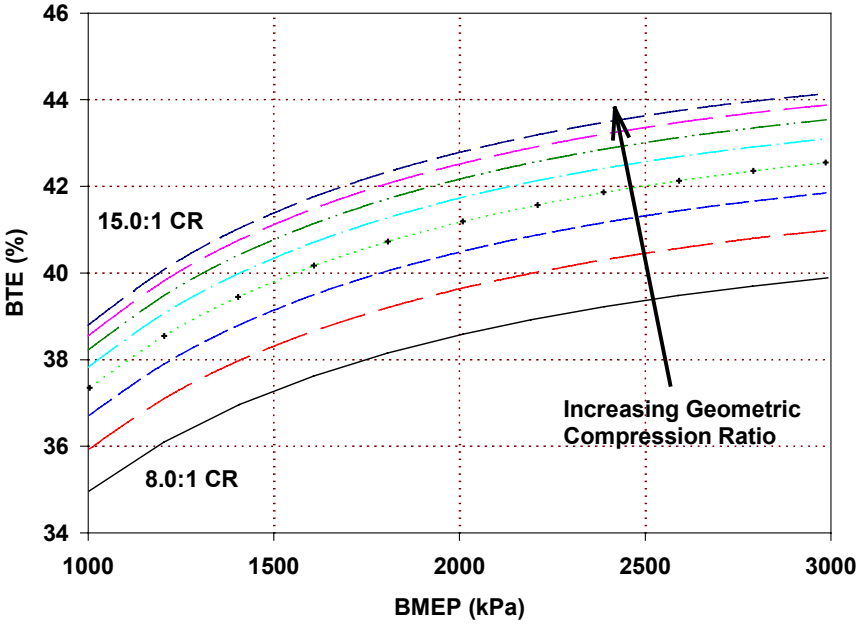

Figure A3-1. Predicted BTE for Geometric Compression Ratios Between 8:1 and 15:1 at a Range of BMEP Values

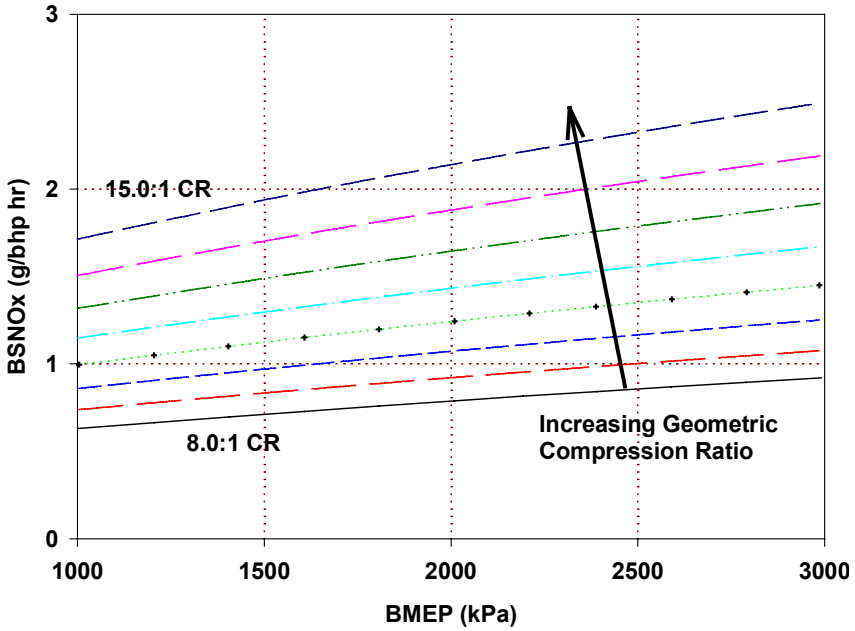

Figure A3-2. Predicted Brake Specific NO_x for Geometric Compression Ratios Between 8:1 and 15:1 at a Range of BMEP Values

A3.2.2 Air-Fuel Ratio

As the operation becomes leaner, the knock-limited compression ratio increases and the burned gas temperature and hence specific heat are lower. Both influence BTE and lead to improved efficiency at leaner conditions. In addition, the lower peak gas temperatures resulting from leaner combustion reduce NO_x. Operation at ever leaner conditions will increase the required air flow rate for a given air-fuel ratio and BMEP level. The higher air demands will increase the pumping work required from the turbocharger and will eventually lead to a reduction in BTE because of pumping penalties. As the air-fuel ratio is increased, the balance between lower knock, reduced combustion temperatures, and lower NO_x versus higher pumping work will define the optimum air-fuel ratio. Operation at high air-fuel ratios may be limited by lean combustion limits and the need to achieve a rapid burn.

A3.2.3 Miller Cycle

Figures A3-3 displays results for a range of expansion factors with the geometric compression ratio held at 15:1. Recall that the expansion factor is a measure of the degree to which the Miller cycle is being implemented. Expansion factor is defined as the ratio of the expansion ratio to the effective compression ratio. The brake thermal efficiency in Figure A3-3 shows a high sensitivity to expansion factor at high BMEP levels. This sensitivity was greatly reduced at low BMEP levels. The optimum expansion factor can be seen to range between 1.2 and 1.3.

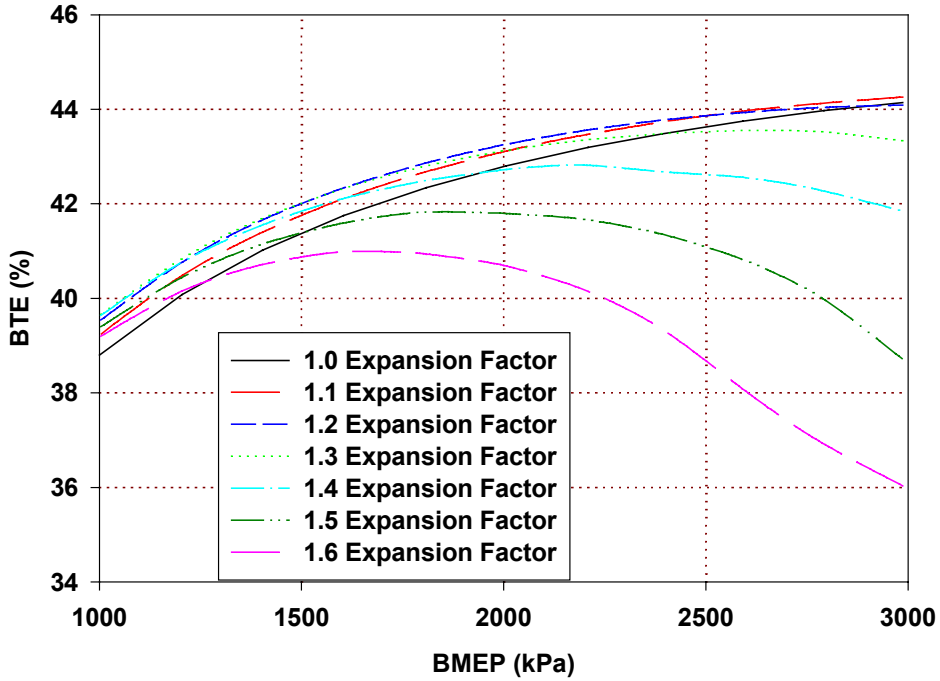

Figure A3-3. Predicted Brake Thermal Efficiency for Expansion Factors Between 1.0 and 1.6 at a Range of BMEP Values

Increasing the expansion factor requires increasing the boost level to maintain BMEP. In addition, increasing the BMEP of an engine operating at a fixed air-fuel ratio increases the required boost. Exhaust restriction across the turbocharger turbine must be increased to provide sufficient compressor power for high boost levels. Beyond a critical boost level, the exhaust manifold pressure will start to exceed the intake manifold pressure, with the rate of increase of the exhaust manifold pressure becoming greater as boost is increased further. The pumping work required to fill and empty the cylinder will then impose an ever greater efficiency penalty on the engine.

Knock severely limits the ability to operate at the high BMEP levels with a 15:1 geometric compression ratio. As previously described, compression ratio can be modulated to maintain a constant predicted knock parameter. Figure A3-4 shows brake thermal efficiency lines at different expansion factors when the compression ratio is varied to maintain a knock parameter of 1.0. The highest brake thermal efficiency occurred at a BMEP of about 2200 kPa and an expansion factor of 1.3. The optimum BMEP was reduced as the expansion factor increased due to unfavorable turbocharger balance conditions at both high BMEPs and high expansion factors. Note that the optimum expansion factor of 1.3 was close to that previously shown when the compression ratio was held constant.

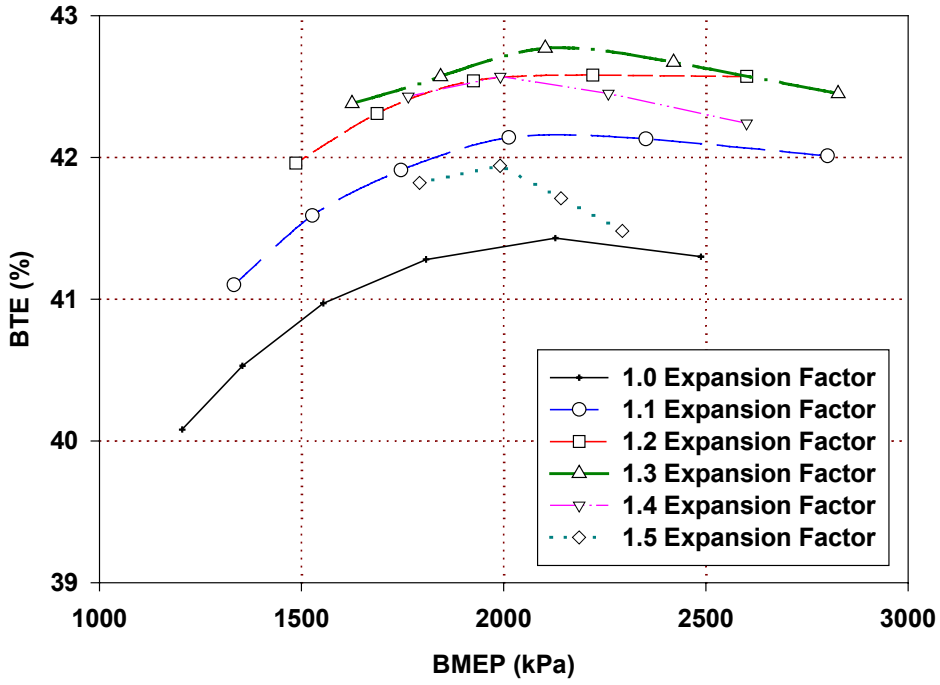

Figure A3-4. Predicted Brake Thermal Efficiency for Expansion Factors Between 1.0 and 1.5 at a Range of BMEP Values – Knock Parameter = 1.0

A3.2.4 Turbocompounding

A mechanically coupled turbocompounder model was added to the ALAMO_ENGINE code to determine the efficiency improvement possible from additional expansion of the exhaust gas. Because turbo-compounding and the Miller cycle are both intended to achieve further expansion of the exhaust gas, one of the goals of this work was to understand the interaction of these two technologies. The turbocompounding investigations were done at a fixed BMEP of 2400 kPa (350 psi). This value was chosen based on the results of the previous studies, that showed an optimum BMEP value of roughly 2200 kPa (320 psi), and consideration of the literature which claims improved gains from turbo-compounding systems as BMEP is increased. The turbocompounder gear train efficiency was set to 90-percent. Note that results from the turbocompounding investigations are not directly comparable to earlier results because of changes in the amount of heat rejected from the exhaust system. The results indicate that, for the engine configuration simulated in this initial study, a turbocompounder did not prove to be beneficial.

A3.2.5 Summary of Baseline Engine with Modifications

The results in Figure A3-4 showed a peak brake thermal efficiency of 43.4-percent at 2400 kPa BMEP, 1.3 expansion factor, with almost no turbo-compounding. The expansion factor was below the best possible value of 1.5 because of the lack of exhaust gas energy, forcing the turbocharger to operate with much greater exhaust pressure than intake manifold pressures when the expansion factor was extended beyond 1.3. The lack of turbocompounding also indicated that insufficient exhaust gas energy was available for expansion to overcome the additional pumping penalties resulting from the power turbine.

Reducing the heat rejected from the cylinder and the exhaust system will increase the amount of energy available for useful expansion in the turbocharger and power turbines. In addition, increasing the flow performance of the intake and exhaust ports will reduce the power required from the compressor to make the engine breathe and hence, leave more energy in the exhaust stream for expansion by the turbocompounder.

A3.3 Application of Enhanced Technologies

To help reach the brake thermal efficiency goals of the ARES program, various technologies were applied to the engine being simulated. The modifications made to the model are described as follows

- Burn duration – The 10 to 90-percent burn duration was reduced from 20 to 18 degrees for a 32:1 air-fuel ratio.

- Friction – The mechanical efficiency was increased from 85 to 91-percent.

- Exhaust system heat loss - The heat loss in the exhaust ports and exhaust manifolds was reduced by 60-percent.

- Two-stage compression with interstage cooling - Because of the high boost pressures utilized by the ARES engine, two-stage turbocharging was introduced. Interstage cooling to 40°C was used to reduce the required compression power.

- Power turbine mechanical efficiency - The power turbine mechanical efficiency was increased from 90 to 95-percent.

- Port flow - The flow multiplier within ALAMO_ENGINE was increased from 1.0 to 1.2. This change increases the volumetric efficiency of the engine by 20-percent, which is assumed to be achievable by optimizing the port geometry, using valve sizes designed to achieve the optimum port gas velocities, and through the application of the Miller cycle. The Miller cycle will increase charging efficiency by restricting the charge flow out of the cylinder during the part of the compression stroke prior to intake valve closing. ALAMO_ENGINE does not account for the gas momentum or intake flow restriction in its calculations, and hence the breathing effects brought about by the application of the Miller cycle must be accounted for empirically.

A3.3.1 Results

ALAMO_ENGINE was used to predict the performance of a turbo-compounded engine utilizing the Miller cycle and all of the enhanced technology changes listed in the previous section. The geometric compression ratio was varied to maintain a knock parameter of 1.0. Figure A3-5 shows the predicted brake thermal efficiency for this engine as a function of turbocompounder power expressed as the percentage of the total engine system power. Higher percentages of the total power from turbocompounding were achieved by using increasingly small power turbine sizes. Lines representing a range of expansion factors are included in Figure A3-5. The best brake thermal efficiency was achieved at an expansion factor of 1.5. This value contrasts with the optimum 1.3 expansion factor determined previously, and shows that, once the technology enhancements listed in Section A3.3 have been made, sufficient exhaust gas energy is available for a beneficial turbocharger balance. As previously shown, the optimum efficiency occurred when the energy was allocated to expansion by the Miller cycle first, up to an expansion factor of 1.5. Additional expansion is then allocated to the turbocompounder. At an expansion factor of 1.5, the optimum brake thermal efficiency occurred when 6-percent of the total engine system power was being obtained from the turbocompounder.

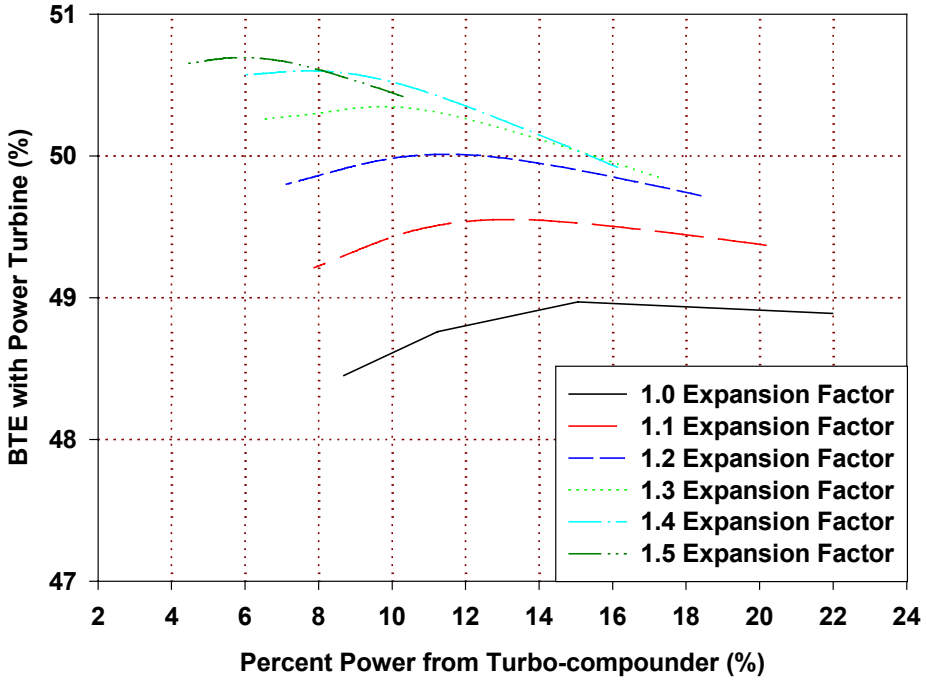

Figure A3-5. Predicted Brake Thermal Efficiency with Power Turbine Contribution for a Range of Expansion Factors and Plotted as a Function of Percent of Total Engine Power Produced by the Turbocompounder-Knock Parameter = 1.0

Note that the peak thermal efficiency in Figure A3-5 was 50.7 percent, meeting the ARES program BTE goals. This efficiency was predicted to occur with 0.7 g/bhp-hr NO_x and without knock. This engine configuration was dubbed the ARES 50-percent BTE Engine. Table A3-3 lists the distribution of fuel energy for the ARES 50-percent BTE Engine. Note that the ARES engine performance is, at this time, only a prediction. The accuracy of the prediction is limited by the assumptions involved with the ALAMO_ENGINE modeling methods. Further work is required to improve the confidence in these results.

Table A3-3. Energy Balance for the ARES 50-percent BTE Engine

	Energy Per Cylinder (J)	Percent of Total Fuel Energy (%)
Fuel LHV	20,351	100
Brake Power (engine w/o turbocompounder)	9,769	48.0
Turbocompounder	549	2.7
Friction	875	4.3
Heat Rejection (cylinder + exhaust system)	3,083	15.2
Intercooler and Aftercooler Heat Rejection	2,631	12.9
Incomplete Combustion	407	2.0
Turbocharger and Turbo-Compounder Friction *	65	0.3
Exhaust Gases	2972	14.6

* Assumed 98% mechanical efficiency of turbocharger and turbocompounder bearings

A4.0 SUPPORTING ENGINE TEST RESULTS

The modeling effort undertaken in this project was supported by engine test results that are discussed in more detail in the following sections of this report. Various concepts were investigated to achieve the targets identified as part of the technical path evaluation. These included the use of the Miller cycle, high-BMEP engine development, multi-site ignition technologies, direct water injection, and exhaust aftertreatment. The current state-of-the-art engine performance and the ARES targets are shown in Figure A4-1. Barriers to achieving high efficiency are:

- Knock (uncontrolled combustion)
- NO_x emissions
- Structural limitations
- Combustion efficiency (unburned fuel)
- Combustion rate (slow reactions at low temperature)
- In-cylinder heat loss
- Frictional losses
- Pumping losses
- Exhaust port and manifold heat loss
- Inefficiency exhaust energy recovery

Figure A4-2 illustrates some of the technologies required for overcoming the barriers listed above. Some of these technologies were evaluated in detail during this program while others were only examined in enough detail to define development targets. Table A4-1 lists development targets for some typical engine performance parameters as well as current levels of performance. While some of the performance targets were met with the single-cylinder test engine, there were some limitations imposed by the test hardware. One such limitation was the limit on peak cylinder pressure. The test engine was limited to peak cylinder pressures in the range of 1900-2300 psi, below the target for the ARES engine. This limitation was based on structural limitation of the test pistons. However, given the constraints on peak cylinder pressure various performance targets were achieved. Figure A4-3 illustrates the friction losses (100 – mechanical efficiency) as a function of IMEP for the single cylinder engine. These numbers were adjusted to multi-cylinder results from the single-cylinder data. Mechanical efficiencies of 92-93 percent were obtained at IMEP levels of 340 psi. This corresponds to an approximate BMEP level of 310 psi, close to the target value of 350 psi. Multi-site ignition concepts were explored to increase combustion rate and mitigate knock. These concepts included both multiple spark plugs arranged about the periphery of the combustion chamber as shown in Figure A4-4 and pilot ignition as shown in Figure A4-5. Application of these concepts resulted in faster combustion rates, extended lean limit performance, and reduced knock tendency. Combustion rates were highly dependent on in-cylinder turbulence and equivalence ratio. At high BMEP levels, observed combustion rates for pilot ignition ranged from 15 to 22 crank angle degrees.

Table A4-1. ARES Targets for Selected Performance Parameters

Parameter	Current Technology	ARES Technology
Power Density (BMEP)	170-200 psi	350 psi
Peak Cylinder Pressure	1500-1800 psi	3200 psi
Turbocharger Efficiency	56 %	65+ %
Mechanical Efficiency	87-89 %	91+ %
Combustion Rate	25-30 Crank Angle Degrees	15-18 Crank Angle Degrees
Aftertreatment	No	Yes
Turbocompounding	No	Likely

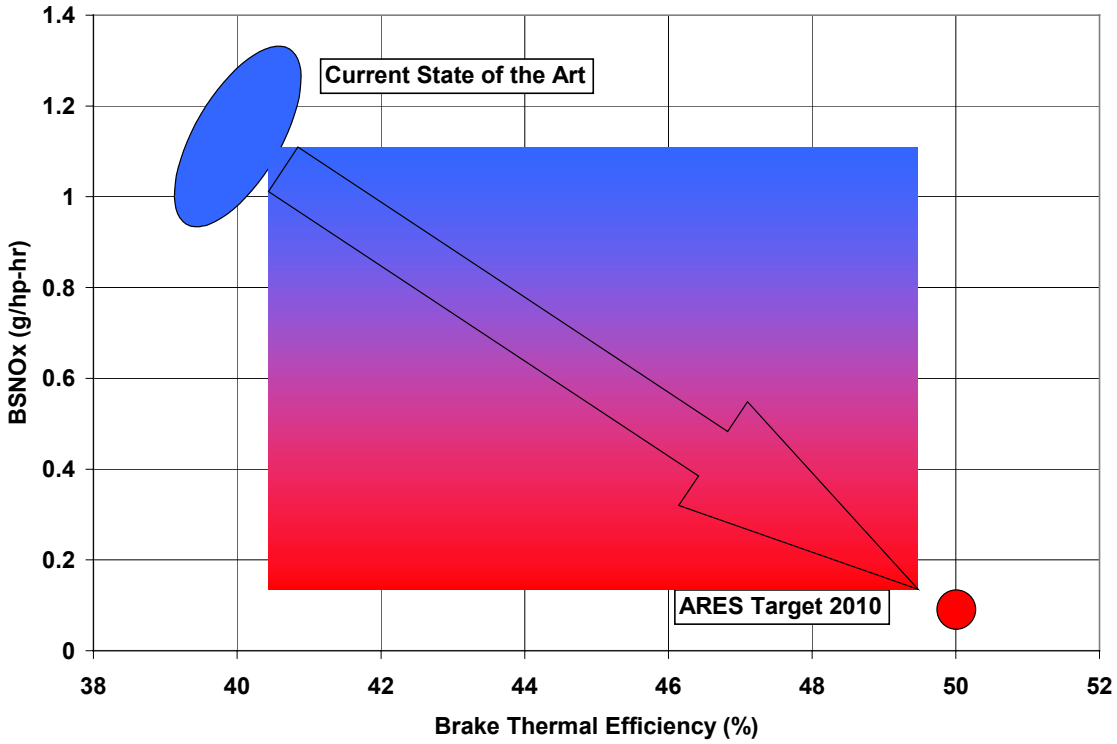

Figure A4-1. Current Engine Performance and ARES Targets

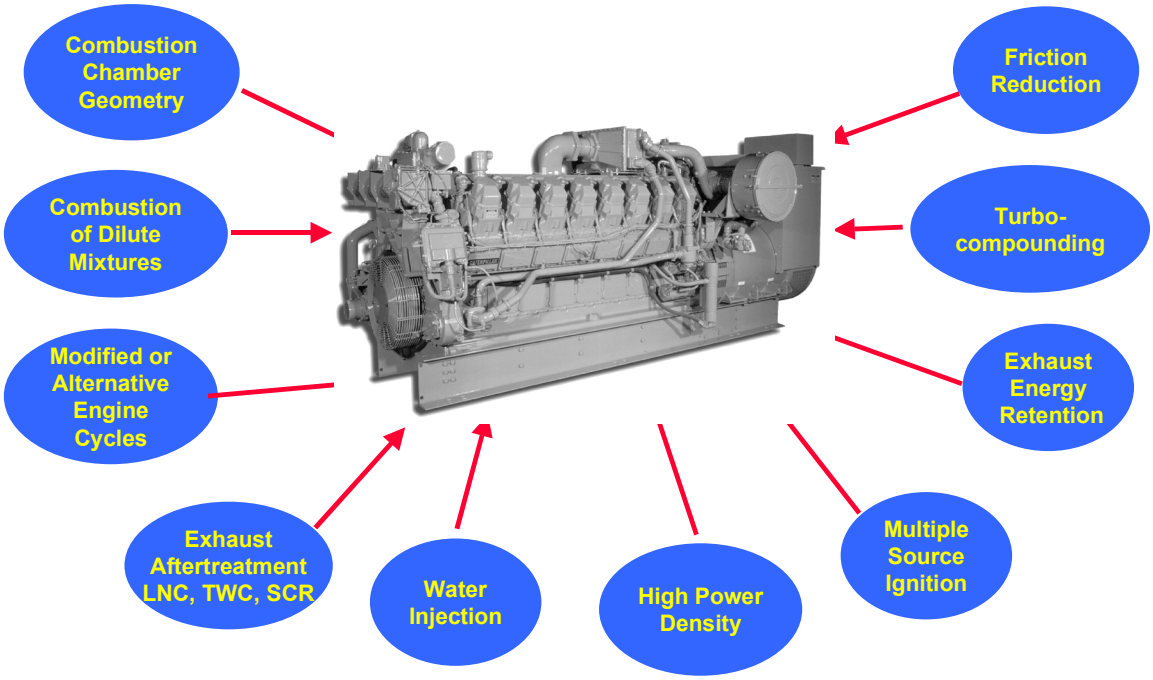

Figure A4-2. ARES Technologies

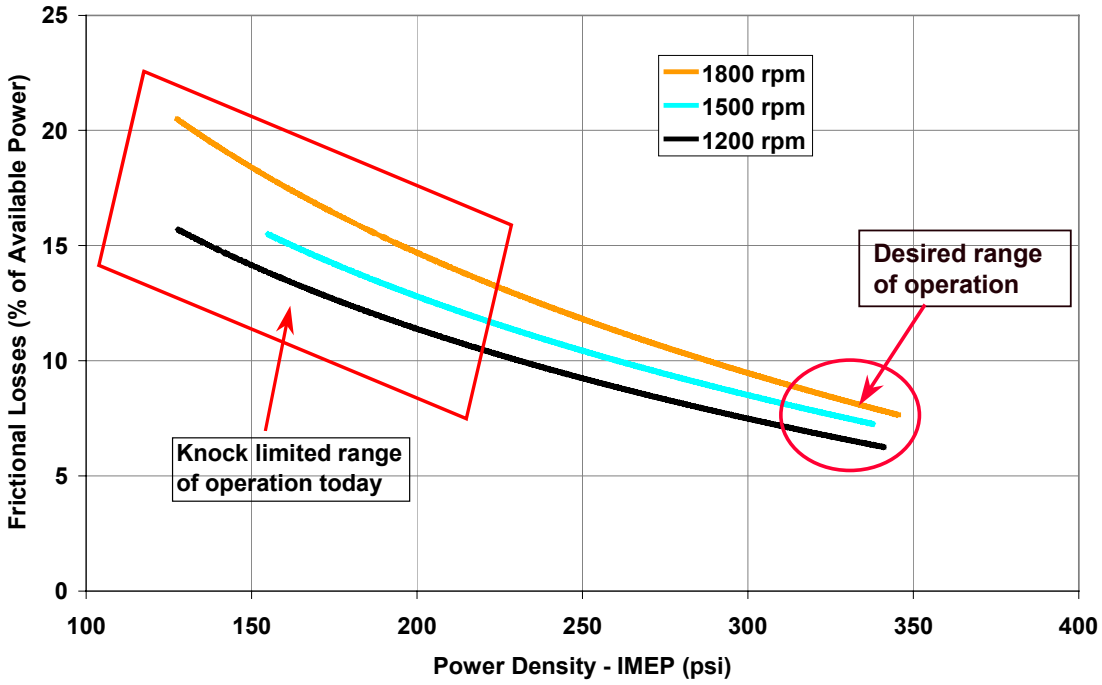

Figure A4-3. Frictional Losses as Function of Power Density

Figure A4-4. Multiple Spark Plug Ignition Concept

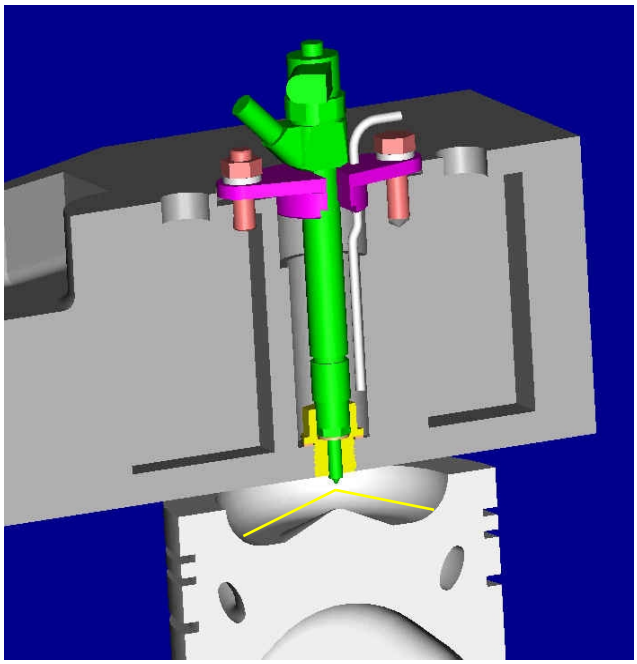

Figure A4-5. Pilot Ignition Concept

The single-cylinder engine data was used as a basis for further modeling. Combustion characteristics, air-fuel ratio, ignition timing, boost and exhaust pressures and temperatures, and emissions were input into the model. The model was used as a means for applying ARES technology that had not been applied on the research engine (i.e. turbo-compounding). Various combustion strategies were evaluated in combination with exhaust aftertreatment options. The results of this modeling exercise are shown in Figure A4-6. This figure illustrates the expected NO_x-efficiency data for four combustion strategies representing both lean burn configurations with a SCR catalyst and stoichiometric with a 3-way catalyst. As shown in the figure, a low-pressure loop EGR system with multi-site ignition and a 3-way catalyst was estimated to achieve below 0.03 g/bhp-hr NO_x with BTE approaching 48 percent. Figure A4-7 illustrates the energy balance of the current engine, the estimated balance for a multi-cylinder engine based on single-cylinder results, and the projected ARES engine. Figure A4-8 illustrates the technologies required to achieve the ARES goals.

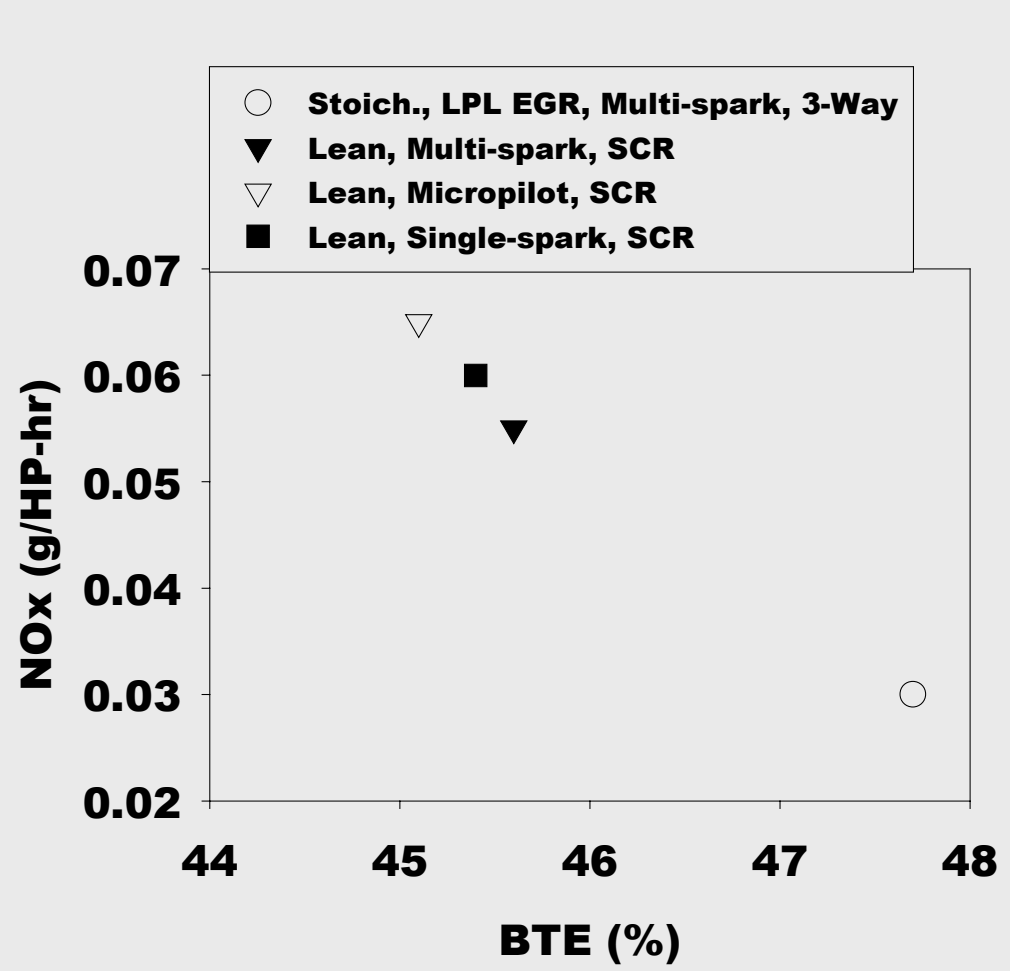

Figure A4-6. Engine Performance Based on Single-Cylinder CAT3501 Results Coupled with Application of ARES Technology via Modeling

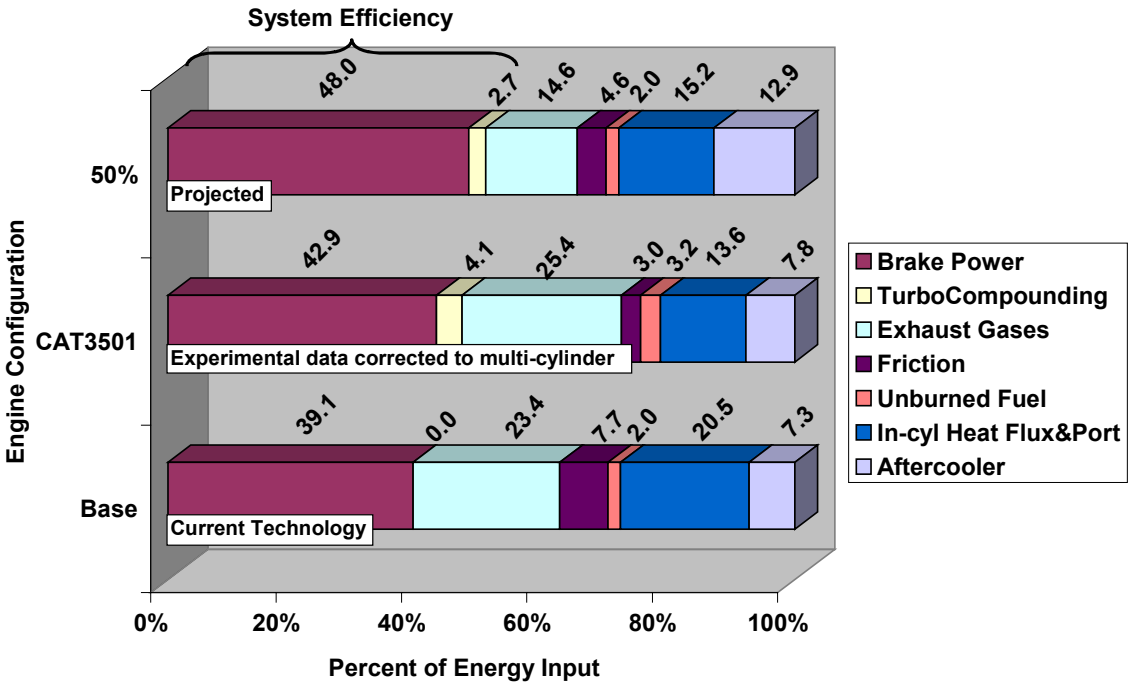

Figure A4-7. Energy Balance for Current Technology, Estimated Multi-Cylinder Results, and Projected ARES Engine.

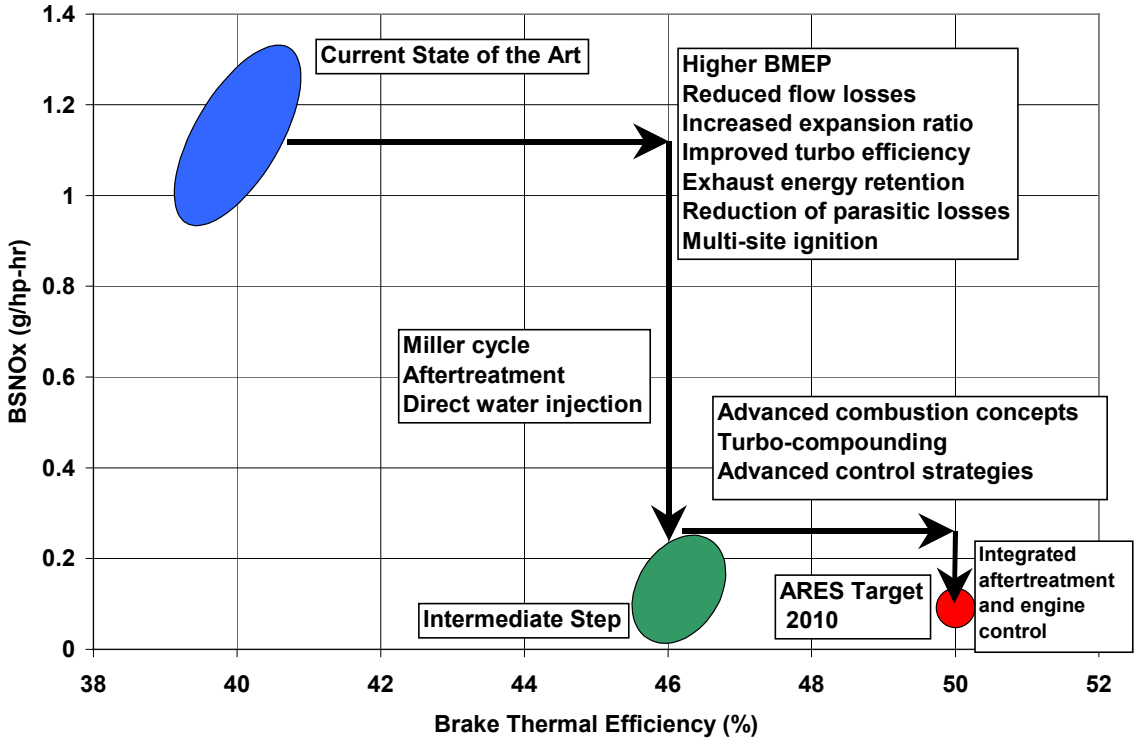

Figure A4-8. Technology Required for Achieving ARES Targets.

A5.0 CONCLUSIONS

An analytical investigation was performed to determine the feasibility of an optimum design for achieving 50-percent brake thermal efficiency with 0.05 g/bhp-hr NO_x in a natural gas, heavy-duty, stationary power generation engine. The investigation was done using SwRI's proprietary ALAMO_ENGINE simulation software. The intent was to provide guidance for the overall ARES program by estimating gains possible through the application of each new technology. Technologies were investigated both analytically and through examination of current and expected technology limitations. Because significant interactions were expected between some of the potential technologies, the technical path evaluation phase was tasked with determining the optimum combination of technologies for achieving the overall goals. Parametric investigations led to an optimum engine design and conclusions regarding the application of many of the technologies investigated.

The predicted performance for the optimized engine design was 50.7 percent brake thermal efficiency with 0.7 g/bhp-hr NO_x. The NO_x target for the ARES program was not met with this engine design. However, exhaust aftertreatment is being examined as part of the ARES program to further reduce NO_x emissions. The 50 percent BTE engine utilized two-stage turbocharging with inter-stage and after-cooling. The Miller cycle was also applied. A fully insulated exhaust system retained heat for use by the turbocharger and turbocompound turbines.

Utilizing experimental data from the CAT3501 single-cylinder research engine further extended the modeling. Using experimental data as input, the model was used to estimate multi-cylinder performance. This exercise indicated that for low NO_x and high BTE a stoichiometric-EGR combustion system with a 3-way catalyst was a promising approach. The estimated multi-cylinder performance was 0.03 g/bhp-hr NO_x at over 47 percent efficiency.

B. KNOCK MODELING AND MITIGATION FOR LARGE BORE NATURAL GAS ENGINES

EXECUTIVE SUMMARY

The objective of this project was to provide recommendations toward optimum knock mitigation strategies and combustion chamber designs for future large-bore, high BMEP, natural gas engines. The goal was accomplished through use of a Southwest Research Institute cycle-simulation package, the Rapid Prototyping Engine Modeling System (RPEMS^{TM}). The RPEMS model allows multiple cycle predictions of the chemical kinetics for the air-fuel mixture within premixed charge engines. Additionally, the model predicts the effects of combustion chamber geometry, ignition location, turbulence level, mixture composition, and previous cycle history.

The project was initiated with algorithm development and coding to add multiple ignition sites to the RPEMS model. Multiple, interacting flame zones are possible within the framework of this model. Validation efforts were performed for the multiple flame zone model in which its predictions were compared to results obtained from simple, ideal analytic solutions for spherical flame growth. The results from these tests showed that the geometric modeling method used for this study could accurately represent complex geometries and multiple flames.

A literature survey was conducted to identify available natural gas chemical kinetic mechanisms with the potential to be used for knock predictions. The most noteworthy of the mechanisms identified was the GRI v2.11 mechanism, developed originally for high temperature combustion within gas turbine engines. It was shown that large discrepancies in low-temperature kinetic predictions existed between available natural gas mechanisms, leading to a high degree of uncertainty in knock predictions derived from their combination with a suitable engine model. Hence, it was decided that an initial effort would be performed to modify the GRI v2.11 mechanism, adding reactions necessary to more accurately predict low-temperature knock reactions. Reaction steps were added for low-temperature pyrolysis and oxidation of methane, ethane and propane. Results from this effort showed that extension of the GRI v2.11 mechanism allowed it to be "tuned" to match experimental knock measurements. Once "tuned", the mechanism was used with the RPEMS code to explore the knock tendencies of various bowl-in-piston combustion chamber designs. Results from this effort led to recommendations for an optimal bowl-in-piston combustion chamber design.

The knock mitigation potential of a novel, multiple spark plug combustion chamber design was assessed. The new chamber utilizes piston-induced squish and distributed combustion zones to increase the overall mass burning rate, thus improving the knock characteristics of the engine. Modeling studies indicated that a potential increase in

knock-limited IMEP (at equivalent squish levels) of approximately ten percent could be afforded by the new chamber design.

The RPEMS package was extended to allow studies of pre-chamber combustion systems. This task was accomplished by utilizing the multiple ignition-site routines tested previously. The pre-chamber was modeled as a separate combustion system, attached to the main chamber by a parallel system of orifices. Each orifice acted to direct a modeled plume of burned gases into the main combustion chamber. The characteristics of the flame plume were assigned through a variety of fluid-dynamic sub-models. Initial results were presented as proof-of-concept of the method. No further work was conducted toward prechamber combustion system development, as experimental evaluation of the model would be required and no experimental prechamber task was conducted.

A numerical analysis of the effects of bowl design and squish on combustion rate was conducted. More specifically, the bowl radius and Top-Dead-Center (TDC) clearance were varied to create different levels of squish, allowing the resultant combustion rate to be compared to basic combustion chamber design parameters. The results of this work showed that for typical engine operating conditions, combustion rate was directly related to squish velocity, but that the fundamental source of the squish velocity was unimportant. Hence, bowl radius and TDC clearance traded-off against each other equally.

A subsequent numerical study to determine optimal knock-limited squish-area was conducted. Here, eight different piston designs were simulated, at various load conditions. Each piston differed in piston bowl design, yielding pistons that exhibited squish that varied from very low to very high. Spark timing sweeps were simulated at constant fuel rate for each speed and boost level, so that maximum knock limited IMEP could be predicted. The results of this effort showed that for conventional combustion systems, operating near 200 psi BMEP and 1500 rpm, the optimal squish area was approximately 70 percent.

Another task initiated on this project utilized a simplified version of the RPEMS package to “reverse-engineer” the combustion system design problem. Parametric studies of a large number of heat release profiles were analyzed to identify the optimal heat release pattern for highest engine efficiency at best engine-out NO_x. After identification of an optimal heat release profile, a follow-on task was initiated to design a combustion system that could provide the targeted heat release rates. This analysis concluded that the optimal heat release rate could be provided by a new multi-chamber combustion system, for which a patent application was prepared.

Experimental tests of the multi-chamber combustion system were conducted utilizing a small, 450 cc, gasoline, side-valve engine. This test apparatus was used only to provide proof-of-concept for the multi-chamber combustion system. Results of this effort showed that the multi-chamber combustion system could control the heat release rate as required by the original concept. Further, the multi-chamber combustion system was insensitive to spark timing over a large spark-timing window. Hence, the multi-chamber system

allowed very aggressive spark advance to be utilized without the occurrence of knock. This result indicated that the multi-chamber concept could be used to allow aggressive spark timing for high BMEP engines, thus extending spark plug life. The results of this effort led to an extended experimental program, utilizing the CAT3501, single cylinder gas engine.

The multi-chamber CAT3501 tests used a custom-machined piston with a removable upper-crown. The removable portion of the piston contained the central, or primary combustion bowl, while the outer region of the piston acted as the secondary combustion chamber. The piston blanks used for prototyping the multi-chamber concept limited the relative volumes of each bowl such that the central bowl was much smaller than the optimal size that previous numerical studies had predicted. It was decided that limited experiments should be conducted anyway, and two removable primary combustion bowls were tested. The first had a relative bowl volume of 1 percent, while the second had a relative bowl volume of 3 percent. The results of the experiments showed that even with severely non-optimal bowl volumes, the multi-chamber concept still provided the ability to operate the engine with more spark advance. However, the highest engine efficiencies measured with the multi-chamber combustion system were well below those measured previously for a traditional open-chamber combustion system. It is believed that much of the efficiency difference is due to the non-optimal bowl volumes used for this study. Future tests of this concept should utilize piston blanks that allow more range in the relative bowl volumes.

B1.0 INTRODUCTION AND BACKGROUND

B1.1 Introduction

Detailed kinetic models for autoignition provide the most insight into the chemical behavior of the fuel-air mixture under the broadest range of conditions. Because these models are based upon very large numbers of elementary coupled reactions, the knowledge base has grown slowly and computational solution times were exorbitant. However, advances in computer technology and detailed kinetic modeling studies have led to the availability of kinetics mechanisms and solution methods that are tractable for modern engine design studies. Probably the best known of the detailed mechanisms for methane combustion was developed by the Gas Research Institute[1]. Later versions of this mechanism include nitrogen chemistry, allowing studies of NO_x formation for a large variety of combustion processes. The project described herein explores methods of increasing the maximum efficiency of the modern, spark-ignited engine through elimination or control of engine knock. The methods employed seek to couple state-of-the-art engine and combustion simulations with modern autoignition models, culminating in an engine design tool that allows iterative autoignition modeling to be performed at multiple levels of complexity for large-bore, natural gas engines.

B1.2 Background

A set of general rules is presented here for designing an engine so that the onset of knock is delayed and maximum efficiencies can be increased. As part of this task, the knock problem is divided into three different areas of investigation. Because autoignition manifests itself as a function of engine design, operating conditions, fuel properties and other factors, a rough division of knock control methodologies can be presented as follows:

- Knock control: chemical
- Knock control: thermal
- Knock control: mechanical

The following chapters describe in detail the engine cycle simulation, the physics of the chemical descriptions of the fuel-air mixture, results generated from multiple combustion chamber designs, and discussion and recommendations for future combustion chamber design efforts.

B2.0 THE RAPID PROTOTYPING ENGINE MODELING SYSTEM (RPEMS™)

B2.1 Introduction

The following is a description of the Rapid Prototyping Engine Modeling System (RPEMS). RPEMS can be run as a stand-alone engine combustion simulation program or as a subroutine to other engine simulation codes. RPEMS has been developed to simulate various in-cylinder events that occur throughout the four-stroke SI engine cycle. Throughout development, emphasis has been placed upon insuring accurate solutions without sacrificing expensive computer time. To achieve this goal, considerable time was spent testing various solution methods and the formulation of each in-cylinder submodel was carefully developed so that desired information could be predicted without excessive computational effort.

B2.2 RPEMS Architecture

The global architecture of the RPEMS package is shown in Figure B2-1. The CHEMKIN thermodynamic property package consists of the CHEMKIN interpreter package that reads thermodynamic inputs from the Kinetics Data Base and the Thermodynamic Data Base, and the CHEMKIN subroutine libraries which are accessed by the RPEMS program. Similarly, the TRANFIT transport property package includes an interpreter for reading and compiling the user defined Transport Property Data Base, the TRANFIT subroutine libraries which communicate directly with RPEMS. The final stage of preprocessing is the GEOMETRY program, which reads a user defined boundary-meshed representation of the combustion chamber and spark plug. The GEOMETRY preprocessor creates an output file, the Geometry Linking File, which communicates directly with RPEMS to provide chamber geometry and flame/wall interaction information.

RPEMS produces numerous output files containing time-resolved solutions for all of the state variables solved within the engine simulation. Other output files for flame locations, chamber geometry conditions, gas compositions, etc. are included.

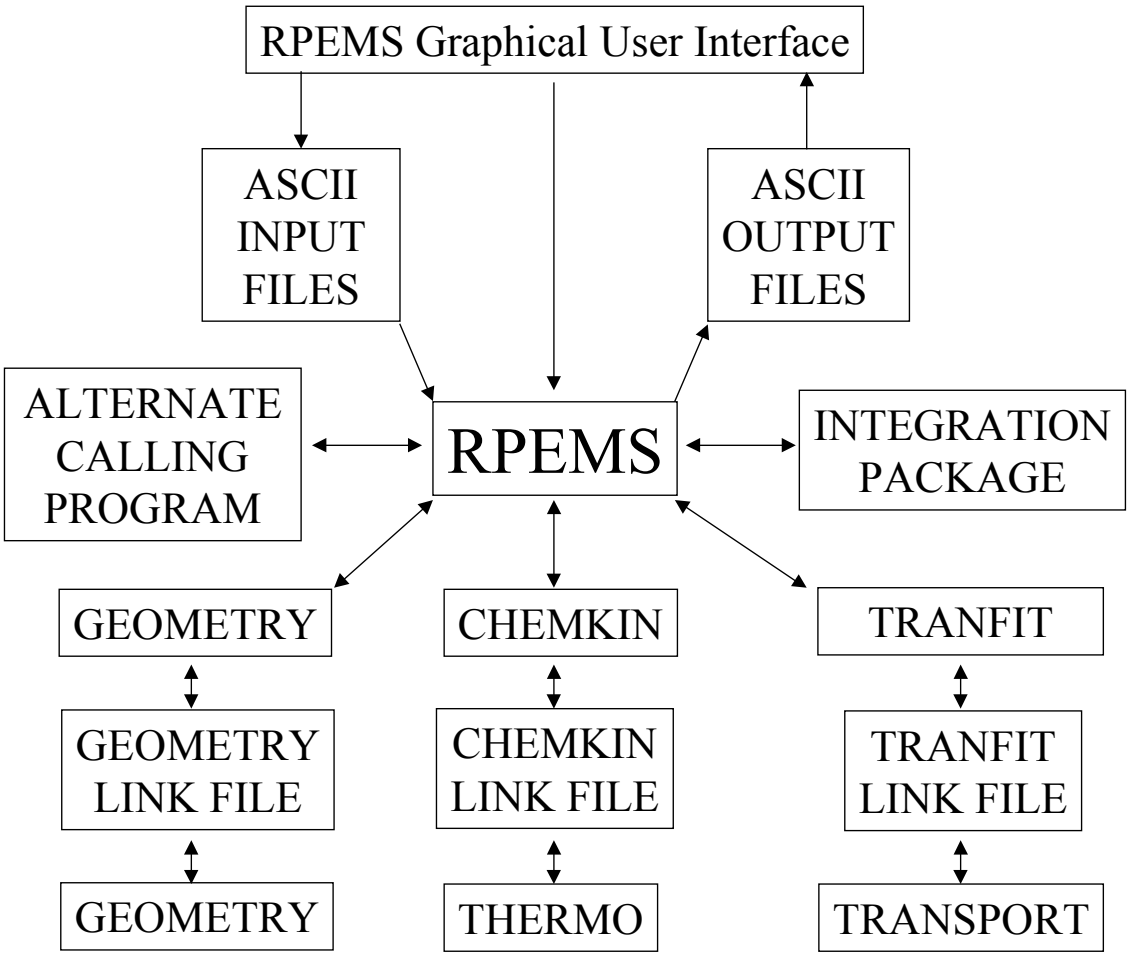

Figure B2-1. RPEMS Package Global Architecture

B2.3 General Governing Equations

Quasi-dimensional, or zonal, engine models require relatively few equations to be solved for most engine simulations. In earlier models,[2, 3] the most detailed of the in-cylinder events, combustion, was modeled with the chamber subdivided into as few as one zone. It was shown that most of the variables of interest could be resolved adequately with a zero-dimensional (in space) model such as this. RPEMS was developed based upon the quasi-dimensional method of engine modeling. However, RPEMS divides the combustion chamber into higher numbers of lumped zones, with a minimum of two zones for basic engine combustion calculations and an unlimited number of additional zones available for resolution of unburned and burned gas chemistries. The division of the chamber into numerous, smaller zones allows RPEMS to better resolve information that could not be predicted by earlier zonal models.

The governing equations for the major in-cylinder processes are all modeled in a similar fashion. Mass conservation within the cylinder is always maintained. Also, a volume conservation equation can be written for the overall chamber volume. Finally, an energy equation and gas law equation is written for each zone within the combustion

chamber. Variations to this modeling theme are made when necessary. However, the basic equations necessary to model compression, combustion, expansion, and gas exchange can be generalized and presented as follows. Note that all inflows are considered positive and outflows are considered negative for the remainder of this text.

General mass conservation for each zone can be written,

$$\frac{dm_z}{dt} = \sum m_{inflow\ z} - \sum m_{outflow\ z} \tag{2.1}$$

where *z* represents individual zones within the chamber. The Right Hand Side (RHS) of Equation (2.1) represents inflows and outflows of mass to each zone.

Volume conservation is similarly written for the entire chamber,

$$\frac{dV_u}{dt} + \frac{dV_b}{dt} = \frac{dV_{cyl}}{dt} \tag{2.2}$$

An ideal gas relation is written for each zone,

$$\frac{1}{P_{cyl}}\frac{dP_{cyl}}{dt} + \frac{1}{V}\frac{dV}{dt} - \frac{1}{m}\frac{dm}{dt} - \frac{1}{R}\frac{dR}{dt} - \frac{1}{T}\frac{dT}{dt} = 0 \tag{2.3}$$

and finally, an energy equation is written for each zone of the form,

$$\frac{d}{dt}(mh) - V\frac{dP_{cyl}}{dt} = \left(\sum mh\right)_{inflow} + \left(\sum mh\right)_{outflow} + Q \tag{2.4}$$

Differences in compression, combustion, expansion, and gas exchange are handled completely through the definitions of the inflow, outflow, and mixing terms from Equations (2.1) through (2.4). The following sections discuss these terms in more detail and present the final forms of the equation sets. The final set of governing equations for the compression process consists of a set of seven, nonlinear, ordinary differential equations. The state variables are:

$$\begin{bmatrix} P_{cyl} & V_u & V_b & T_u & T_b & m_u & m_b \end{bmatrix} \tag{2.18}$$

and submodels are used to describe all other variables and their time derivatives. These submodels are described in further detail in later sections of this text.

B3.0 MASS BURNING RATE AND HEAT TRANSFER MODELS

B3.1 Introduction

First, the mass burning rate model is discussed, along with sub-models used to enhance or support the predictive capability of the combustion process calculations. Second, the heat transfer model formulation is discussed.

B3.2 The Fractal Model of Combustion

The turbulent wrinkling hypothesis leads to the conclusion that the turbulent flame speed is a function of the ratio of the turbulent wrinkled flame area to the unwrinkled laminar flame area. This is expression can be written as,

$$u_t = \frac{A_t}{A_L} u_L \tag{3.1}$$

The simplicity of this equation belies the difficulty encountered in trying to characterize the degree to which turbulence wrinkles the flame. Gouldin[4] proposed that the wrinkled flame front could be characterized as a fractal surface. The use of fractals to describe surfaces has become popular because the fractal description allows an overall Euclidean geometry such as a smooth sphere to be superimposed with a roughness effect created by a fractal surface. The two descriptions together more completely describe real-world geometries, which invariably exhibit both Euclidean and fractal characteristics. The attractiveness of fractals to describe the turbulent flame front in quasi-dimensional engine models is apparent in that the flame front can be characterized as an expanding spherical surface that is wrinkled locally by turbulence effects.

B3.3 The Turbulence Model

The calculation of turbulence intensity is made through a one-equation, turbulent kinetic energy submodel or by inclusion of measured turbulence intensity data. The turbulent kinetic energy rate equation is given by,

$$\rho \frac{dK}{dt} = P_{intake} + P_{exhaust} + P_{tumble} + P_{swirl} + P_{squish} - \rho\varepsilon, \tag{3.2}$$

where all of the P_i terms on the RHS are turbulent kinetic energy production terms and are modeled individually within the RPEMS code.

B3.4 Wall Heat Transfer Model

The effect of wall heat transfer has been shown to reduce the peak pressure in the combustion chamber by about five percent.[5] Obviously, this is an engine specific approximation, but the general trend is a loss of usable energy from the combustion chamber during the combustion process. Heat transfer effects are modeled by RPEMS through use of Woschni's correlation.[6] This correlation assumes that the major mode of heat transfer from the in-cylinder gases to the chamber walls is by convection, with the convective heat transfer coefficient being a strong function of Reynolds number. The reader is directed to the original source for details of the model[6].

B3.5 Closure

This section detailed the development of the sub-models used within RPEMS to model. A summary of the work accomplished on this program toward extension of the fractal model of flame propagation to regimes characteristic of large-bore, lean, natural gas engines was also presented.

B4.0 COMBUSTION CHAMBER GEOMETRY MODEL

B4.1 Introduction

A method for modeling any arbitrary combustion chamber wall geometry was proposed by Poulos, et al.,[2, 3] and has subsequently been incorporated for use within RPEMS. The following sections review in detail the geometry model and its use within RPEMS. Changes to the original model are described as they occur within the description. The reader is encouraged to review the original literature for a more detailed description and code listing.[2, 3]

B4.2 The Geometry Model

Combustion chamber surfaces are described by a set of flat, triangular facets, approximating the actual combustion chamber geometry. The modeling mesh is most easily generated from solid models derived from an outside source, such as Pro-Engineer™. The accuracy of the modeled chamber is limited only by the complexity of the modeled parts and the number of facets used for their representation. Each facet is identified by an integer index and by Cartesian coordinates of the three apices of the triangle. The coordinates are measured from an origin located at the intersection of the cylinder's line of symmetry and the plane formed by the mating surface of the engine deck and cylinder head. The geometry routine reads the chamber geometry data and simulates the geometric interaction of an assembly of spherical flames with all of the chamber surfaces. The simulation really occurs in a two-step process. The flame itself is represented by multiple (if necessary) spherical flamelets that truncate against each other and the combustion chamber surfaces. First, at each time-step of the flame simulation, the total, exposed flame area is calculated from the assembly of flame spheres. Figure B4-1 illustrates the method by which the total flame area is determined. Each sphere surface is subdivided into a large number of smaller sub-areas, labeled dA in Figure B4-1. At each time-step of the cycle-simulation, vectors corresponding to every sub-area (R1, R2, etc.,) on every flame sphere are tested to determine whether they are part of the "true" flame surface (example R1) or are instead truncated by another flame (example R2). Ultimately, at the end of this procedure, all surface elements corresponding to the modeled flame have been labeled as "true" or "truncated".

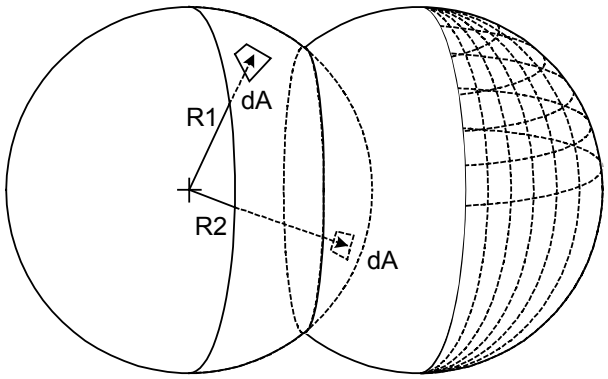

Figure B4-1. Multiple Sphere Approach to Modeling Flame Area

Next the interaction of the flame assembly with the chamber wall and piston is determined. In this calculation, only the flame sub-areas labeled "true" in the previous step are checked for interaction with chamber walls and the piston, thereby reducing the computational effort required, refer to Figure B4-2. The total flame area of the assembly of spherically propagating flames is determined by summing all flame sphere sub-areas labeled "true" after the two-step calculation described above.

$$A_f = \sum_{i=1}^{m}\sum_{j=1}^{n}\sum_{k=1}^{s} dA_{true} \tag{4.1}$$

The outcome of the calculations described above result in an instantaneous approximation of the overall flame area at each time-step of the cycle-simulation. The step-size for flame growth is set by the main calling program. Multiple, interacting flame zones are possible within the framework of this model. Additionally, for simulations of axially symmetric combustion chambers with centrally located spark plugs, the geometry model can be disabled within the RPEMS input file and analytic solutions for the geometric flame/wall interaction are used. Figure B4-3 diagrams the inter-relationship of the geometry model to the main cycle simulation program.

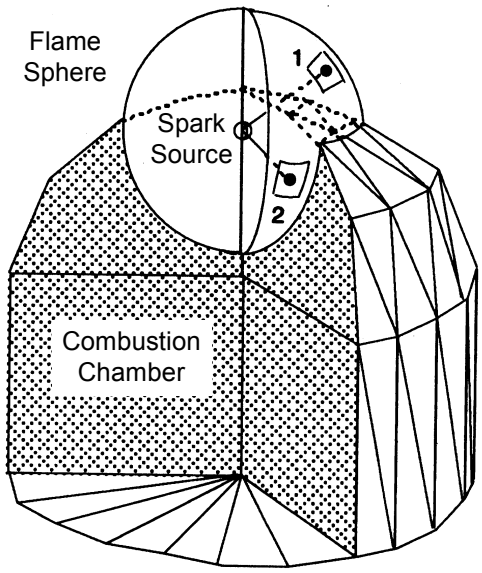

Figure B4-2. Flame/Wall Interactions

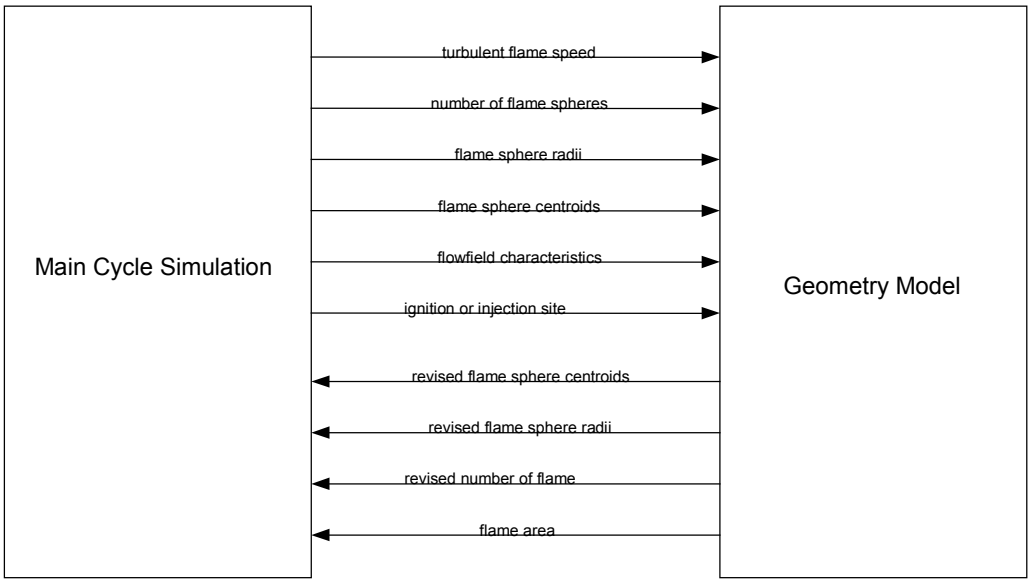

Figure B4-3. Geometry Model Communication with Main Cycle Simulation

B4.3 Closure

Additional tests and use of the geometry routines are provided in Section B5.0, where traditional bowl-in-piston combustion chambers are modeled, implementing single and multiple spark plugs. Additional results are included for a novel, multiple spark plug combustion chamber that may provide improved resistance to knock while increasing mass burning rates.

B5.0 CYCLE-SIMULATION RESULTS

B5.1 Introduction

This section presents results produced utilizing the open-chamber features of the RPEMS engine model. First, the model was run for combustion chambers characterized by varying levels of swirl, tumble, and squish, to assess the effects of each type of bulk flow on turbulence production. Next, predictions have been made for knock occurrence in a modern, open chamber design engine and compared to experimental measurements for knock. This validation exercise was split into two subcategories. First, the model was validated for its ability to predict the pressure (and thus, temperature) history produced by the engine during a cycle. Successful prediction of the thermodynamic history of the unburned fuel-air charge insures that the chemical kinetic models are being "driven" by the appropriate time-temperature conditions that lead to knock. The second part of the validation effort compared the actual knock prediction (the chemical part of the problem) to the experimentally measured knock condition. Because no direct experimental measurements were available for the composition of the in-cylinder gases during knocking operation, the only experimental knock data available was at the knock-limited spark timing. Therefore, the validation was conducted by comparing the model's prediction for knock–limited spark timing to experimental values. Additionally, the model utilized two different knock prediction mechanisms. The first was the GRI mechanism, which is based upon fundamental reaction kinetics. The second knock model was based upon a correlation, which had been introduced previously to the ARES consortium as part of the ALAMO_ENGINE cycle simulation. Comparison of knock predictions from both models was made to experimental data.

B5.2 Turbulence Characterization

General trends in the behavior of each turbulence sub-model can be determined. Figure B5-1 shows the relationships between each bulk flow condition and the turbulence produced near top-dead-center (TDC) of the compression stroke. As the figure indicates, squish flow, a dominant feature of large-bore engines, produces a very large level of turbulence during the squish period as the piston approaches TDC and the fuel-air mixture above the piston is squished into the combustion bowl in the piston. The tumble flow condition causes a marked increase of turbulence near TDC of the compression stroke, due to a propensity for conservation of angular momentum of the tumbling gases. The swirl flow results show that swirl tends to create a bulk motion in the chamber that exists throughout the compression stroke and into the expansion stroke. In direct comparison to the tumble-generated flows, the swirl-generated flow is not subject to a decreasing radius for the swirling mass as the piston approaches TDC. Therefore, no pronounced turbulence generation is produced near TDC for the swirl-flow case. The squish flow forces a majority of the chamber mass into the bowl near TDC, thus reducing the swirl radius substantially. In such a combustion chamber, it would be expected that swirl-generated turbulence would increase near TDC. In the current RPEMS model, increases in turbulence near TDC due to a squish type chamber are completely modeled

through the squish submodel. The squish results shown in Figure B5-1 are representative of a 50-percent squish level with no swirl or tumble. Again, note that squish-type combustion chambers create large turbulence values near TDC.

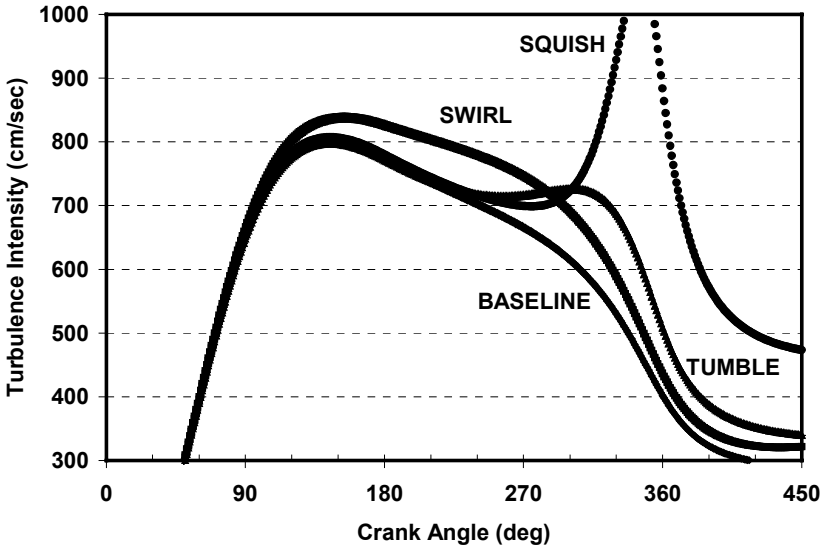

Figure B5-1. Turbulence Characterization for Large-Bore, Natural Gas Engines

B5.3 Spark-Plug Location Effects

An additional set of simulations were run to illustrate the effect of different spark plug locations and the number of spark plugs on mass burning rate. Figure B5-2 shows a comparison of central versus peripheral spark plug location effects and multiple-spark plug effects. These simulations were run for stoichiometric fueling rates, within a flat-piston, axis-symmetric combustion chamber. The results indicate that single spark plug engines produce the highest rate of pressure rise (mass burning rate) for a centrally located spark plug. Additionally, two peripheral plugs produce pressure rise rates similar to a single, central spark plug.

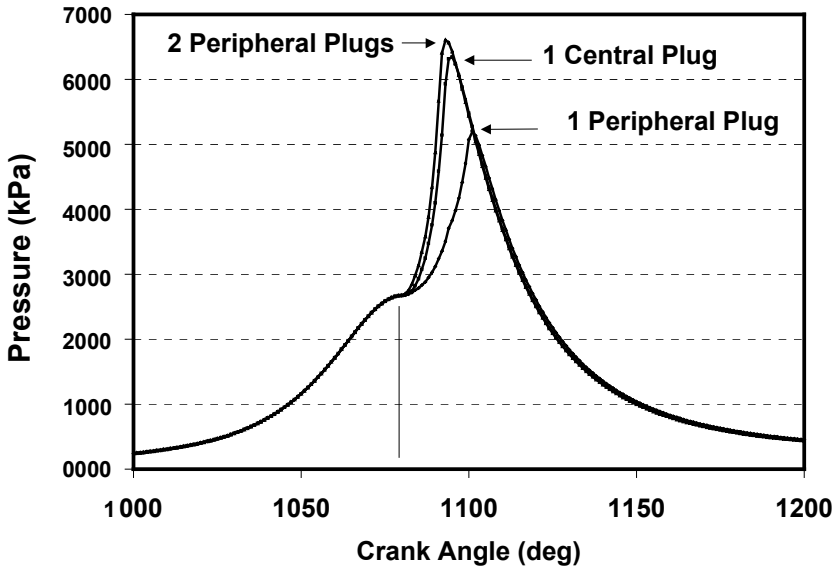

Figure B5-2. Single and Multiple Spark Plug Effects. Modeled Cylinder Pressure at Constant Spark Timing. Engine Speed = 1500 rpm. Compression Ratio = 11.5:1. Squish Area = 0-percent. A/F = stoichiometric

B5.4 Piston-Bowl Geometry Effects

The initial results from the RPEMS model for natural gas combustion within large-bore engines led to a more detailed study of piston bowl geometries. The study was conducted to assess the effects of bowl diameter and depth on mass burning rates. Additionally, a detailed chemical kinetic model for natural gas was used to investigate the likelihood of knock for each of the tested pistons. The pistons investigated are shown in Figure B5-3. The compression ratio was held constant at 11.5:1. The squish areas ranged from 10 to 80-percent, with bowl depths being varied to maintain constant compression ratio.

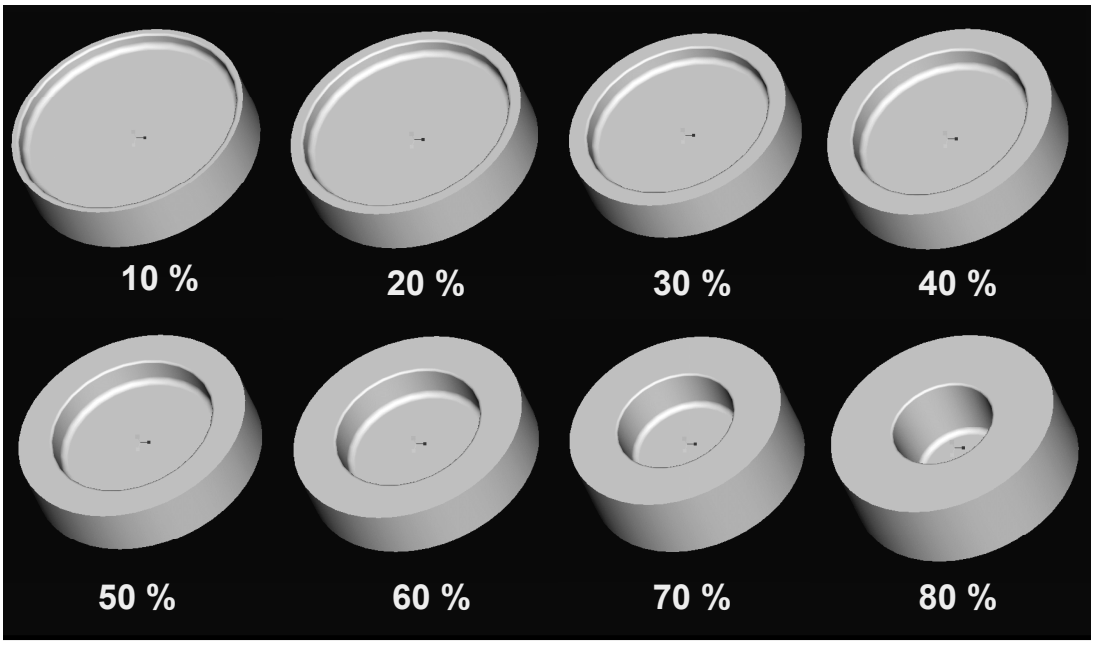

Figure B5-3. Piston Designs Tested for Piston Bowl Effect Study

Figure B5-4 illustrates the predicted cylinder pressure histories for each of the test pistons. Additionally, experimental data was available for a 42-percent squish area piston, also shown in the figure. The 42-percent squish area data was taken at knock-limited spark timing. The simulations run for this set of tests did not include knock predictions. Instead, the tests were conducted to assess the relative changes in mass burning rate that would be expected to occur for each of the piston designs.

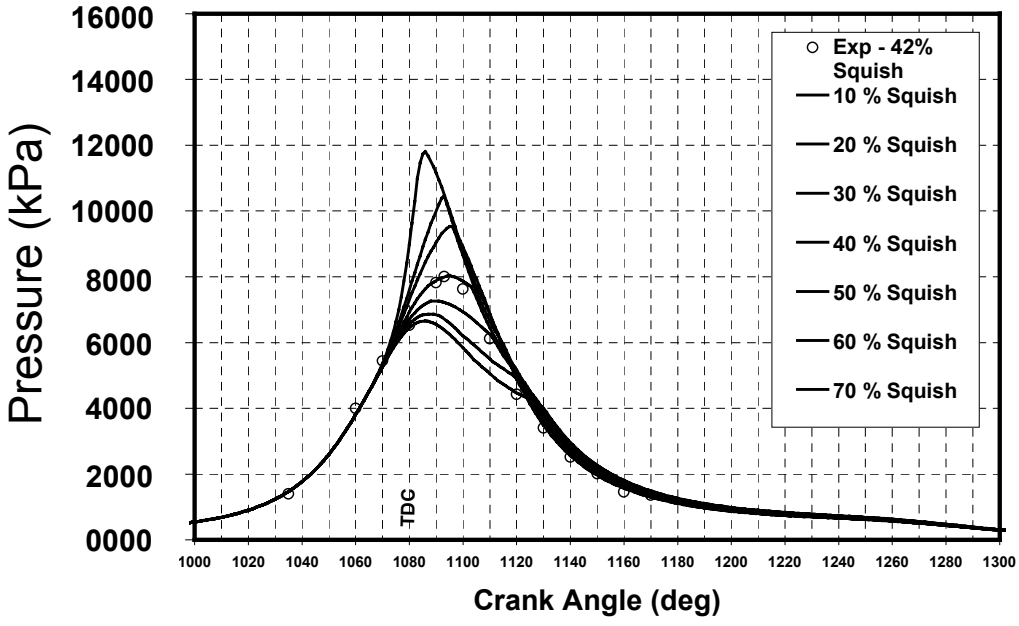

Figure B5-4. RPEMS Predictions for Cylinder Pressure for Various Piston Bowl Designs.

B5.5 Design for Knock Mitigation

B5.5.1 Chemical Kinetics

The knock modeling effort combined the predictive capabilities of the engine model with a chemical kinetic description of the autoignition chemistry of natural gas. Two kinetic models were used for this study. First, a correlation was employed that allowed very fast calculations for the state of the unburned gases during the compression and combustion portions of the cycle. The correlation was based upon a representative induction time approach that can be described by,

$$\frac{d\tau}{dt} = \frac{C_1 P^{1.15} \phi^{1.04}}{(\frac{RON}{100}) e^{\left(\frac{3800}{T}\right)}}, \tag{5.3}$$

where pressure effects are represented by P, in atmospheres, equivalence ratio by ϕ, octane number by RON and temperature by T, in Kelvin. The induction time, τ, is obtained by integrating Equation 5.3, starting at bottom-dead-center, BDC, of the intake stroke and continuing throughout the combustion period. Knock is predicted to occur when the induction time reaches a value of one (1.0). A quantitative measure of the knock intensity is obtained through comparison of the mass of fuel consumed after knock is predicted versus the total unburned mass at the beginning of combustion.

Knock predictions were also made utilizing detailed kinetic descriptions of natural gas mixtures. Generally, the detailed kinetics are described by rate equations for the production and destruction of each species within the unburned mixture.

The species histories predicted using the detailed chemical kinetic description fully account for chemical energy release within the unburned gas mixture of the combustion chamber. Therefore, unlike the induction time knock correlation, the detailed mechanism releases chemical energy into the combustion chamber, thus causing elevated unburned zone temperatures and associated knock characteristics. As with the induction time correlation, a quantitative description of the knock intensity can be derived from the amount of fuel consumed during the knock process.

B5.5.2 High Cycles Versus Averaged Cycles and Previous-Cycle Effects

Knock prediction requires that the modeler pay special attention to details of engine operating conditions that are often not critical to prediction of power or emissions. When validating a knock model against experimental data, it is imperative that the model's predictions be compared to experimental data that was derived during a knocking engine cycle. Because knock occurrence can damage expensive test engines and instrumentation, it is common to stop testing (and data acquisition) if knock becomes severe. Therefore, not much "true" knocking data is available. Where data is available, the engine is usually knocking intermittently, on only a few percent of the actual firing cycles. Additionally, the measured data is usually presented as cycle averaged data,

calculated over tens to hundreds of cycles. Even though the engine may have exhibited audible knock during the test (as is common during spark sweeps for MBT timing), the only real knocking cycles occurred when peak cylinder pressure was higher than the averaged trace. An example of this phenomenon is presented in Figure B5-5, in which multiple, successive large-bore, natural gas engine cycles are presented from an experiment with the engine set at knock-limited MBT timing. Figure B5-5 indicates a rather large variation in cycle-to-cycle variability of combustion, especially in measurements of peak cylinder pressure. This is a very important feature of the data set because it is the variation in peak pressure that causes large swings in the peak unburned zone temperature from cycle-to-cycle. In the results depicted in Figure B5-5, only the high-pressure (with correspondingly high temperatures) cycles actually exhibited autoignition.

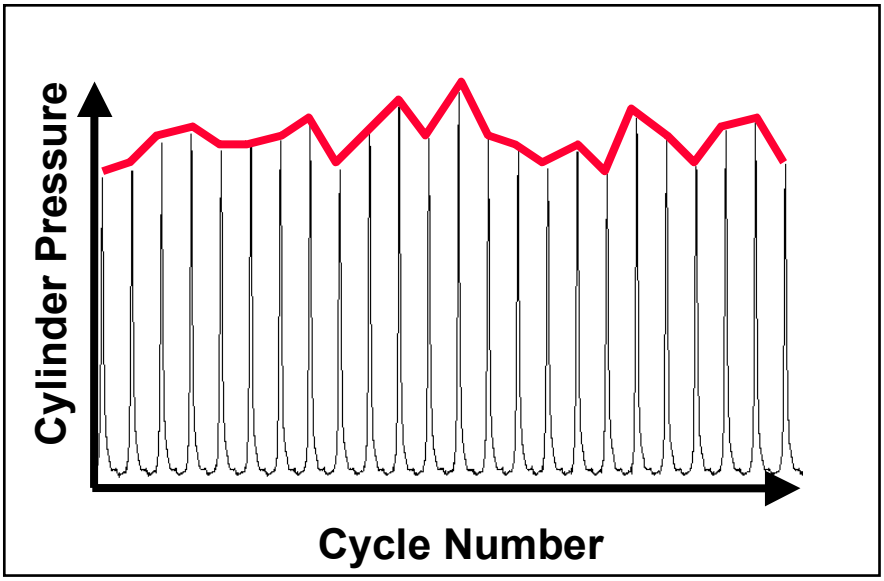

Figure B5-5. Cylinder Pressure Measured for Successive Cycles in a Large-Bore, Lean, Natural Gas Engine Running at Knock-Limited MBT Timing

Calculation of the statistical coefficient of variance (COV) of the magnitude of peak pressure, the location of peak pressure, and traditional indicated mean effective pressure (IMEP) reinforces the need to validate knock models against relevant knocking data. Figure B5-6 shows a comparison of calculated COV values for each of the three parameters mentioned previously and derived from the experimental data from Figure B5-5. The raw data were acquired in an open-chamber engine running near the lean limit. Hence, the COV of IMEP is slightly high at about 3 percent. Additionally, notice that the COV of location of peak pressure is very low (approximately 1 percent). The location of peak pressure is relatively stable while the variance in magnitude of peak pressure is very high (8 percent). This translates into a variance in peak unburned temperature of 4 percent from the mean. For a mean peak unburned zone temperature of 1000 K, this would lead to temperature excursions of 40 K for one standard deviation of the cyclic data set.

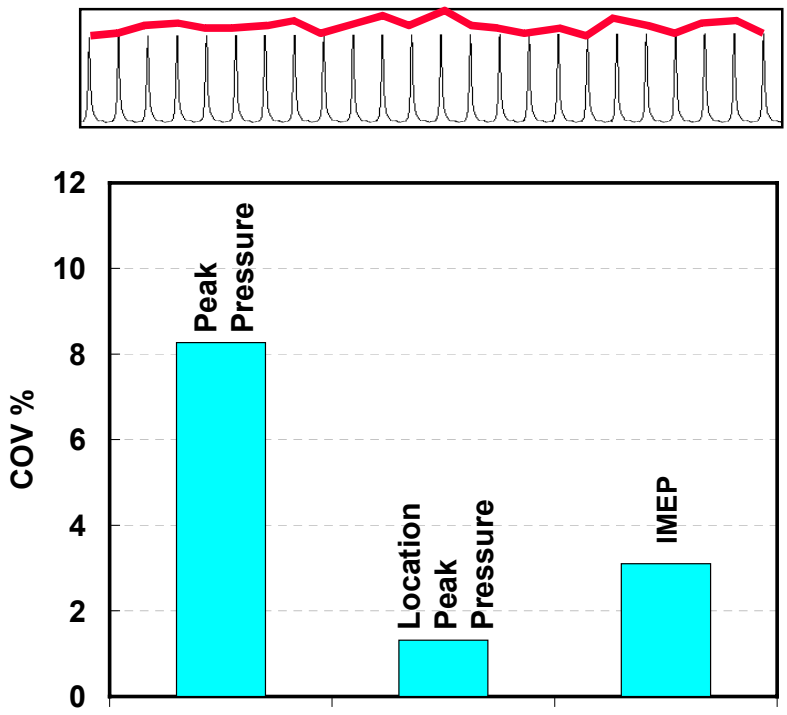

Figure B5-6. Coefficient of Variance for Peak Pressure, Location of Peak Pressure and Indicated Mean Effective Pressure for Raw Data Set Illustrated in Figure B5-5

B5.5.3 Development of Knock Mitigation Design Strategy

A first step in the development of a procedure for developing knock resistant combustion chambers was to run a set of cycle-simulations without knock predictions to provide a baseline for later comparison. Therefore, a spark timing sweep was simulated for a specific combustion chamber design. Because this study was conducted in parallel with the extension of the fractal combustion model, the results in this section are all calculated for combustion chambers without squish (flat pistons) and using *stoichiometric mixtures* of pure methane and air. Hence, the cylinder pressure predictions in this section are much higher than typical for this class of engine. The choice of operating conditions and simple chamber geometries eliminated uncertainties in the results that would have been compounded by the sub-models for squish and combustion being developed at that time. Later sections will present results generated for traditional, bowl-in-piston combustion chambers burning lean, natural-gas/air mixtures.

Figure B5-7 shows a comparison of the pressure traces for the single and dual spark plug combustion chambers. Note that the peak cylinder pressure is labeled in the plot. This cylinder pressure is high compared to conventional, lean-burn natural gas engines. As with the previous tests, note that the high cylinder pressure is a consequence of simulating high boost (2 atm), stoichiometric operating conditions.

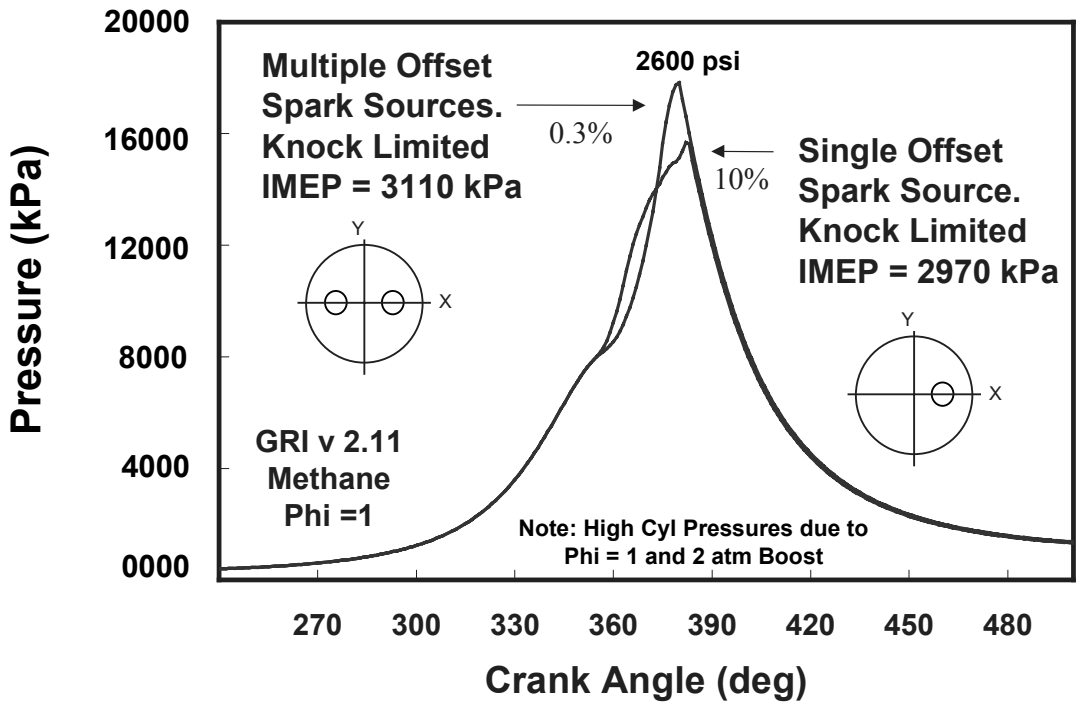

Figure B5-7. Comparisons of Pressure Traces for Large-Bore, Stoichiometric, Methane-Fueled Engine at MBT Ignition Timings with Single and Dual Spark Plugs

A final set of simulations was run to compare the effects of high swirl flow on knock-limited IMEP. Swirl levels of zero and eight were used for the calculation. Figure B5-8 shows a comparison of the knock-limited pressure traces for single spark plug combustion chambers operated with zero and high swirl. As with previous plots, the knock intensity is labeled next to each pressure trace. The improvement in knock-limited IMEP was predicted to be approximately 6.4-percent for the high swirl combustion chamber versus the low swirl chamber. As with earlier simulations at these operating conditions, the peak cylinder pressure was high compared to conventional lean-burn, natural gas engines. This set of tests was conducted to gain insight into a methodology for comparing the knock resistance of various combustion chamber designs. Therefore, the absolute values of IMEP and pressure were not of primary importance. However, subsequent tests were conducted at more conventional operating conditions and are presented in later sections of this report.

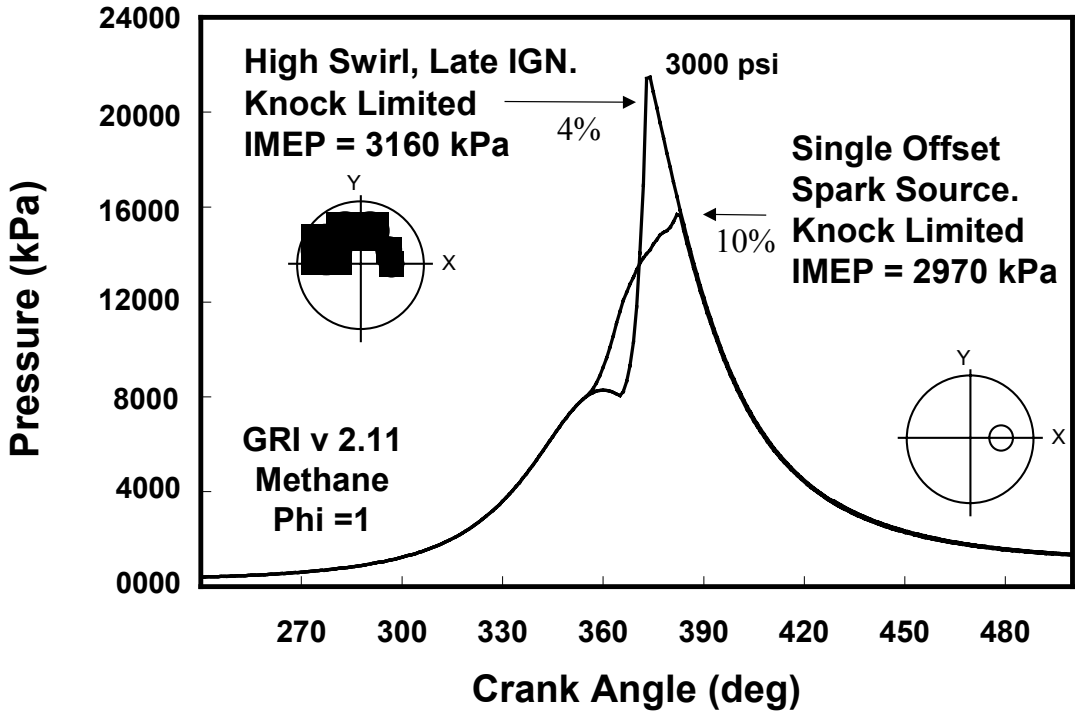

Figure B5-8. Comparisons of Pressure Traces for Large-Bore, Stoichiometric, Methane-Fueled Engine at MBT Ignition Timings with Low and High Swirl Combustion Chambers

B5.5.4 Distributed Combustion Piston Design

A separate project funded as part of the ARES program was tasked with developing an overall ignition system that provided a potential for improvements in ignitability and combustion rate for large-bore, open-chamber, lean-burn natural gas engines. The RPEMS model was used as a design support tool for this effort. A solid model of the proposed piston design was created using Pro-Engineer^{TM}. The test piston was designed to allow single or multiple spark plug tests, utilizing multiple different ignition coils and associated hardware.

Figure B5-9 illustrates the piston design proposed for the ignition system development project. The design allows up to four peripheral spark plugs and one central spark plug. The RPEMS code was used to predict the knock tendencies and IMEP improvement potential for various spark plug locations and spark timings. The piston is referred to as the Distributed Combustion (DC) piston design throughout this text.

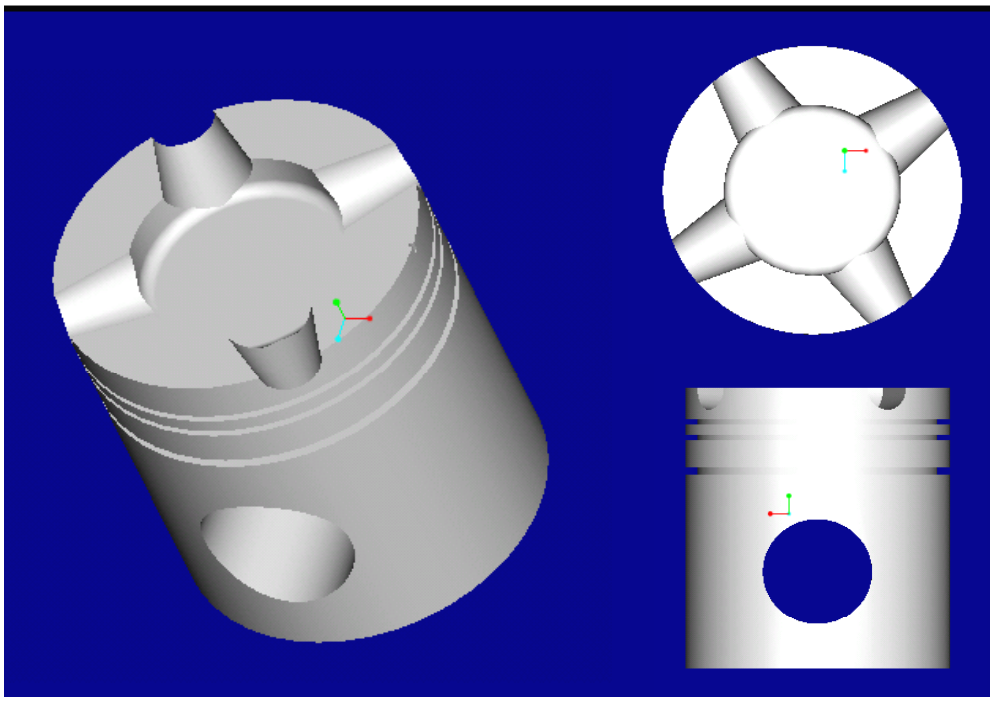

Figure B5-9. Solid Model of the Proposed Test Piston for the Ignition System Development Project

A simulation was run using the DC piston with four peripheral spark plugs. Again, spark timing was held at 18 degrees BTDC, to allow direct comparison to the previous tests. Figure B5-10 shows the results of this simulation. The four spark plug DC piston exhibited combustion rates much higher than the single, central spark plug tests. Note that no changes to the bulk flow or turbulence were made and that the increased mass burning rate is primarily due to the use of multiple spark plugs. Additionally, because the combustion flame is initiated at the periphery of the chamber, much of the mass outside of the bowl is consumed early in the combustion process, followed by a high turbulence combustion period within the bowl. This succession of events creates a higher average mass burning rate than conventional designs.

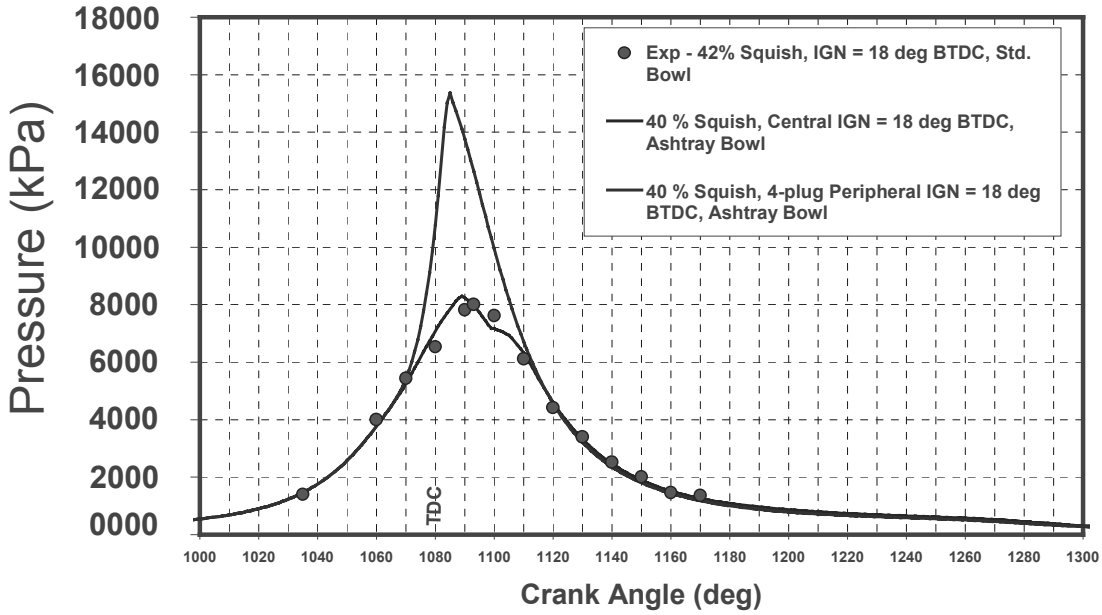

Figure B5-10. Pressure Predictions for DC Piston Design with Central Spark Only Versus Case Run With Four, Peripheral Spark Plugs, at Same Spark Timing

The conventional bowl-in-piston design with central ignition exhibits highly turbulent combustion in the bowl, but lower turbulence, slow combustion outside of the bowl. The DC piston design offers improved combustion outside of the bowl. The spark timing chosen for the tests presented in Figure B5-10 was chosen for comparison purposes only. The knock model indicated severe knock at this spark timing, thus requiring additional timing retard.

A further set of simulations was run for the DC piston, recognizing that all five spark plugs could be utilized. The spark timing was held equal for all five spark plugs in the tests conducted. Again, as had been the case with the previous tests, an increase in the number of spark plugs (flame initiation sites) led to an increased mass burning rate. However, addition of a single spark plug to the chamber with four, peripheral spark plugs did not produce as dramatic of an increase in mass burning rate as had occurred in the previous tests comparing single spark plugs to multiple spark plugs.

A spark timing sweep was conducted for the five spark plug version of the DC piston (See Figure B5-11). Knock predictions from each simulation showed that even ignition timings of 8 degrees BTDC caused excessive knock. Again, as had been done in the previous testing, the bulk flow (tumble) was reduced. The overall tumble was reduced from a value of two (2.0) to one-half (0.5). Even at this tumble level, knock was predicted for spark timing of 8 degrees BTDC. Therefore, the ignition timing was further reduced to values of 6 and 3 degrees BTDC. The knock model predicted that knock would be avoided for both of the final spark timings tested. The results of all the single-, four-, and five- spark plug tests with the DC piston are presented in Figure B5-12. The highest, knock-free IMEP was predicted when using four spark plugs, with tumble equal to two, and spark timing of 8 degrees BTDC. The IMEP improvement was predicted to

be approximately 12 percent, compared to the conventional piston with a single, central spark plug. The five spark plug DC piston tests predicted an IMEP improvement of 11 percent, compared to the conventional piston with a single, central spark plug.

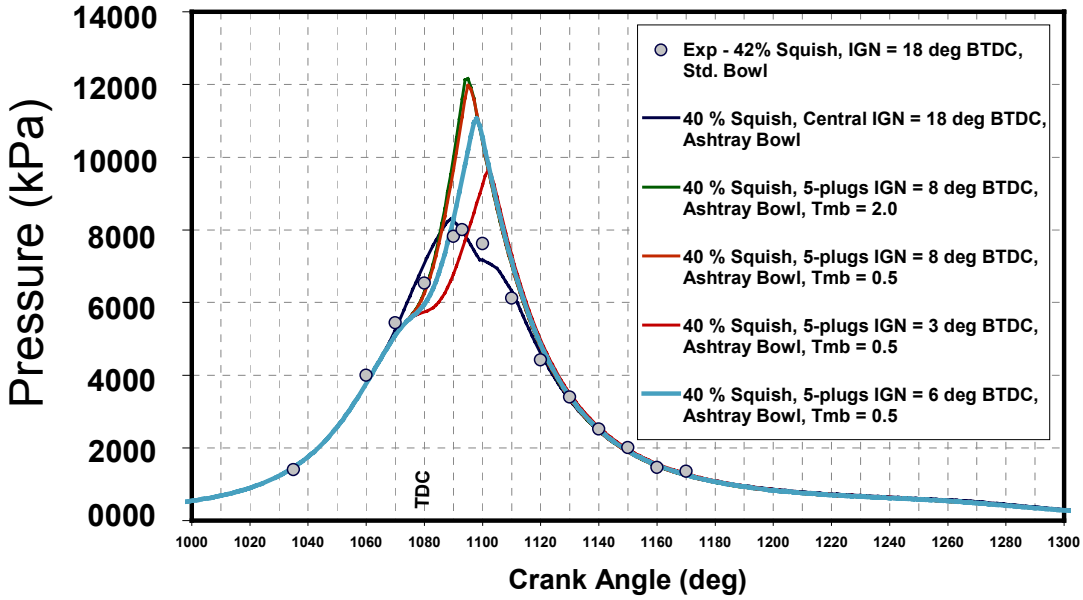

Figure B5-11. Pressure Predictions for DC Piston Design with Central Spark Only Versus Case Run With Four Peripheral- and One Central- Spark Plug at Various Spark Timings and Bulk Flow Conditions

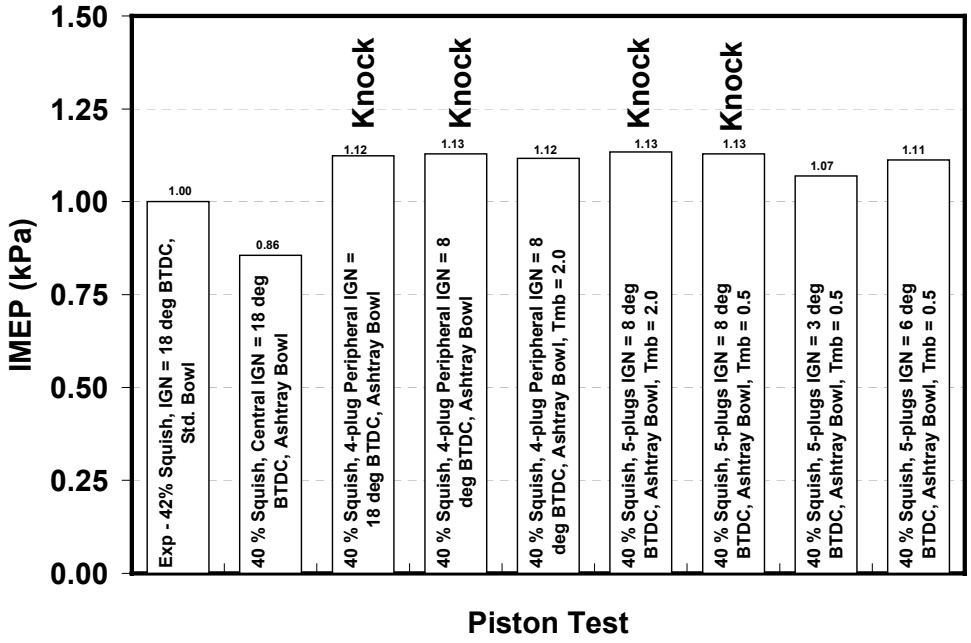

Figure B5-12. Knock and IMEP Detail for Simulations of the DC Piston at Various Spark Timings and Bulk Flow Conditions

B5.6 Bowl Radius vs. TDC Clearance as a Means of Controlling Squish Velocity

Effort was devoted to studies of the individual combustion-speed effects of piston-to-head TDC clearance and piston bowl radius. Both variables lead directly to squish flow, but questions existed in regard to the sensitivity of combustion to each variable. For example, the squish flow local to the bowl edge requires a finite amount of time to reach the center of the combustion chamber (typically where the spark plug is located). The question arose: How will combustion rate be affected if we change the bowl radius, but adjust TDC clearance to hold peak squish velocity constant? The expectation was that larger bowl radii would allow a longer "ignition delay" period before squish affected the flame kernel. Hence, more spark timing would be possible for a piston with a large bowl radius and tight TDC clearance than for a piston with smaller bowl radius and large TDC gap.

Four test pistons were machined to test the hypothesis presented above. Figure B5-13 shows engineering drawings of the test pistons. Note that the measurements indicated in the drawings are for cold dimensions. As the engine and components warm up, all dimensions change, with TDC clearance being affected substantially. The squish velocities noted in Figure B5-13 were calculated for cold clearances. Additionally, the piston-to-head clearance and squish velocity details for the final machined version of piston 2 did not match those from Figure B5-13, due to piston-to-valve clearance limits that required slight valve relief to be machined in the piston crown.

Figure B5-14 shows results for calculations of the warm-engine squish velocities expected for each of the test piston designs. Note that pistons 2 and 3 were expected to exhibit very similar squish velocity profiles, thus providing the possibility of assessing the effects of TDC clearance vs. bowl radius.

The RPEMS model was used to simulate the expected burn rates from the four piston designs. Figure B5-15 and 5-16 show comparisons of the modeled and experimental results (modeled = dashed lines, expt = solid lines). The experiments were designed such that the total air mass and fuel energy provided for combustion were equal in all tests. More specifically, the air-fuel ratio was constant and the compression pressures were equivalent for each comparison. The RPEMS model predicted the expected trends for all tests very well. However, the absolute values for peak cylinder pressure and location of peak cylinder pressure indicated that some modeling inadequacies still exist.

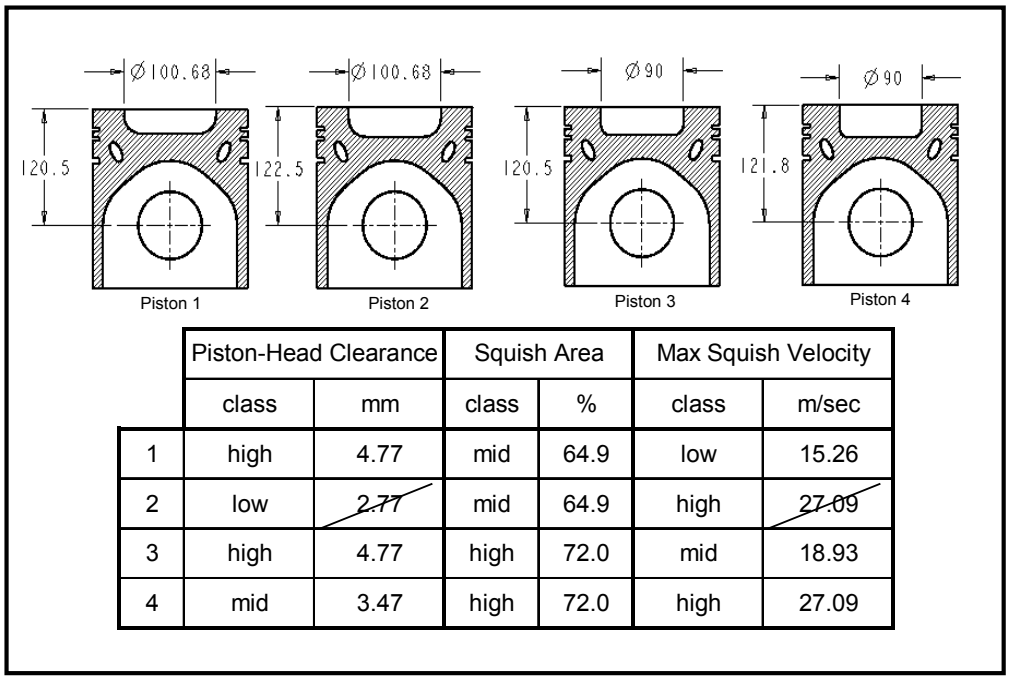

	Piston-Head Clearance		Squish Area		Max Squish Velocity	
	class	mm	class	%	class	m/sec
1	high	4.77	mid	64.9	low	15.26
2	low	~~2.77~~	mid	64.9	high	~~27.09~~
3	high	4.77	high	72.0	mid	18.93
4	mid	3.47	high	72.0	high	27.09

Figure B5-13. Piston Designs Utilized for Experimental Evaluation of Squish Parameter Effects on Combustion.

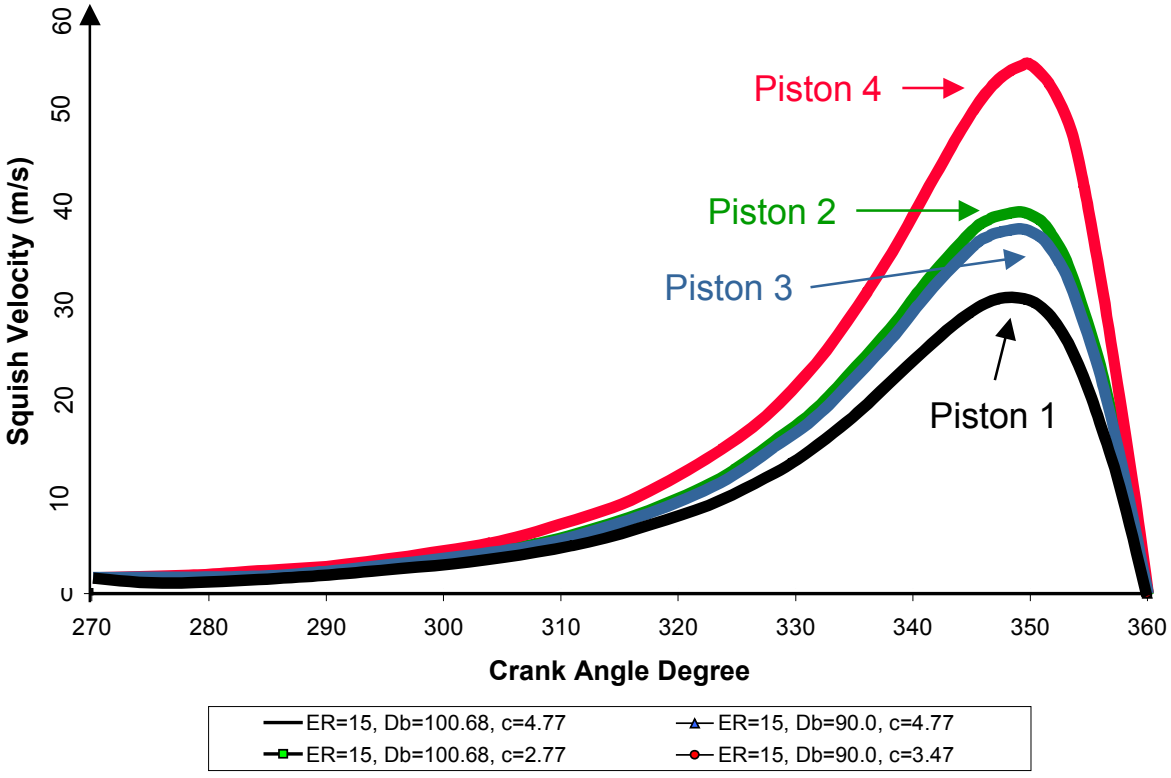

Figure B5-14. Fully-Warm Engine Squish Velocities Resulting from Four Different Piston Designs.

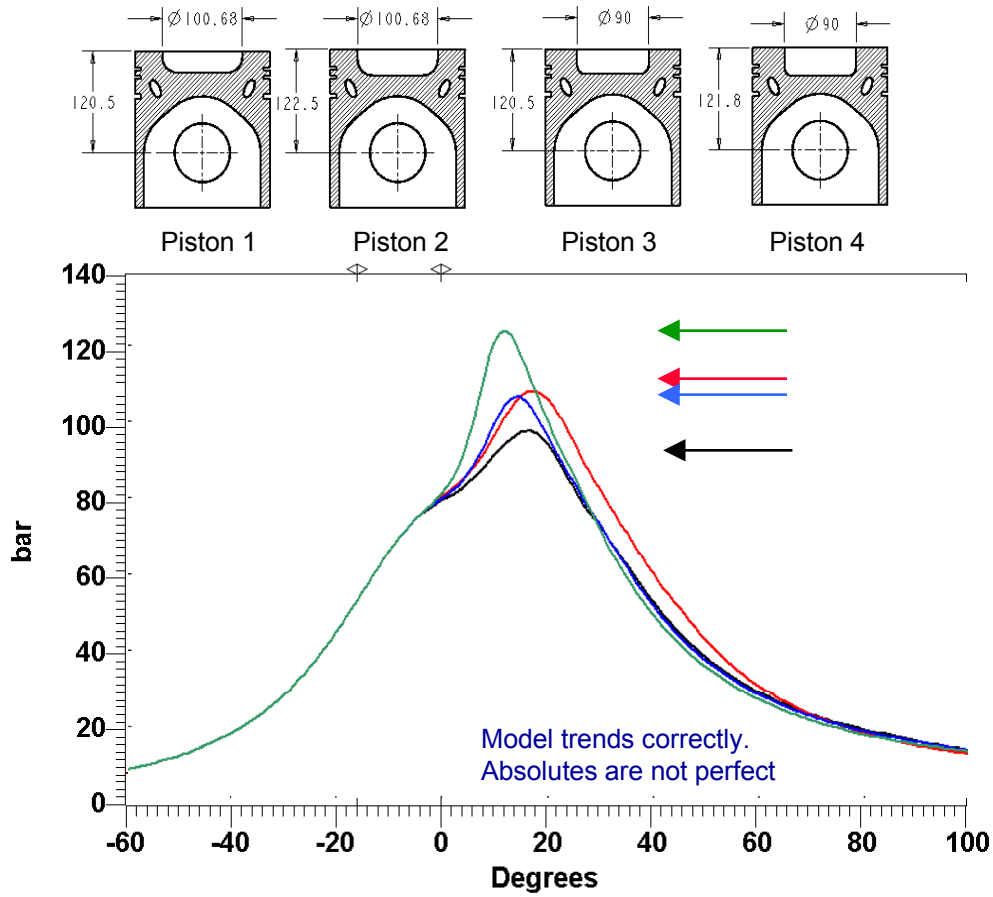

Figure B5-15. Modeled vs. Measured Combustion Pressures for Each Piston Design

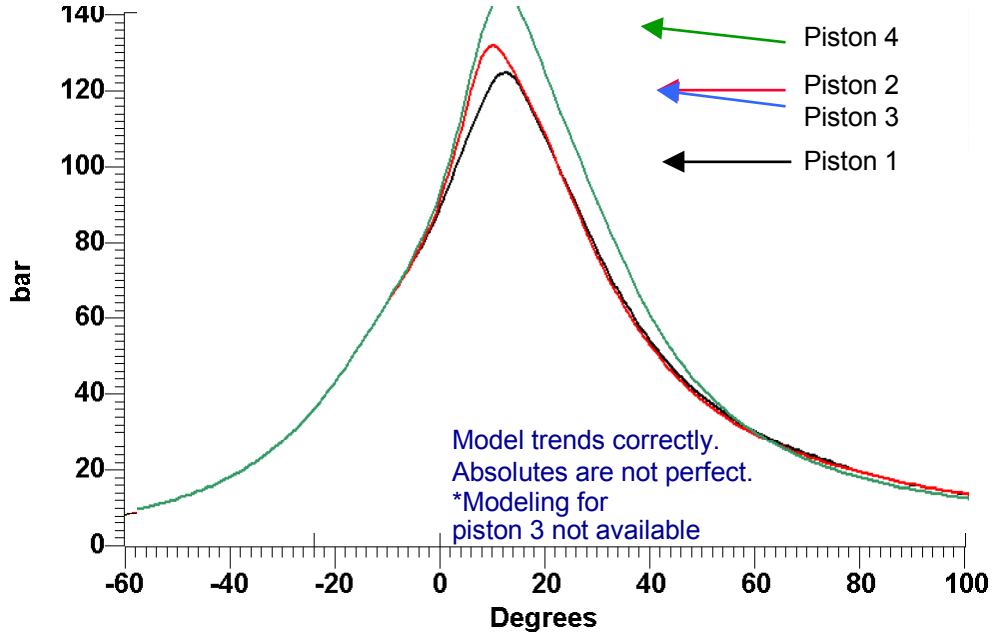

Figure B5-16. Modeled vs. Measured Combustion Pressures for Each Piston Design

For advanced spark timings, Piston 4 (highest squish velocity) knocked severely and no experimental data was acquired. The comparison of Piston 2 and 3 results from Figure B5-15 indicate that as the bowl radius was increased, combustion rate slowed, as expected. However, the overall results of this work indicated that for the range of piston-related dimensions tested, the difference in combustion rates due to the tradeoff in TDC clearance for bowl radius was very small. Hence, our conclusion was that bowl radius and TDC clearance could be traded against each other as necessary to create desired squish velocities, without a combustion preference existing for one design variable over the other.

B5.7 Squish Effects on Knock-Limited IMEP

Throughout the ARES program, various piston designs were evaluated on separate phases of the program. See Figure B5-17 for the various piston designs evaluated. It was decided that a modeling study would be conducted to assess the probable best conventional piston for the CAT 3501 test engine. The term "probable best" was used because the piston design would be evaluated for its ability to create fast efficient burn rates without the onset of knock, with no evaluation of the NO_x reduction potential of the piston design. Therefore, this study would be directly applicable to a lean-burn open-chamber engine configuration that would utilize a NO_x reduction aftertreatment system. Hence, the engine would provide high thermal efficiencies without knock, while the aftertreatment system would insure low NO_x emissions.

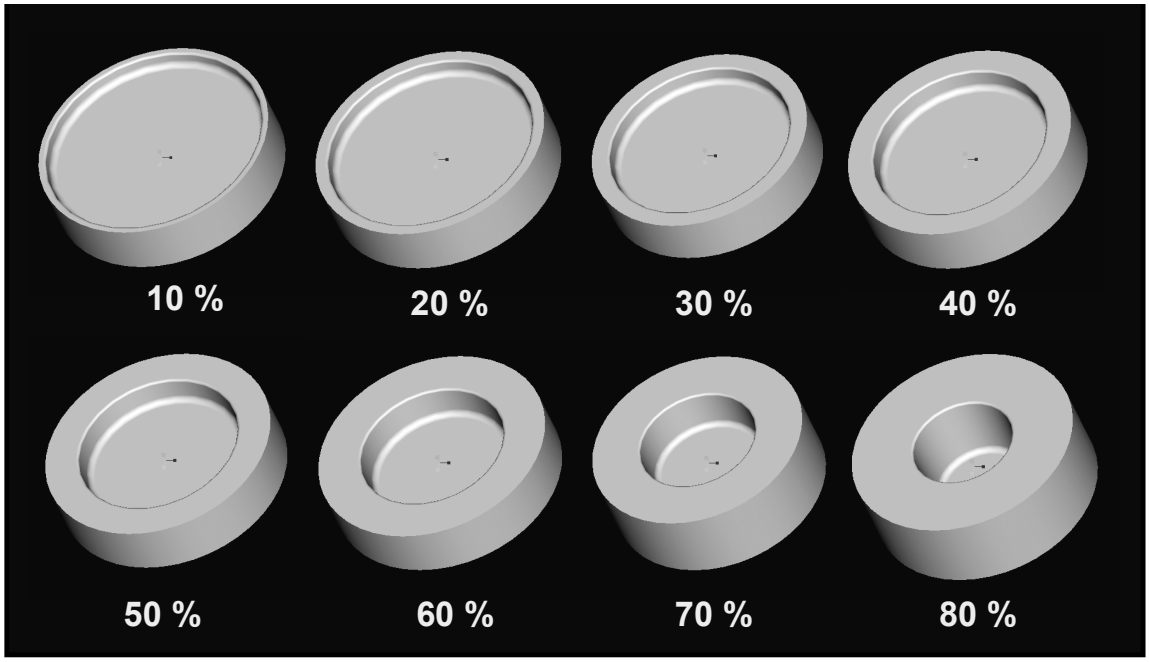

Figure B5-17. Piston Designs for Evaluation of Squish Area Effect on Combustion

Eight different piston designs were simulated, varying squish area from 10 percent to 80 percent. The TDC clearance for all pistons was held constant, at the tightest value possible without piston-to-valve interference. All simulations were run at 1500 rpm, with fixed compression pressures and air-fuel ratios (A/F=25/1). For each piston design simulated, engine spark timing sweeps were conducted. Figures B5-18 and B5-19 show predicted results for engine Indicated Mean Effective Pressure (IMEP) and Knock Index (KI). Note that a knock index greater than unity would indicate excessive knock. Combining the IMEP map with the knock index map yields the optimum piston configuration for the conditions examined. For a 190 psi BMEP baseline target at 1500 rpm, best performance was obtained using a 70 percent squish piston

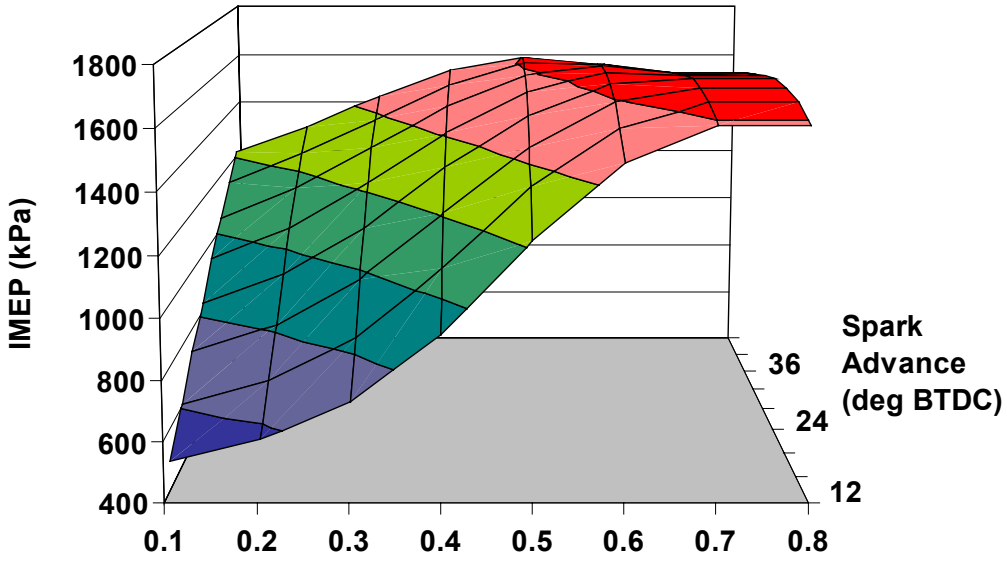

Figure B5-18. IMEP Predictions for Test Piston Designs

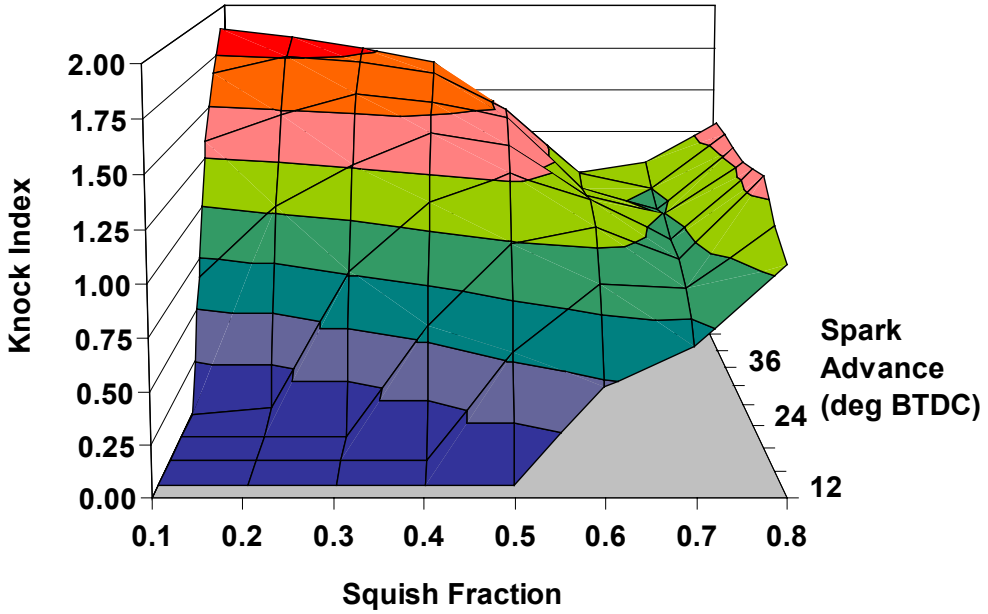

Figure B5-19. Knock Predictions for Test Piston Designs

B5.8 Reverse-Engineering a Combustion Chamber Design from Idealized Heat Release Analysis

As the ARES program progressed, it was decided that increased attention should be directed toward development of a combustion system that could provide high thermal efficiency while also providing reduced NO_x. This shift in focus was made to help evaluate the possibilities for meeting efficiency and NO_x targets in-cylinder, instead of through a combination of combustion system redesign and aftertreatment. An analysis task was initiated that sought to find the ideal mass burn rate profile for a large-bore gas engine and then to perform a subsequent effort that would design a piston and chamber that could produce the required burn rate.

A simple, lumped, single-zone model for the CAT 3501 engine was created. This model would accept idealized burn rate profiles as inputs to the combustion calculations. Outputs for thermodynamic, performance, and emissions variables of interest were generated for a variety of different burn rate profiles. Figures B5-20 through B5-25 show typical inputs and outputs for the single-zone engine simulation. The primary outputs of interest from the modeling tasks were NO_x production and work delivery to the piston. Note that the absolute value of the NO_x prediction is given as an "NO_x indicator". This term represents expected NO_x emissions and can be used for relative comparisons different combustion rate profiles. Similarly, the work delivery to the piston is directly related to IMEP and efficiency of the combustion process, thus allowing relative comparisons of different burn rate profiles for expected changes in engine efficiency.

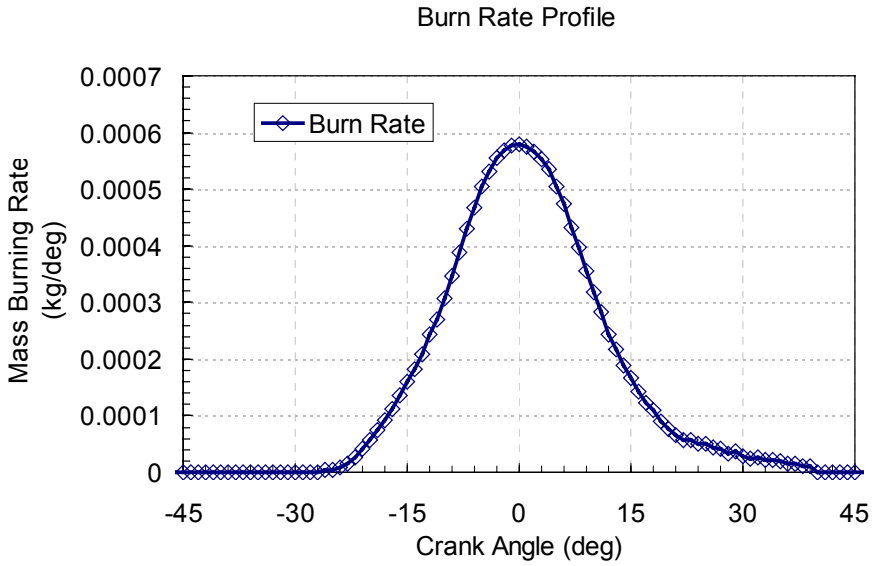

Figure B5-20. User-Supplied Burn Rate Profile

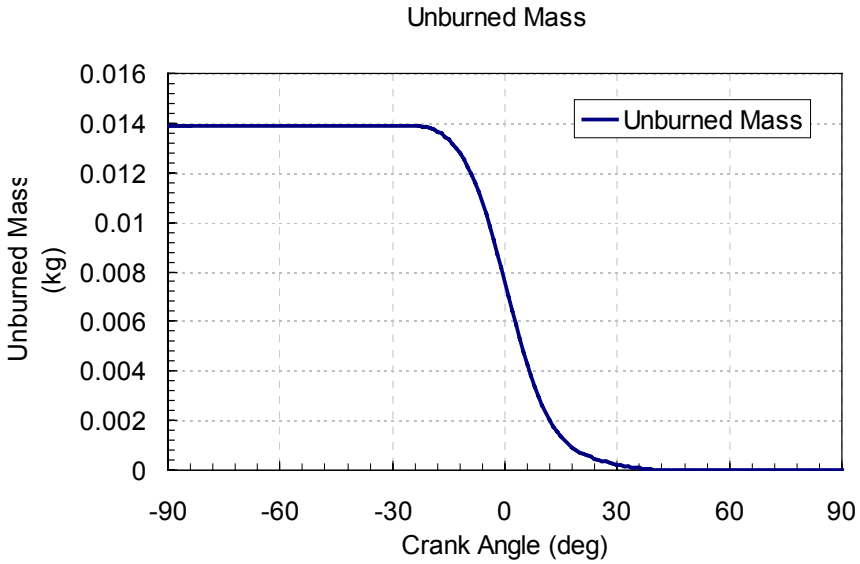

Figure B5-21. Unburned Mass History

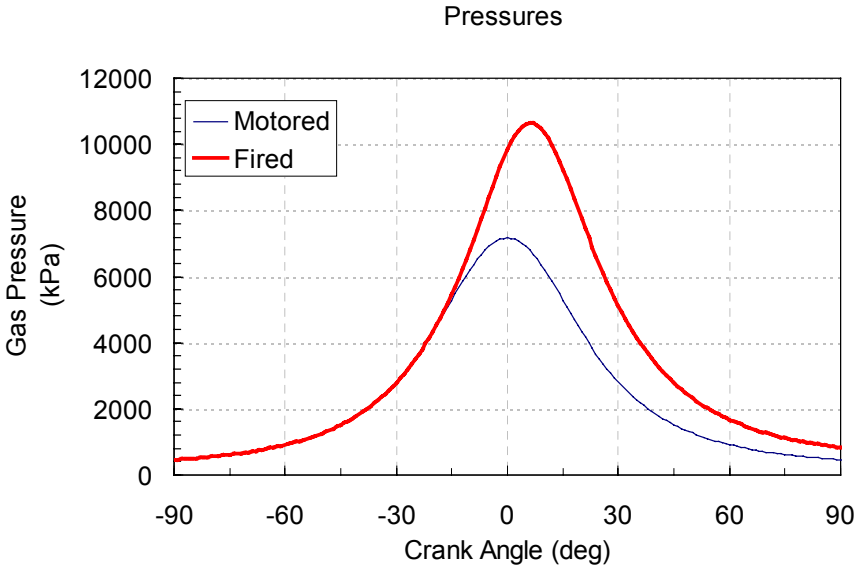

Figure B5-22. Cylinder Pressure History

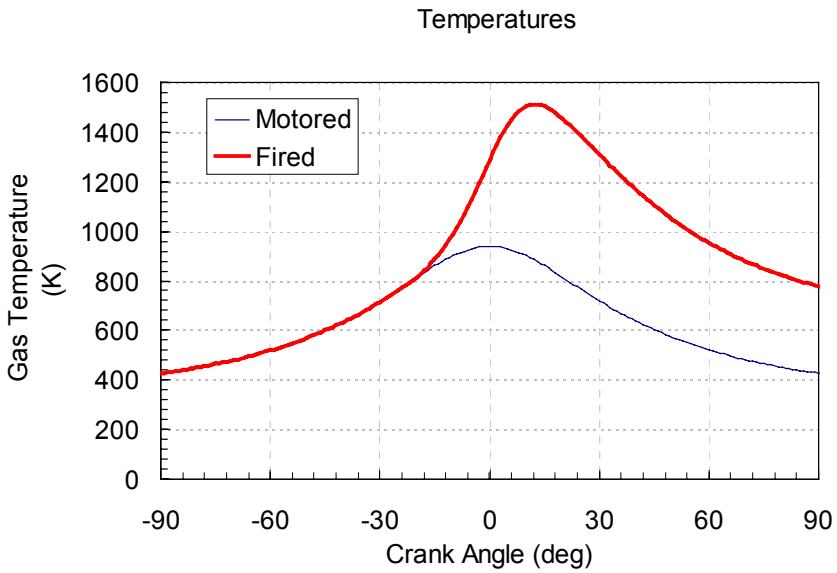

Figure B5-23. Bulk Temperature History

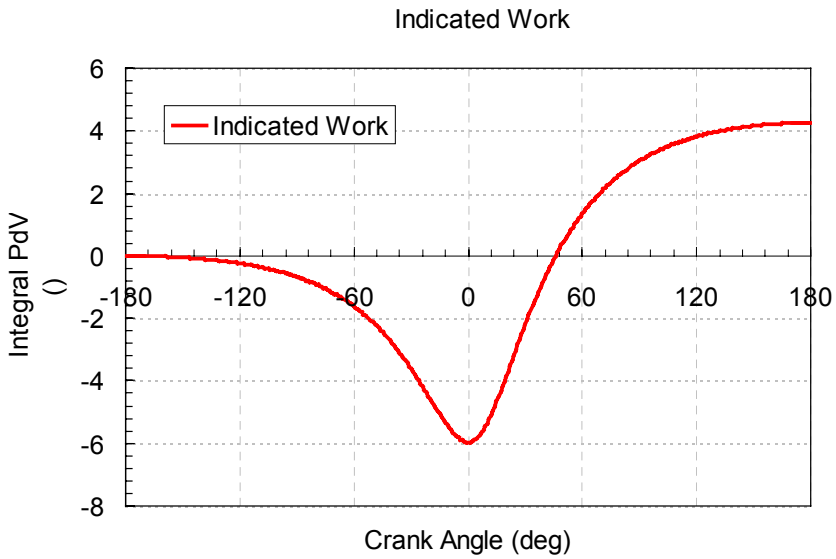

Figure B5-24. Work Delivery to Piston

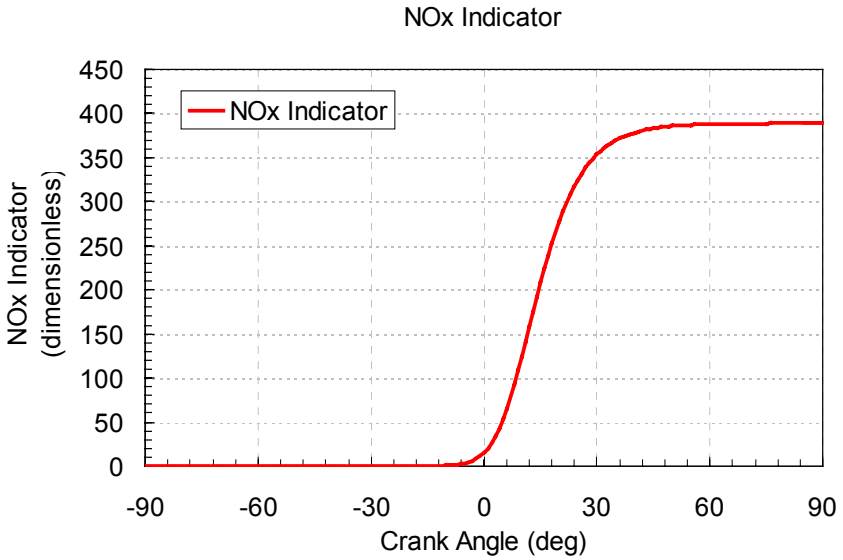

Figure B5-25. Approximate NO_x Emissions

Ultimately, a large number of different idealized burn rates were studied. Figure B5-26 shows an example of six different profiles analyzed. The results of analysis from each individual heat release profile were summarized in a plot of NO_x vs. expected efficiencies to produce an NO_x-Efficiency tradeoff curve, as shown in Figure B5-27. Also shown in the figure is the burn rate profile identifed as the most desirable for low NO_x at highest efficiency. Note also in Figure B5-27 that numerous burn rate profiles produced higher efficiencies than that which was deemed "best". Typically, those burn rates that exhibited high efficiency also had a very fast and extended burn rate, approximating ideal Otto-cycle conditions. For an engine equipped with aftertreatment system, the "best" burn rate may differ from that chosen herein.

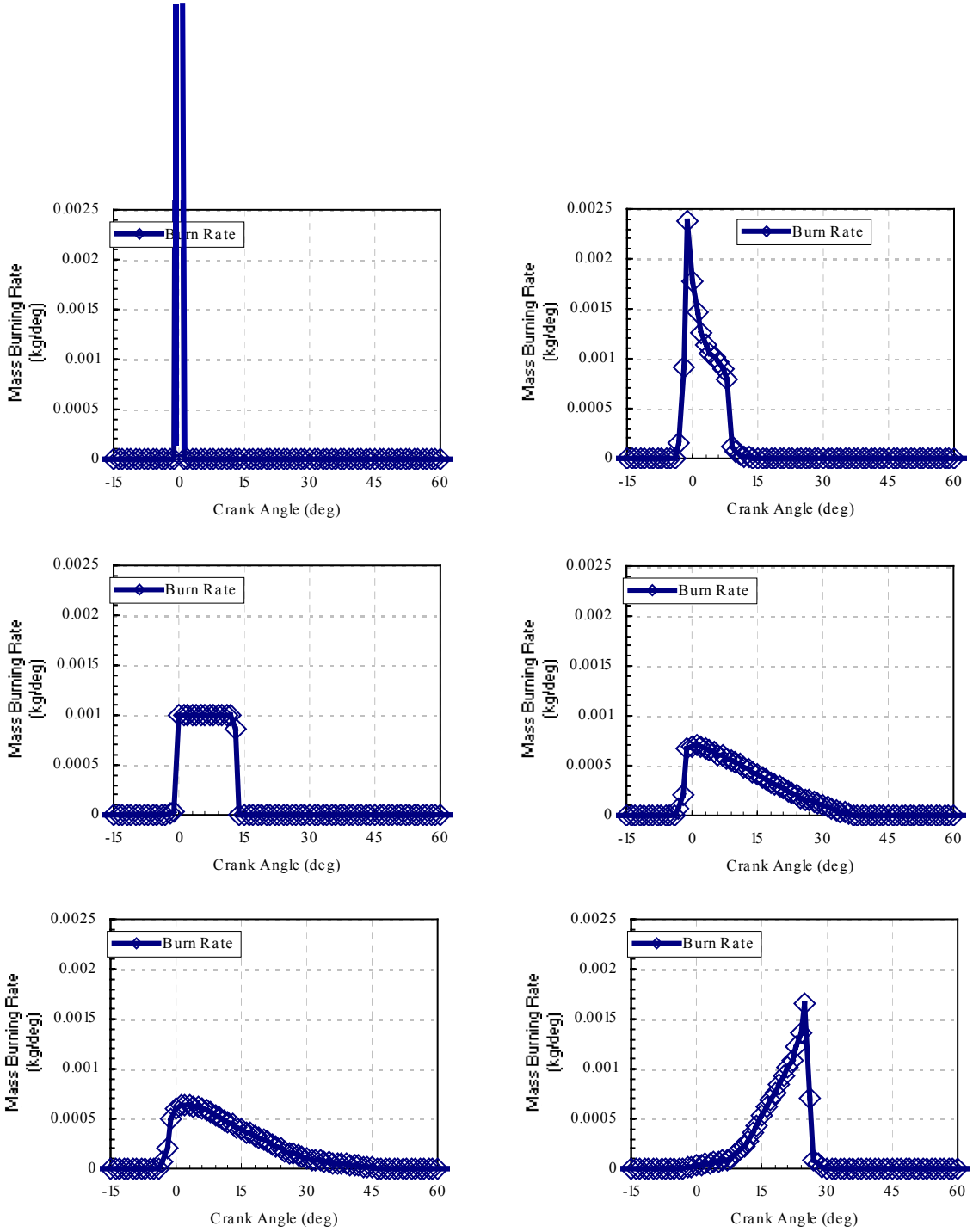

Figure B5-26. Examples of Variety of Burn Rate Profiles Studied

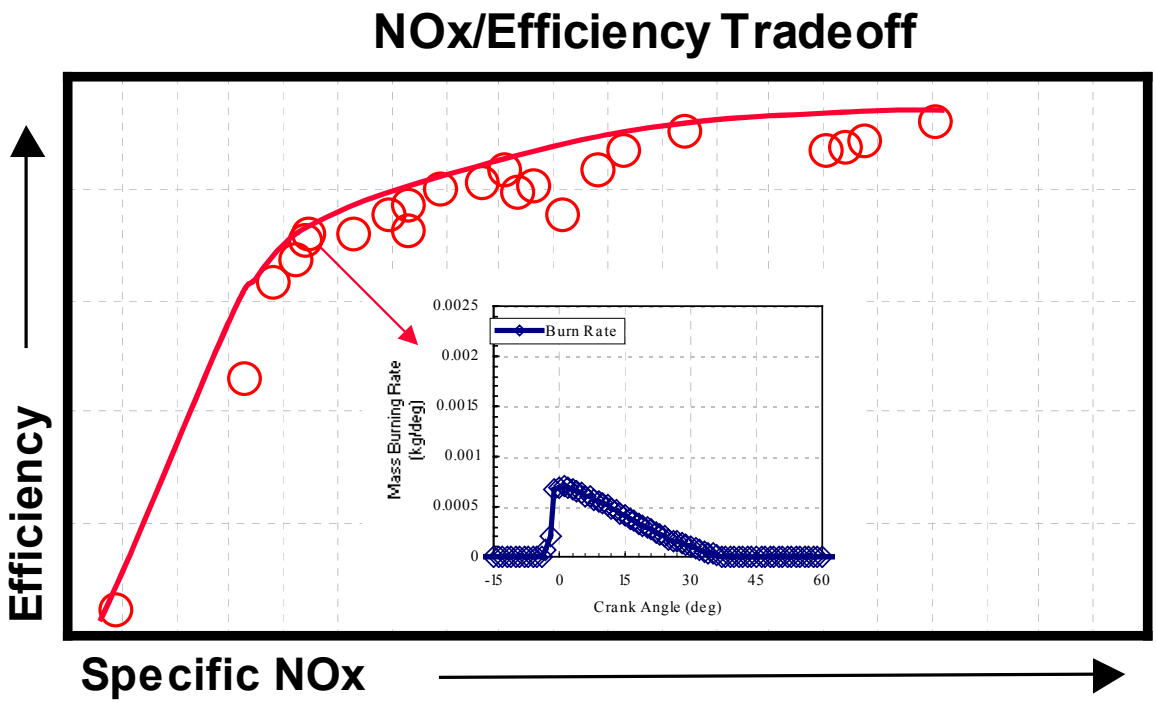

Figure B5-27. Resulting NO_x-Efficiency Tradeoff and Optimal Burn Rate

Upon review of the burn-rate analysis task, it was determined that the "ideal" burn rate exhibited a fast initial burn, followed by a much slower burn-off of the last 60-70% of fuel-air mixture. The question then arose, "how do we design a piston to achieve the desired burn rate?". Review of earlier results from the RPEMS code gave an indication of a possible solution. Figure B5-28 shows an example of the effect of piston bowl design on burn rate. Experimental points for 10 percent, 50 percent, and 90 percent mass burned are included in the figure. The bowl design effect on combustion is as follows:

Just after spark (CAD = 340), the flame propagates nearly spherically, without wall effects. Thus, the flame area exhibits a radius-squared dependence (shown in Figure B5-16 for small flame radii). Later, as the flame truncates against the bowl-bottom (CAD = 356), the flame area exhibits a more linear dependence with flame radius (markers for bowl locations shown in Figure B5-28). As the flame reaches the bowl edge (CAD = 378), the flame area truncates severely, slowing the mass burning rate noticeably. Finally, near the end of combustion, the flame reaches the cylinder edge (CAD = 396) and the flame area truncates to zero, effectively quenching the traditional flame propagation process.

The key to Figure B5-28 is the fact that the piston shape affected the predicted mass burning rate noticeably. Therefore, it was assumed that a piston might be designed to provide the "ideal" burn rate profile recognized in Figure B5-27.

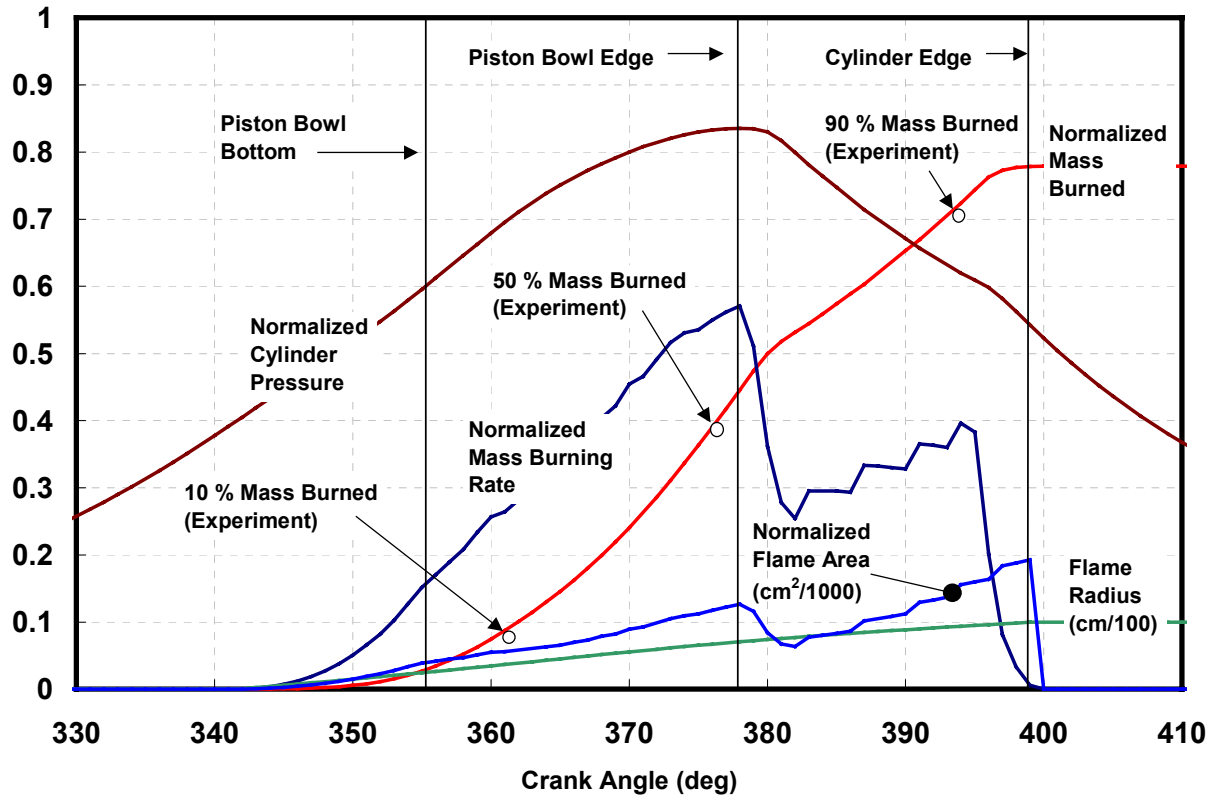

Figure B5-28. Earlier Modeling Results Indicating Relationship Between Piston Shape and Combustion Rate

B5.9 A New, Multichamber Combustion System Concept

Conceptually, it was a simple matter to envision a piston that had the potential to provide the target burn rate. The target burn rate required a high initial burn rate, followed by a controlled heat release. It was assumed that a high squish flow, local to the spark plug would create the fast initial burn. It was recognized that this technique could also lead to poor lean-limit performance if the squish flow tended to "extinguish" the flame kernel in a manner similar to the results generated from previous ARES work utilizing direct water injection and two spark plugs. After initial fast combustion, the combustion chamber would be designed to "slow" the flame through contact with a solid surface. The shape of the solid surface would be designed to allow the flame to propagate in a controlled fashion until all unburned mixture was combusted.

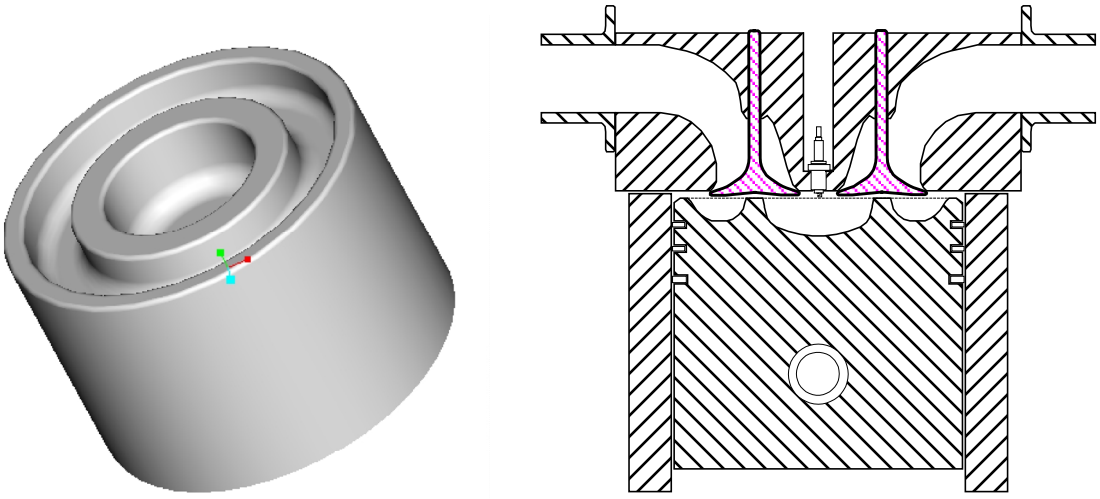

Figure B5-29. Multi-Chamber Concept for Simultaneous Control of Burn Rate and Emissions

Figure B5-29 shows the conceptual piston and chamber design for testing of the flame control methodology. It was decided to attempt full flame control through piston design alone, with no changes to the traditional cylinder head. This decision was made to allow final experimental verification of the design. A second benefit of the proposed piston and chamber design is that the fast spark-ignited, initial burn is separated from the secondary burn through design of the piston. Therefore, the secondary burn should be relatively insensitive to ignition timing and more sensitive to instantaneous piston-to-head clearance. A benefit of this effect is that a large secondary burn can be designed to occur at an ideal crank-angle timing, even if very advanced ignition timing is utilized to ignite the first charge. The proposed piston/chamber design concept, termed "multi-chamber", was disclosed to the clients of the ARES program and a patent is pending. Interested parties should contact SwRI's Engine and Vehicle Research Division for further information.

The basis of the proposed combustion control chamber is to utilize the piston-to-head clearance to "slow" the flame propagation process when cylinder pressures and temperatures reach values that could lead to knock and/or high NO_x. A simple analysis of flame quenching distances for pure methane showed that at standard conditions, stoichiometric methane/air flames quench at pore diameters of approximately 1.8 mm. At elevated temperatures and lean conditions, the flame quenching distance is reduced.

The proposed concept requires that the flame speed be reduced, without total flame quenching. Figure B5-30 shows instantaneous piston-to-head clearance and the crank-angle window in which flame speed reductions may be possible. This window spans nearly fifteen crank angle degrees, for flame quenching distances of 2 mm. Based upon these results, it was decided by the members of the ARES program to pursue the multi-chamber concept further.

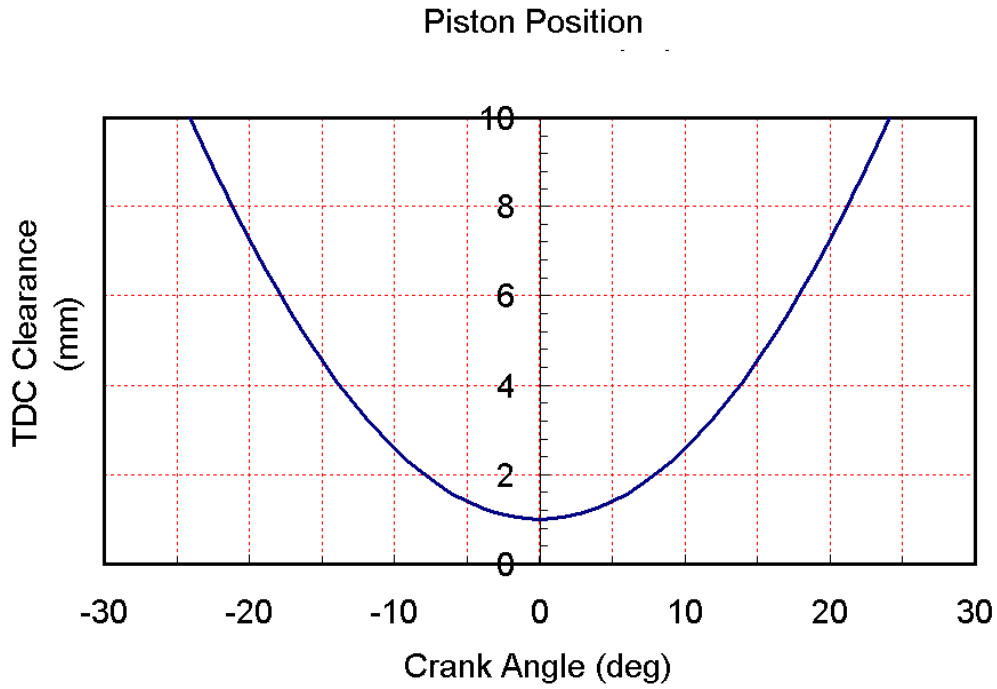

Figure B5-30. Piston-to-Head Clearance for Typical Large-Bore Combustion Chamber

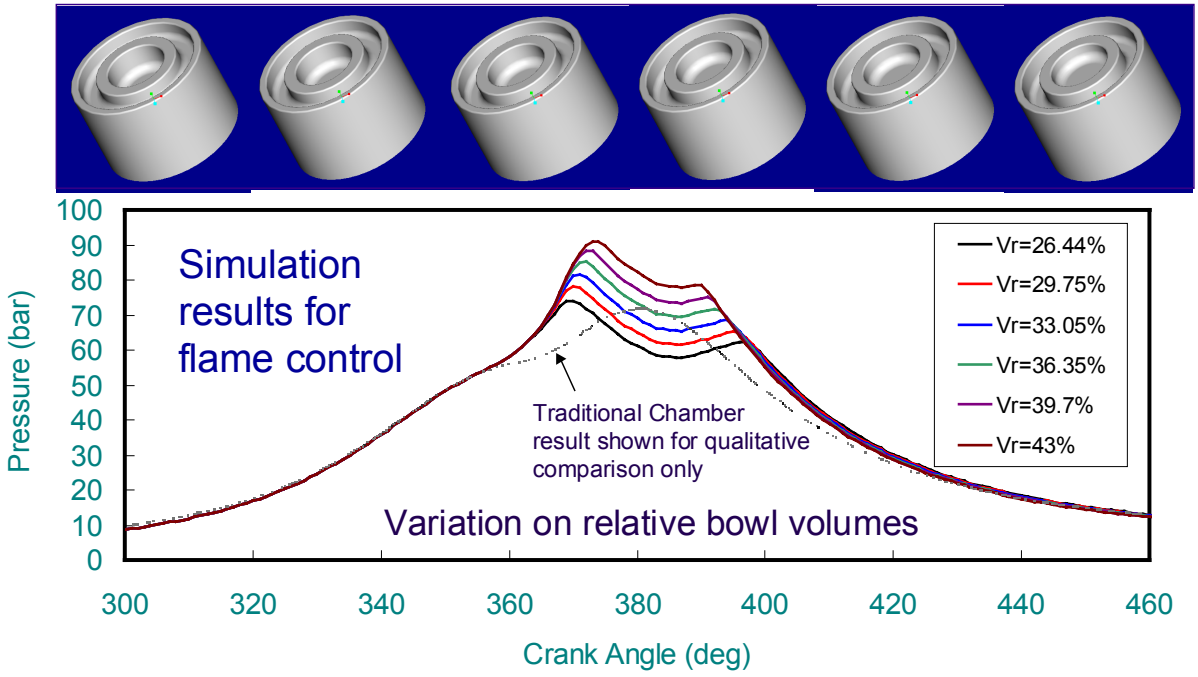

Figure B5-31. Results of Simulations for Proposed Multi-Chamber Concept

Figure B5-31 shows results of simulations for the proposed multi-chamber concept. Simulations were performed for various piston designs, where the volume of the central, primary chamber was varied, while holding the overall chamber volume constant. In Figure B5-31, the relative volumes of the simulated primary chambers are labeled "V_r". Also included in Figure B5-31 is an example of an experimental pressure trace from a conventional combustion chamber, drawing attention to the increased early flame speed and later flame control predicted for the multi-chamber concept.

Figures B5-32 and B5-33 show further predictions of the effect of bowl separation distance and TDC clearance for the multi-chamber concept. As expected, as the physical segregation between chambers is reduced, the flame transitions more easily from one chamber into the next.

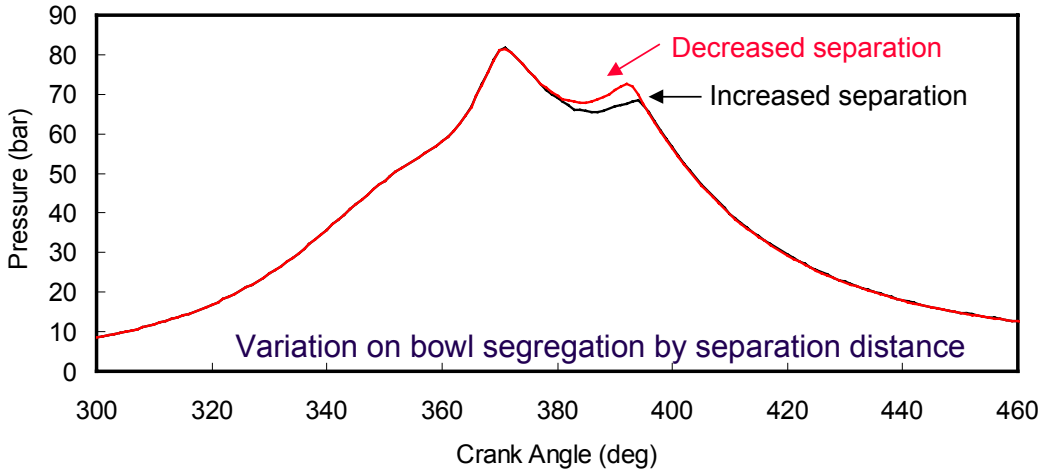

Figure B5-32. Effect of Segregation Barrier Width

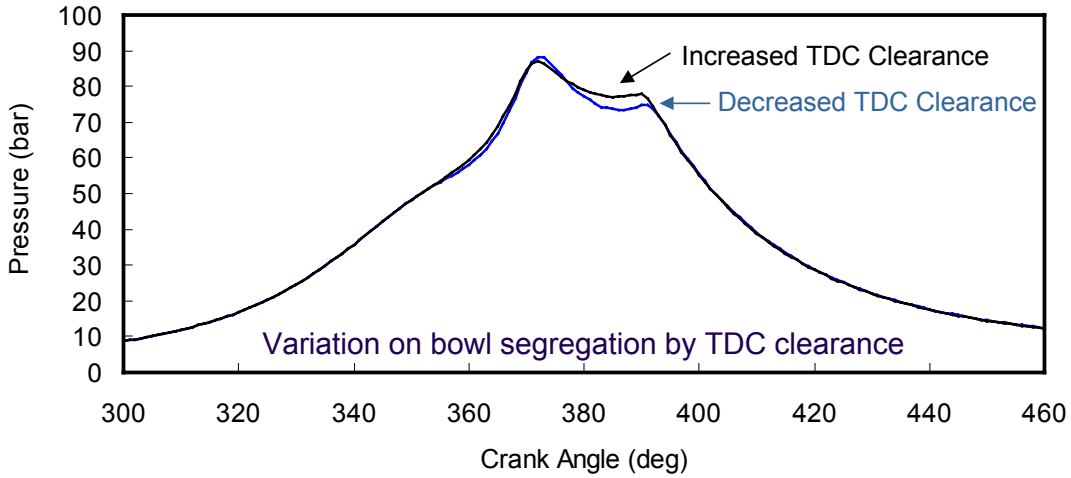

Figure B5-33. Effect of TDC Clearance

B5.10 Initial Experimental Evaluation of the Multichamber Combustion System Concept

Upon completion of the numerical analysis for multichamber combustion concepts, an experimental, proof-of-concept task was proposed to the ARES program members. The proposed experiment utilized a small displacement (~450 cc), single cylinder, side-valve engine. This engine was readily available within the SwRI laboratory, and provided an experimental test bed that could be modified easily for evaluation of the multi-chamber concept. Figure B5-34 shows the SwRI side-valve test engine.

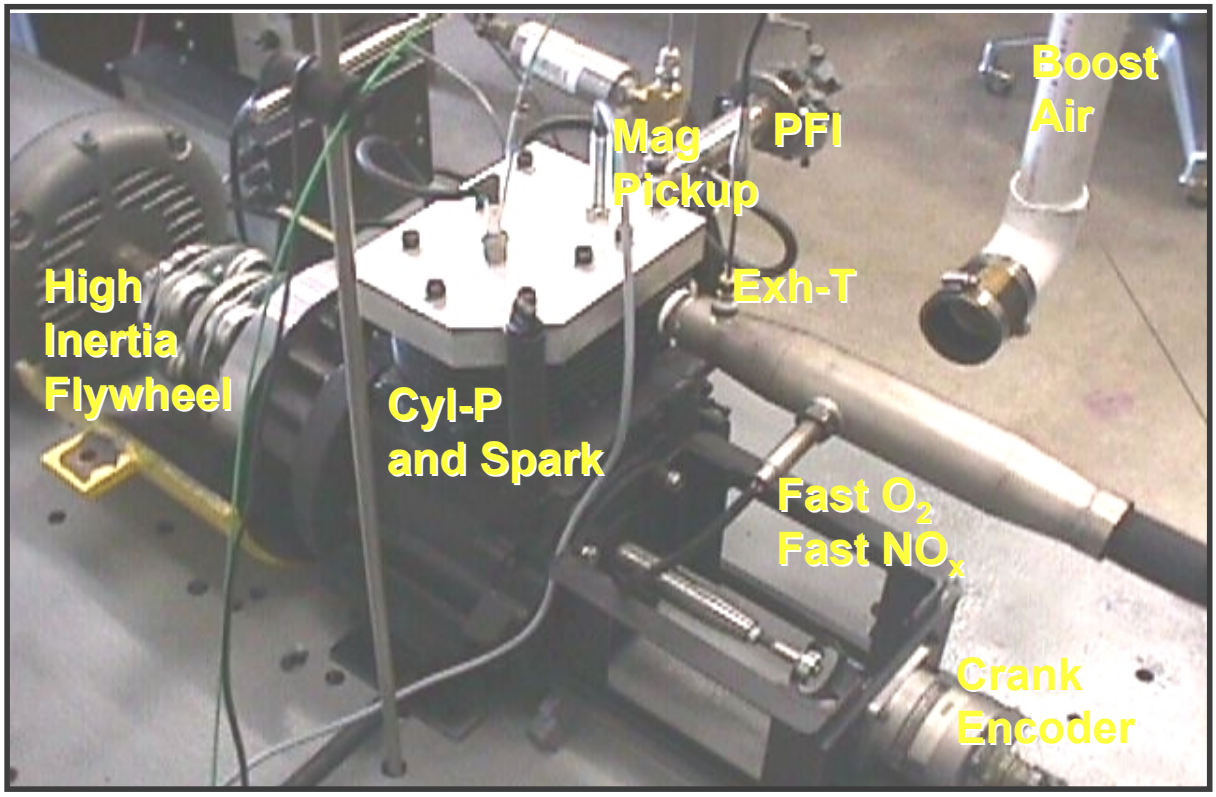

Figure B5-34. Small-Scale Experimental Setup

The side-valve test engine was equipped with a gasoline port fuel-injection system, as well as instrumentation for high speed combustion analysis. The side-valve arrangement of the test engine allowed easy machining of different cylinder heads for testing. Figure B5-35 is a schematic of the piston, cylinder head and valve train layout. Notice in Figure B5-35 that a test design for a multi-chamber combustion system has been included. The segregation space between the two chambers is formed by the distance between the cylinder head and the piston crown. The spark plug was located in the primary chamber (just above the piston), with the secondary chamber located above the valves. Because of the close proximity of the segregation region to the cylinder wall, some engine breathing reduction was expected, thus reducing volumetric efficiency and increasing pumping losses.

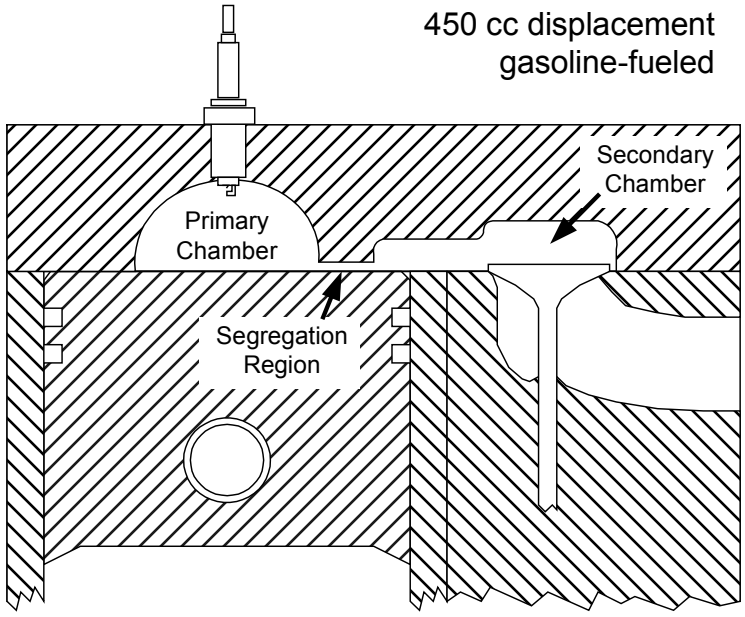

Figure B5-35. Schematic of Small-Scale Experimental Setup

The test plan was to start testing with a combustion system designed to have a very tight segregation region, thus producing the most pronounced flame-wall interaction. Subsequent tests would be made using incrementally larger segregation distances, thus providing incrementally less flame propagation control. Note that the primary goal of this experimental effort was to demonstrate the effectiveness of the proposed flame control technique, not necessarily to optimize engine operation.

Figure B5-36 shows the effect of various chamber segregation designs on combustion pressure. The engine was operated at 1700 rpm and light load. Spark timing, fueling rate and compression pressure were held constant for all runs. A motored engine trace is included for comparison purposes. As hypothesized and predicted numerically, the flame travel in the combustion chamber was affected strongly by the segregation region of the chamber. Early flame growth (before TDC firing) was similar for all test cases, but near TDC, cases with small piston-to-head clearance exhibited slower secondary burn rates than the more open-chamber designs.

Figure B5-37 shows how changes in air-fuel ratio also affect the performance of the segregated or multi-chamber combustion system. As predicted by simple flame quenching arguments, richer mixtures propagated more readily through the flame-quench regions of the multi-chamber system. Therefore, use of this combustion system in a production engine would require that air-fuel ratio effects on flame control be calibrated into the design.

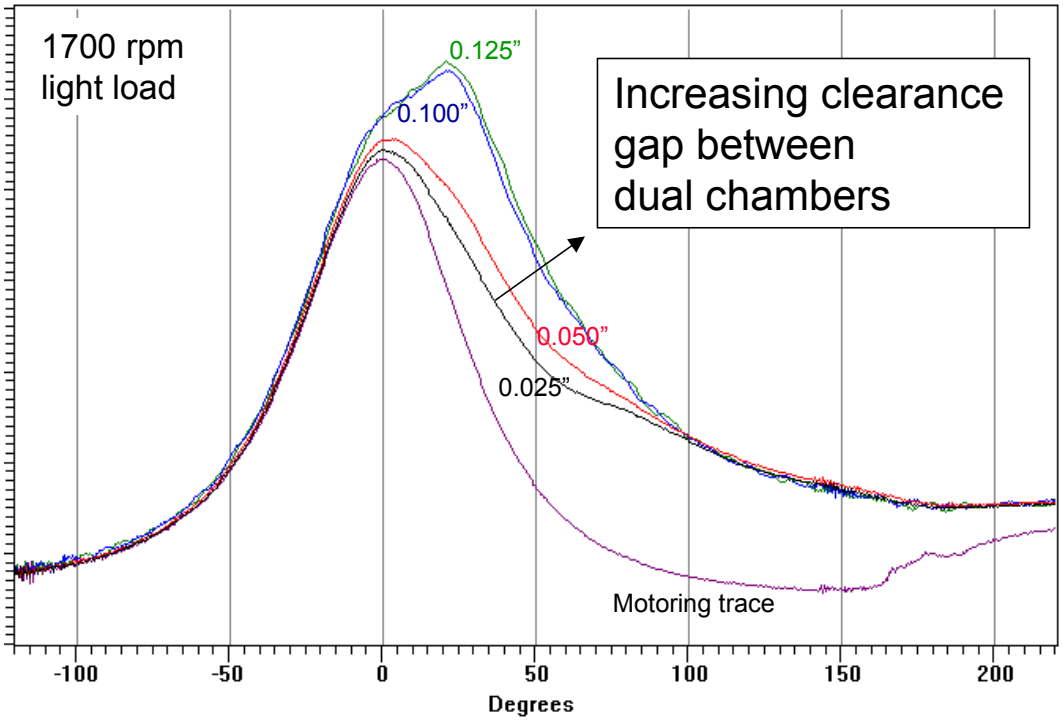

Figure B5-36. Effect of Clearance Gap on Combustion Performance

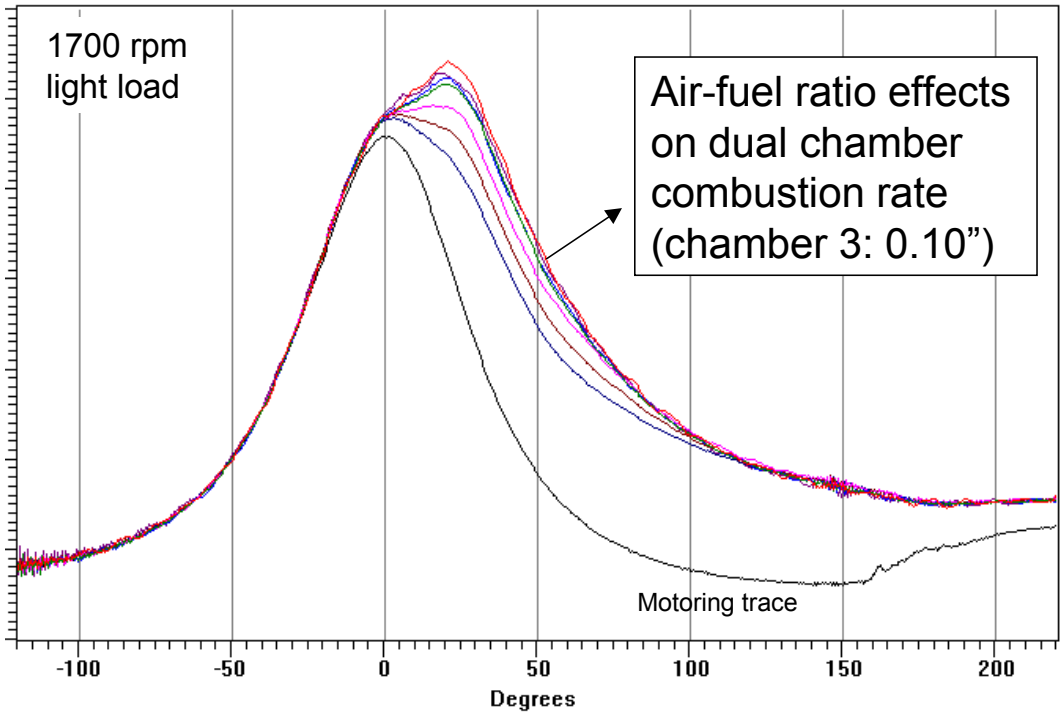

Figure B5-37. Effect of Air-Fuel Ratio in Dual-Chamber Engine

A second effect made available by the multi-chamber design is that location of peak combustion pressure is less sensitive to spark timing than for traditional open-chamber designs. Figure B5-38 shows the relative sensitivity of each chamber type to spark timing. Spark timing was varied from zero to twenty-one degrees before TDC, at high load and 1700 rpm. The traditional single-chamber combustion system exhibited typical behavior, in that peak cylinder pressure location moved toward TDC as spark timing was advanced. The multi-chamber combustion system allowed much more aggressive ignition advance, while maintaining peak pressure locations well to the right of TDC.

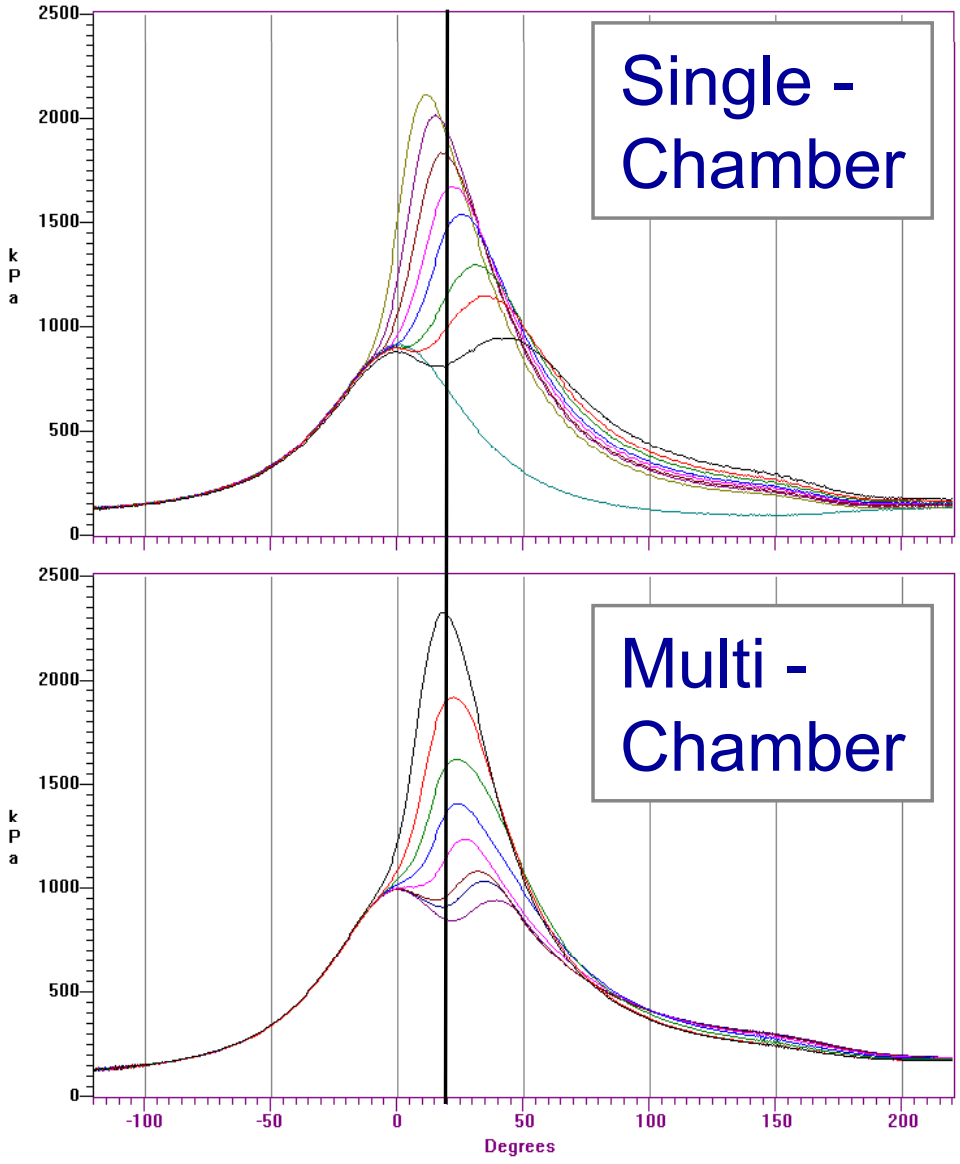

Figure B5-38. Ignition Timing Sensitivities of Traditional, Single-Chamber vs. Dual-Chamber Combustion System

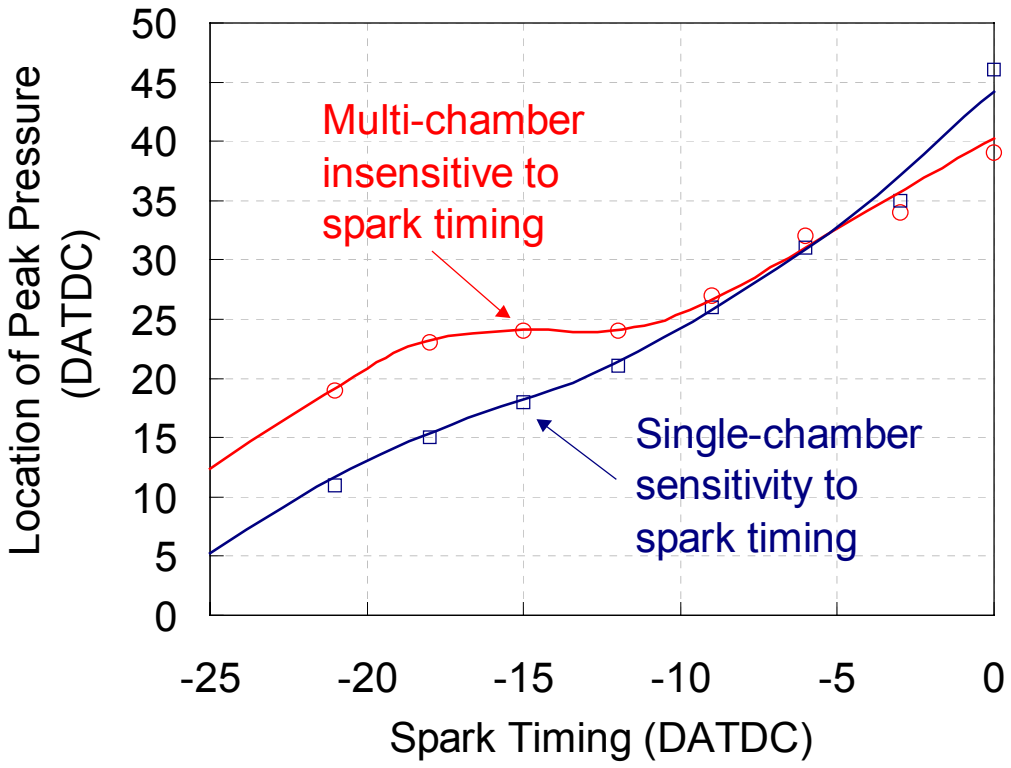

Figure B5-39 Ignition Timing Sensitivity Comparison for Traditional, Single-Chamber vs. Dual-Chamber Combustion System

Figure B5-39 shows location of peak pressure as a function of spark timing for the single- and multi- chamber combustion systems. Note the severe insensitivity of the multichamber system to spark advance between –10 and –20 degrees spark timing. For equivalent locations of peak pressure, the multichamber combustion system allowed up to 10 degrees more spark advance than the traditional combustion system. For boosted, lean-burn or highly-dilute combustion systems, reductions in ignition energy requirements and associated spark plug life could be realized by utilizing a multi-chamber combustion approach with advanced ignition timing.

The results of the side-valve engine tests were successful enough to justify further experimental efforts on a full-scale engine. During testing, it was recognized that burn rate was affected by more than just the chamber geometry. Equivalence ratio, coolant temperature, ambient temperature and other variables affect flame propagation. Hence, a second invention disclosure and patent application were submitted for burn rate management utilizing controlled local coolant temperature and flow rate.

B5.11 Full-Scale Experimental Evaluation of the Multichamber Combustion System Concept

The results from the side-valve experimental evaluation of the multi-chamber combustion concept led to a limited set of experiments utilizing the CAT 3501 single-cylinder test engine at SwRI. Figure B5-40 shows the CAT 3501, as installed at SwRI. This test-bed would allow evaluation of the multi-chamber combustion system's performance in an engine representative of a large-bore, lean-burn, stationary natural gas engine. Figure B5-41 shows a schematic of the test engine layout, including EGR and supplemental boost system.

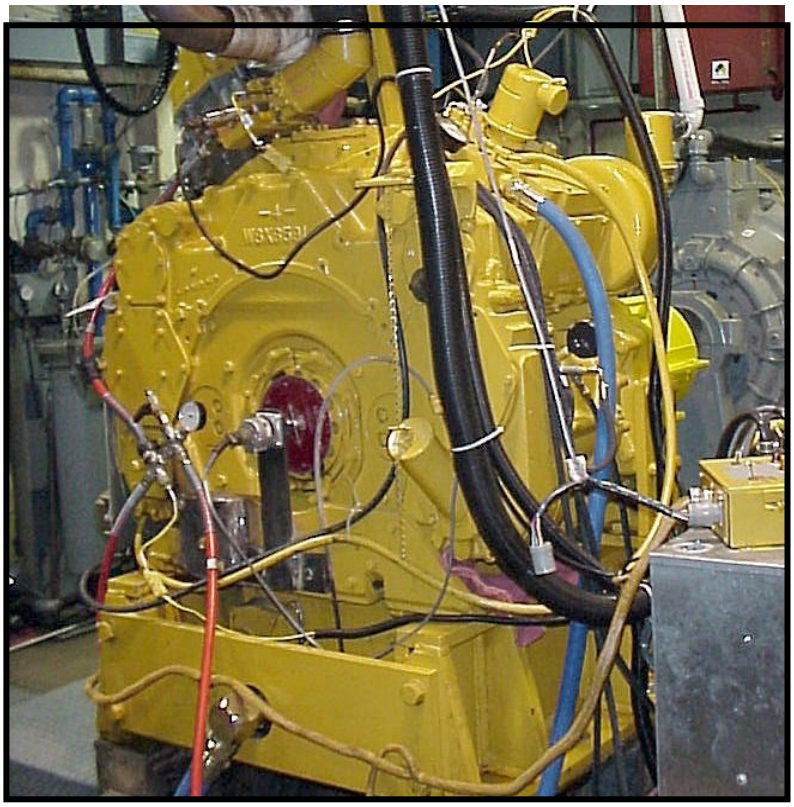

Figure B5-40. CAT 3501 Single-Cylinder, Large-Bore Test Engine at SwRI

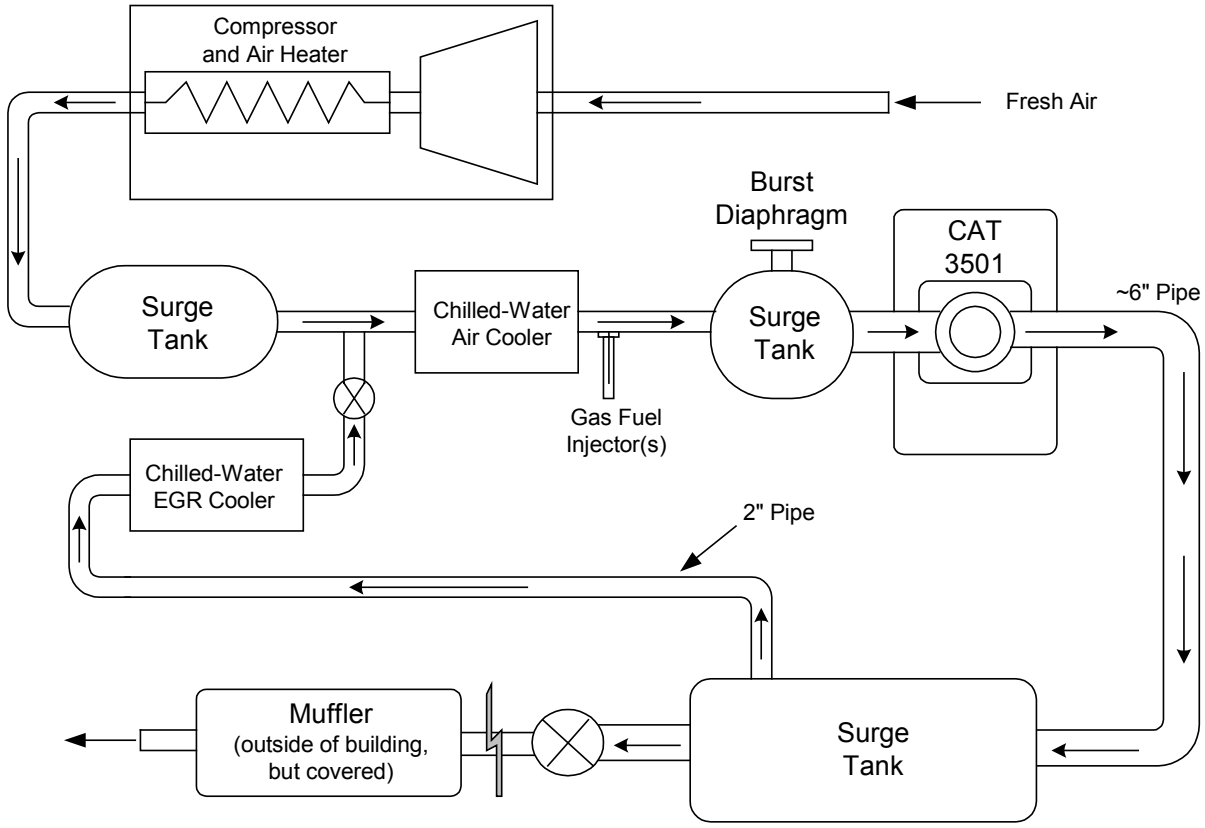

Figure B5-41. Schematic of CAT 3501 Single-Cylinder, Large-Bore Test Engine Setup

Caterpillar supplied piston blanks for build-up of the test combustion system. The test pistons were designed and machined to allow the primary (central) combustion chamber to be removed and replaced with other chambers to evaluate the effect of relative chamber volumes. Figure B5-42 shows the test piston design. Based upon earlier numerical simulations, the original target primary chamber (ignition chamber) volume was approximately 40 percent of the total chamber volume. The original-design primary chamber squish target was approximately 60 percent. Notice in Figure B5-42 the relatively small central chamber (bowl) volume. The production-design of the piston blanks limited the relative volumes of the multi-chamber systems to be tested. Hence, all tests were conducted with primary chamber volumes much smaller than predicted optimal.

Figure B5-43 shows the final machined test piston before installation in the engine. Notice that valve reliefs were necessary to insure safe fully-warm engine operation.

Figure B5-44 shows a post-test image of the multi-chamber piston, after being run in the CAT 3501 test engine. The piston discoloration is primarily due to oxidation of the prototype crown material. No indication of knock or abnormal combustion was apparent.

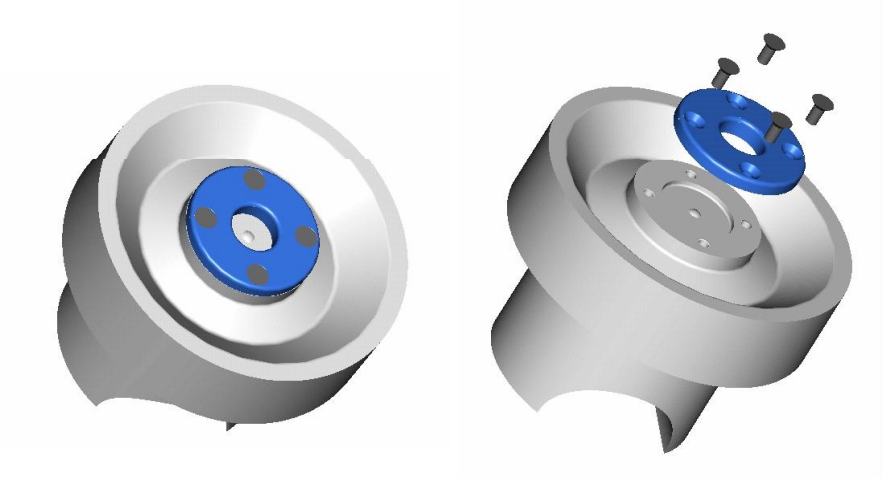

Figure B5-42. Final Piston Design

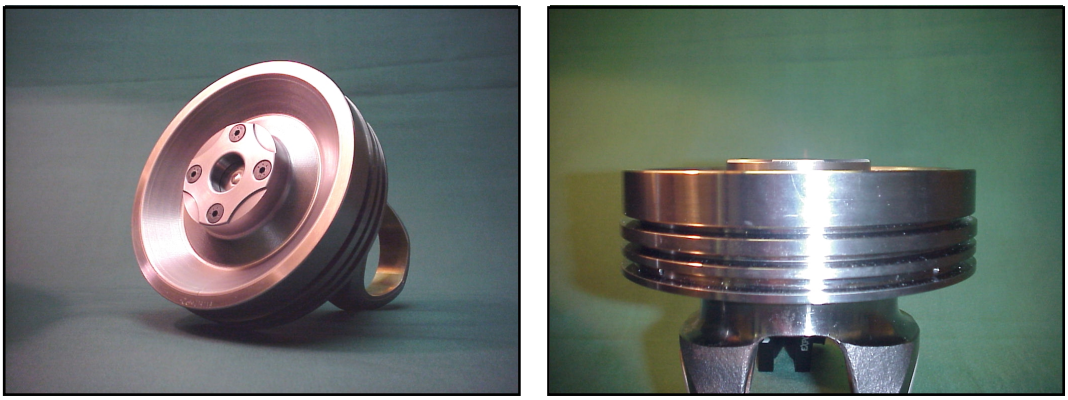

Figure B5-43. Final Version of Machined Test Piston

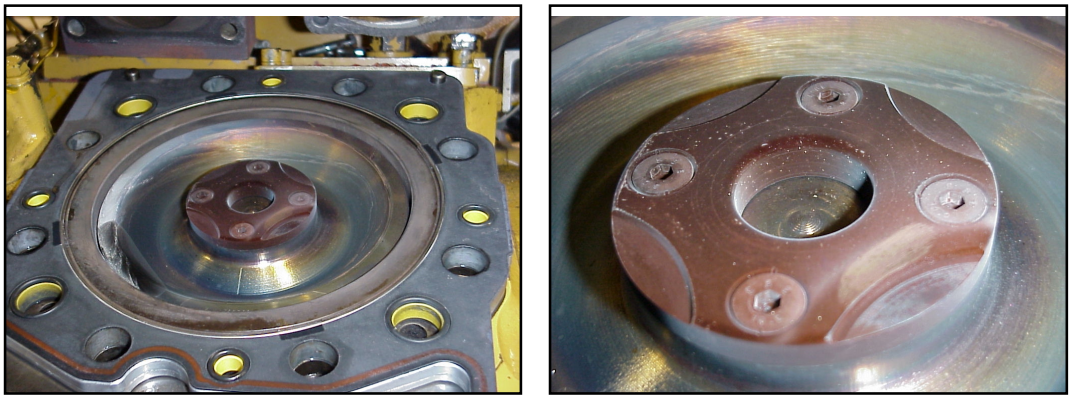

Figure B5-44. Post-Test Images of Prototype Piston

Figure B5-45 shows brake thermal effciency results for the multi-chamber combustion system tests. Included in Figure B5-45 is a result from a traditional open-chamber combustion system. The reduction in brake thermal efficiency from the multi-chamber design is attributable in part to the severely compromised volume of the primary combustion chamber. Recall that the primary chamber volume ranged between 1 percent and 3 percent of the total TDC chamber volume, where numerical predictions indicated that optimal combustion performance would be obtained at much larger primary chamber volumes. The combustion efficiencies for the multi-chamber experiments ranged from 94 percent-96 percent. It is believed that the relative volume and dimensions of the multi-chamber designs tested caused local squish velocities too high to repeatedly ignite lean mixtures. The experimental system could not operate at air-fuel ratios as lean as a conventional combustion system, thus further explaining the low thermal efficiency results. Again, it is believed that a larger primary bowl would have reduced local squish velocities enough to allow leaner engine operation, while simultaneously providing burn rates closer to the target for combined high efficiency and low NO_x.

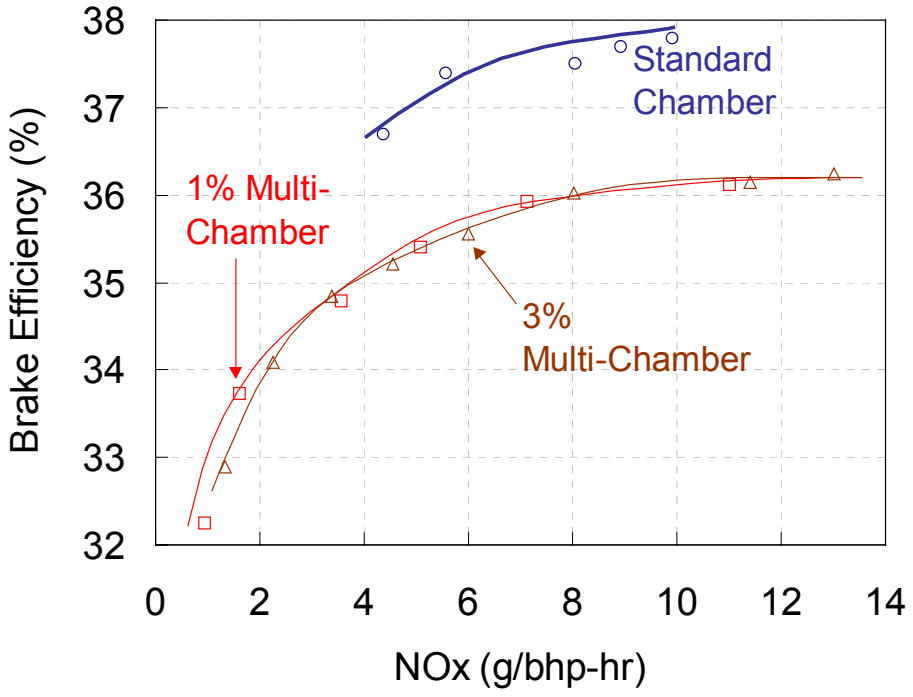

Figure B5-45. BTE Results for Prototype Multi-Chamber Combustion System vs. Traditional Open-Chamber

Figure B5-46 shows the location of peak pressure (LPP) as a function of spark timing for the multi-chamber combustion system versus the traditional, open-chamber system. The expected insensitivity of LPP to spark timing for the multi-chamber concept was not evident in this set of experimental results. However, the expected ability to run more aggressive spark advance for equivalent location of peak pressure was demonstrated. At equivalent LPP, the multi-chamber combustion system allowed over five degrees added ignition advance, thus providing lower ignition pressures and possible extension of spark plug life.

Review of test results for zero to ten percent mass burned (0-10%) indicated that the multi-chamber combustion system exhibited strong insensitivity to spark timing (see Figure B5-47). This result is in contrast to the results indicated by Figure B5-46, where overall combustion (LPP) was compared to spark timing. It is believed that combustion of the gases in the large relative second combustion volume masked the effects produced by the primary combustion chamber and surrounding walls. Figure B5-47 indicates that for a very large range of spark timings, the first ten percent of the available combustion mass was completely insensitive to the time of ignition for the multi-chamber combustion systems tested. In contrast, the traditional open-chamber combustion system showed a very strong influence of spark timing on first ten percent mass burned.

As with the 0-10% burned analysis, a 10-90% burned analysis showed similar results: The expected spark-timing insensitivity of the multi-chamber combustion system was apparent. Figure B5-48 shows that the time for 10-90% combustion was stabilized for spark timings between –20 and –25 CAD.

The results from the multi-chamber tests provided strong evidence that a flame control technique utilizing piston crown design was possible. Although the designs tested were far from predicted-optimums, they did provide proof-of-concept that the flame can be controlled, such that heat release rate can be slowed/or accelerated by piston or head design. It should be noted that the flame control technique suggested in this work utilizes chamber walls as a geometric barrier and/or heat sink to control flame motion. Therefore, thermal loading of the piston and chamber may increase.

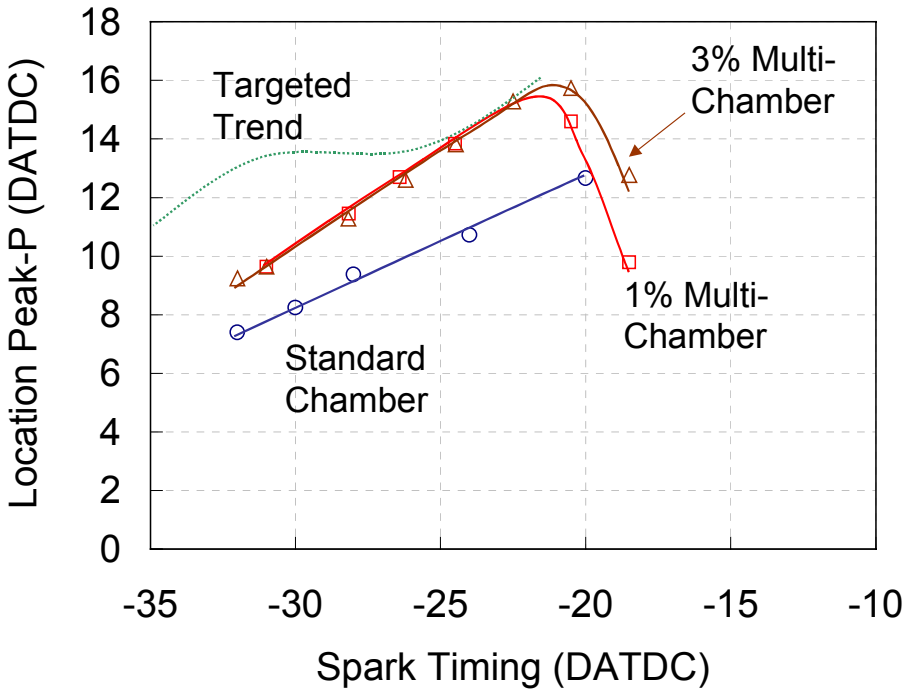

Figure B5-46. Location of Peak Pressure (LPP) Results for Prototype Multi-Chamber Combustion System vs. Traditional Open-Chamber

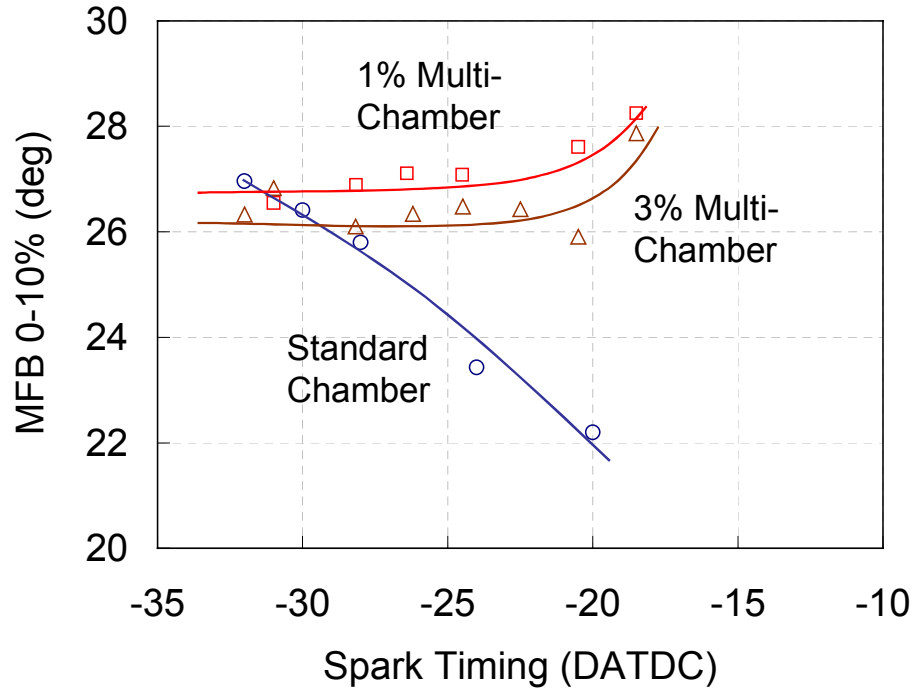

Figure B5-47. 0-10% Mass Fraction Burned Results for Prototype Multi-Chamber Combustion System vs. Traditional Open-Chamber

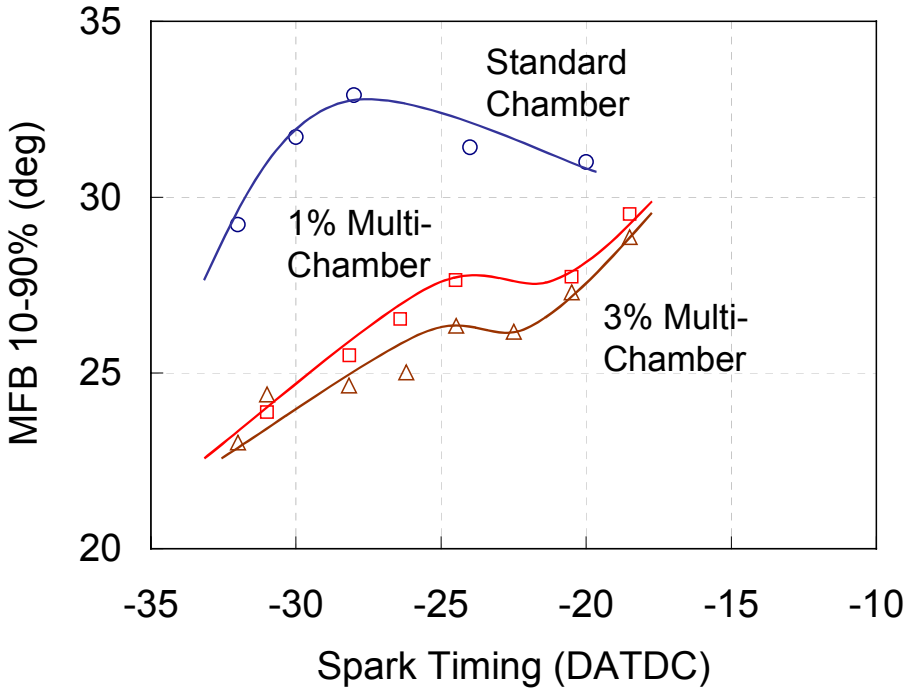

Figure B5-48. 10-90% Mass Fraction Burned Results for Prototype Multi-Chamber Combustion System vs. Traditional Open-Chamber

B5.11.1 Multi-Chamber System Summary

This section presented validations and results from a series of simulations and experiments conducted to evaluate use of an engine model to assist in development of traditional combustion systems. A methodology was developed and utilized in which various piston parameters can be evaluated in regard to performance, knock and emissions.

A second set of tasks were completed to provide proof-of-concept testing for a novel new combustion system design. The design was based upon a multi-chamber combustion concept in which the piston and head were used to create segregated combustion regions that could exhibit quite different combustion characteristics. Additionally, the segregation between the chambers only exists near TDC, when primary combustion occurs. It was demonstrated that partial segregation of the combustion chambers provided the ability to utilize advanced ignition timing. Additionally, the new combustion concept provided a combustion event that was largely insensitive to spark timing. Initial results showed that the multi-chamber designs tested produced lower overall efficiencies than conventional open-chamber combustion systems. However, design limitations imposed by the current test pistons were the probable cause of the efficiency reductions. Future tests with more optimal piston designs would be expected to perform closer to, if not better than, current open-chamber systems.

B6.0 SUMMARY

The objective of this project was to provide recommendations toward optimum knock mitigation strategies and combustion chamber designs for future large-bore, high BMEP natural gas engines. The goal was accomplished through use of a Southwest Research Institute cycle-simulation package, the SwRI Rapid Prototyping Engine Modeling System (RPEMS).

A multi-zone engine model was implemented for the studies performed on this project. The detail of the chemical kinetic calculations is specified by the user and can range from phenomenological correlations to detailed kinetics. Additionally, the model predicts the effects of combustion chamber geometry, ignition location, turbulence level, mixture composition and previous cycle history. An autoignition model for natural gas mixtures was used to predict the onset and severity of knock for various combustion chamber designs.

The project was initiated with algorithm development and coding to add multiple ignition sites to the RPEMS model. Specifically, a subroutine library was developed for simulating flame growth, convection and truncation within a multidimensional combustion chamber. Multiple, interacting flame zones are possible within the framework of this model. Validation efforts were performed for the multiple flame zone model in which its predictions were compared to results obtained from simple, ideal analytic solutions for spherical flame growth. The results from these tests showed that the geometric modeling method used for this study could accurately represent complex geometries and multiple flames.

A literature survey was conducted to identify available natural gas chemical kinetic mechanisms with the potential to be used for knock predictions. The most noteworthy of the mechanisms identified was the GRI v2.11 mechanism, developed originally for high temperature combustion within gas turbine engines. It was shown that large discrepancies in low-temperature kinetic predictions existed between available natural gas mechanisms, leading to a high degree of uncertainty in knock predictions derived from their combination with a suitable engine model. Hence, it was decided that an initial effort would be performed to edit the GRI v2.11 mechanism, adding reactions necessary to more accurately predict low-temperature, knock reactions. Reaction steps were added for low-temperature pyrolysis and oxidation of methane, ethane and propane. Results from this effort showed that extension of the GRI v2.11 mechanism allowed it to be “tuned” to match experimental knock measurements. Once “tuned”, the mechanism was used with the RPEMS code to explore the knock tendencies of various bowl-in-piston combustion chamber designs. Results from this effort led to recommendations for an optimal bowl-in-piston combustion chamber design.

An additional effort was performed to assess the knock mitigation potential of a novel, multiple spark plug combustion chamber design. The new chamber utilizes piston-induced squish and distributed combustion zones to increase the overall mass burning

rate, thus improving the knock characteristics of the engine. Initial modeling studies indicated that a potential increase in knock-limited IMEP (at equivalent squish levels) of approximately ten percent could be afforded by the new chamber design.

The RPEMS package was extended to allow studies of pre-chamber combustion systems. This task was accomplished by utilizing the multiple ignition-site routines tested previously. The pre-chamber was modeled as a separate combustion system, attached to the main chamber by a parallel system of orifices. Each orifice acted to direct a modeled plume of burned gases into the main combustion chamber. The characteristics of the flame plume were assigned through a variety of fluid-dynamic sub-models.

A second task was conducted to extend the RPEMS package to allow studies of pre-chamber combustion systems. This task was accomplished by utilizing the multiple ignition-site routines tested previously. The pre-chamber was modeled as a separate combustion system, attached to the main chamber by a parallel system of orifices. Each orifice acted to direct a modeled plume of burned gases into the main combustion chamber. The characteristics of the flame plume were assigned through a variety of fluid-dynamic sub-models. Initial results were presented as proof-of-concept of the method. No further work was conducted toward prechamber combustion system development, as experimental evaluation of the model would be required and no experimental prechamber task was conducted.

The ARES program began a third task with a numerical analysis of the effects of bowl design and squish on combustion rate. More specifically, the bowl radius and Top-Dead-Center (TDC) clearance were varied to create different levels of squish, allowing the resultant combustion rate to be compared to basic combustion chamber design parameters. The results of this work showed that for typical engine operating conditions, combustion rate was directly related to squish velocity, but that the fundamental source of the squish velocity was unimportant. Hence, bowl radius and TDC clearance traded-off against each other equally.

A subsequent numerical study to determine optimal knock-limited squish-area was conducted. Here, eight different piston designs were simulated, at various load conditions. Each piston differed in piston bowl design, yielding pistons that exhibited squish that varied from very low to very high. Spark timing sweeps were simulated at constant fuel rate for each speed and boost level, so that maximum knock limited IMEP could be predicted. The results of this effort showed that for conventional combustion systems, operating near 200 psi BMEP and 1500 rpm, the optimal squish area was approximately 70 percent.

Another task conducted as part of the ARES program utilized a simplified version of the RPEMS package to “reverse-engineer” the combustion system design problem. Parametric studies of a large number of heat release profiles were analyzed to identify the optimal heat release pattern for highest engine efficiency at best engine-out NO_x. After identification of an optimal heat release profile, a follow-on task was initiated to design a combustion system that could provide the targeted heat release rates. This analysis

concluded that the optimal heat release rate could be provided by a new multi-chamber combustion system, for which a patent application was prepared.

Experimental tests of the multi-chamber combustion system were conducted utilizing a small, 450 cc, gasoline, side-valve engine. This test apparatus was used only to provide proof-of-concept for the multi-chamber combustion system. Results of this effort showed that the multi-chamber combustion system could control the heat release rate as required by the original concept. Further, the multi-chamber combustion system was insensitive to spark timing over a large spark-timing window. Hence, the multi-chamber system allowed very aggressive spark advance to be utilized without the occurrence of knock. This result indicated that the multi-chamber concept could be used to allow aggressive spark timing for high BMEP engines, thus extending spark plug life. The results of this effort led to an extended experimental program, utilizing the CAT 3501, single cylinder gas engine.

The multi-chamber CAT 3501 tests used a custom machined piston with a removable upper-crown. The removable portion of the piston contained the central, or primary combustion bowl, while the outer region of the piston acted as the secondary combustion chamber. The piston blanks used for prototyping the multi-chamber concept limited the relative volumes of each bowl such that the central bowl was much smaller than the optimal size that previous numerical studies had predicted. It was decided that limited experiments should be conducted anyway, and two removable primary combustion bowls were tested. The first had a relative bowl volume of 1 percent, while the second had a relative bowl volume of 3 percent. The results of the experiments showed that even with severely non-optimal bowl volumes, the multi-chamber concept still provided the ability to operate the engine with more spark advance. However, the highest engine efficiencies measured with the multi-chamber combustion system were well below those measured previously for a traditional open-chamber combustion system. It is believed that much of the efficiency difference is due to the non-optimal bowl volumes used for this study. Future tests of this concept should utilize piston blanks that allow more range in the relative bowl volumes tested.

B7.0 REFERENCES

1. C.T. Bowman, Hanson, Davidson, Gardiner, Lissianski, G.P. Smith, Golden, M., Frenklach, Goldenberg, GRI Mech. V.
2. Poulos, S.G. (1982), "The Effect of Combustion Chamber Geometry on SI Engine Combustion Rates - A Modeling Study", M.S. Thesis, Department of Mechanical Engineering, MIT.
3. Poulos, S.G., and J.B. Heywood (1983), "The Effect of Chamber Shape on Spark Ignition Engine Combustion", SAE Paper 830334.
4. Gouldin, F.C. (1987), "An Application of Fractals to Modeling Premixed Turbulent Flames", Combustion and Flame. v68(3). 249-266.
5. Chin, Y.W. (1991), "Fractals and Combustion in Spark Ignition Engines", Ph.D. Dissertation, Department of Mechanical Engineering, The University of Texas, Austin, TX.
6. Woschni, G. (1967), "A Universally Applicable Equation for the Instantaneous Heat Transfer Coefficient in the Internal Combustion Engine", SAE Paper 670931.

C. EVALUATION OF TECHNOLOGIES FOR ACHIEVING HIGH BMEP LEVELS IN NATURAL GAS ENGINES

EXECUTIVE SUMMARY

Achieving high brake thermal efficiencies for natural gas engines will require knock free engine operation at high power levels. The Miller cycle, in which the compression and expansion ratios differ, offers a method of extending the knock free operational range of natural gas engines. Other combustion concepts for igniting lean mixtures or producing fast combustion rates may also extend the operational range.

The objective of the High BMEP Engine Development task was to experimentally determine the effectiveness of various methods in extending the knock-limit in a large-bore, natural gas-fueled engine. An additional objective was to evaluate engine combustion concepts to achieve higher BMEP levels with less susceptibility to knock than current engines.

A Caterpillar G3501, a single-cylinder research engine loaned to SwRI by Caterpillar, was installed and used as a test engine for this project. Various combustion concepts were evaluated to obtain knock free operation at high BMEP levels.

The Miller cycle was utilized to reduce the effective compression ratio and in-cylinder temperatures reducing the knock tendency and NO_x formation. Special camshafts were designed to achieve the desired effective compression ratios. Pistons with different bowl volumes were designed and procured to achieve the desired expansion ratios. Evaluation of the Miller cycle involved the testing of combinations of compression ratio and expansion ratio. These configurations allowed a comparison of the effects of increasing expansion factor (expansion ratio) with constant compression ratio.

Implementation of the Miller cycle resulted in an increase in BTE at a constant NO_x level. Increasing the expansion ratio also resulted in an increase in BTE however, due to higher in-cylinder pressures, the level of BMEP that could be obtained without knock or exceeding the peak cylinder pressure was reduced. Various combustion concepts were evaluated for high BMEP operation. This testing was limited by the peak cylinder pressure limitations of the test pistons. Interrelationships between peak cylinder pressure, BMEP, combustion phasing, and expansion ratio make it difficult to analyze the acquired data. Lean burn and stoichiometric with EGR concepts were evaluated with single-site spark ignition and multiple-site ignition concepts. One Micro-pilot, stoichiometric-EGR concept was able to achieve 350 psi IMEP.

C1.0 BACKGROUND

The Miller cycle has been used in the past to mitigate knock in natural gas engines. This cycle is an over-expanded engine cycle, where the compression ratio is lower than the expansion ratio by altering timing of the intake valve closing event. Reducing the compression ratio will reduce the compression temperatures and reduce the tendency to knock. In the typical Otto Cycle, the compression ratio and expansion ratios are the same. In the Miller cycle, the actual (or effective) compression ratio is reduced from the expansion ratio by either early intake valve closing (before BDC) or late intake valve closing (after BDC). Technical literature suggests that the late intake valve closing (LIVC) strategy is better than early intake valve closing (EIVC) strategy, due to improved trapping efficiency and reduced pumping losses[1]. The lower effective cylinder volume creates a reduced effective compression ratio. The ratio of the expansion ratio to the effective compression ratio is termed the expansion factor.

In the period between BDC and LIVC timing, some of the fresh charge admitted into the cylinder during the induction stroke is pushed back into the inlet manifold and the trapped mass is reduced. To increase the trapped mass to maintain the original engine power output, the inlet manifold pressure must be increased. A simple theoretical analysis of two cycles with the same expansion ratio of 12:1, but different effective compression ratios of 12:1 and 8:1, was performed to illustrate the requirements and benefits of the Miller cycle. A 70 percent increase in manifold absolute pressure (MAP) was required to achieve the same peak compression pressure. Although the peak compression pressures are the same, the compression temperature for the Miller cycle case was approximately 80 K less. This reduced compression temperature should reduce the tendency to knock and allow for an increase in the knock-limited BMEP.

The lower peak compression temperatures would likely allow operation at a higher BMEP and allow some improvement in thermal efficiency. Additional gains in thermal efficiency may be realized by increasing the expansion ratio and gaining additional useful work from the increased expansion.

Maintaining constant expansion ratio and reducing the compression ratio as described above is the typical method for implementing the Miller cycle. However, since efficiency is a function of expansion ratio, ideally one would want to maintain the effective compression ratio at the knock limit and increase the expansion ratio.

C2.0 OBJECTIVE

The objective of the High BMEP Engine Development task was to experimentally determine the effectiveness of various methods in extending the knock-limit in a large-bore, natural gas-fueled engine. An additional objective was to evaluate engine combustion concepts to achieve higher BMEP levels less susceptible to knock than current engines.

C3.0 TECHNICAL APPROACH

The following text provides detailed discussions of engine selection, test plan development, and design/procurement of required hardware.

C3.1 Research Engine Selection

A single cylinder engine representative of stationary gas engines was required for experimentation for ease and cost effectiveness of evaluating various technologies. A single-cylinder Caterpillar G3501 engine was loaned to this program by Caterpillar and installed in a test cell at SwRI for performing these experiments.

The Caterpillar G3501 engine is actually a V-twin design with one cylinder disabled. The piston and connecting rod were removed from one bank and a bob-weight was installed on the crank throw to provide counter-balance. The engine was not entirely balanced, however, and requires an inertia block and bedplate for mounting. Specialized components for this engine include the crankshaft, camshaft, cylinder block, front housings, and balancers. Major components that are in common with the multi-cylinder engine are the cylinder head, liner, piston, and connecting rods. Ratings for the spark-ignited natural gas version of the 3500 series engine are 50.5 kW (67.7 hp) per cylinder at 1200 rpm and 11.7 bar (170 psi) maximum BMEP[2]. The 3500 series engine has a bore of 170 mm and stroke of 190 mm, giving a displacement of 4.3 liters per cylinder.

C3.2 Research Engine Experimental Setup

The Caterpillar G3501 engine was installed into a test cell specifically configured for operation of a single-cylinder, medium speed engine. A photograph of the G3501 engine installed at SwRI is shown in Figure C3-1.

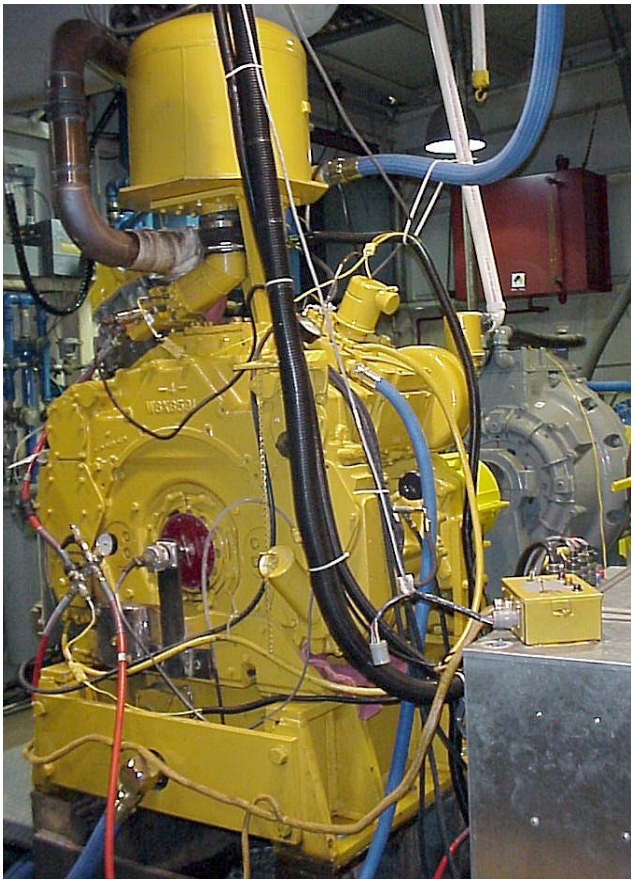

Figure C3-1. Caterpillar G3501 Engine Installed at SwRI

The air handling and exhaust systems allow for simulation of a turbocharger at a wide range of efficiencies. Simulated turbocharger efficiency was calculated using ideal gas relationships and measured boost pressure, exhaust temperature, and exhaust backpressure. Testing at a given turbocharger efficiency was accomplished by altering the exhaust backpressure to achieve the desired efficiency with the measured boost pressure and exhaust temperature.

Fuel composition of the pipeline natural gas fuel was measured by a gas chromatograph and linked directly with the data acquisition system to provide the constituent volumetric percentages, heating value, and stoichiometric fuel-air ratio. An analysis was conducted on the mean pipeline gas composition available in San Antonio (calculated from daily measurements over one year) and was compared to the 90th percentile gas composition. The ARES target gas composition was based on 90th percentile methane and compositional distribution of the published national mean natural gas[3]. Since the average gas composition at SwRI was very close to the ARES target composition, it was decided to use pipeline gas for the majority of tests.

An electronic port fuel injection system was installed on the G3501 engine. This injection system featured two pulse-width modulated fuel solenoid valves, connected in parallel to a spray bar installed in the inlet manifold where it mates to the cylinder head.

An electronic control module and PC interface were provided with a speed-governor control strategy (i.e. closed-loop on engine speed).

Exhaust emissions were measured to provide concentrations of the five gases (NO_x, CO, THC, CO_2, and O_2), from which the brake specific emissions and actual fuel-air equivalence ratio were calculated. Mass airflow was derived from the measured fuel flow and calculated fuel-air equivalence ratio. An NGK universal exhaust gas oxygen (UEGO) sensor was installed in the exhaust system to provide the fuel-air equivalence ratio when exhaust emissions were not being acquired.

Crank angle based data acquisition was performed with a DSP Technologies combustion analyzer. This analyzer acquired cylinder pressure and various other signals at a resolution of one-half crank angle degree (720 measurements per revolution). The software performed calculations of indicated performance and burn rates in real time over a specified range of engine cycles. Specific operating conditions were typically set using the real time calculations and, once set, average and statistical data were acquired over a 100-cycle range. This analyzer was particularly useful for determining the knock-limited BMEP.

C3.3 Experimental Test Plan

The experimental test plan was to conduct an evaluation of an alternative engine cycle (Miller cycle) and perform evaluations of alternative spark ignition systems. However, to ensure proper setup and control of the G3501 engine, a comparison test was performed first to confirm performance and emissions of the engine matched to that recorded at Caterpillar.

C3.3.1 Comparison Testing

Caterpillar provided data acquired at 1500 rpm for comparison to data acquired by SwRI. This data set featured ignition timing and air-fuel ratio sweeps, which ranged from misfire to knock. Several of the data points were repeated with the same conditions, while other conditions near that set by Caterpillar were tested.

C3.3.2 Miller Cycle Test Plan

Development of the Miller cycle test plan was guided by the modeling work performed in the Technical Path Evaluation task. Results from the modeling showed that the expansion ratio must be significantly higher than the original configuration to achieve the target thermal efficiency. However, to reduce the tendency to knock with the Miller cycle alone, the effective compression ratio would likely need to be less than the original configuration. This led to a decision to decrease the effective compression ratio from the original 12:1 to 10:1 and test with increasing expansion ratios. Three expansion factors of 1.0, 1.3, and 1.5 were selected for evaluation. A 9:1 effective compression ratio was also added to the test plan. Table C3-1 shows the configurations selected for evaluation on the G3501engine. The configuration in the first row of Table C3-1 is the stock

configuration as the engine was delivered. The remaining configurations required different pistons and/or camshaft profiles, which are described in detail in the following sections of the report.

Table C3-1. Miller Cycle Test Plan

Expansion Factor	Expansion Ratio	Effective Compression Ratio
1.0	12.0	12.0
1.0	10.0	10.0
1.3	13.0	10.0
1.5	15.0	10.0
1.5	13.5	9.0

C3.3.3 Piston Design – Expansion Ratio

The expansion ratio is a function of the clearance volume at TDC. The clearance volume is the combustion chamber volume (piston bowl) plus the crevice volume. Therefore, the piston bowl volume must be altered to achieve the expansion ratios given in Table C3-1. Special 'blank' pistons were procured from Caterpillar for obtaining the desired bowl volumes. Cross-sectional drawings of the stock and blank pistons are given in Figure C3-2 for reference.

These pistons were machined to achieve the required bowl volumes by altering the depth of the combustion bowl. The bowl diameter and piston-to-head distance of the stock piston was maintained in all pistons (crevice volume remained stock). The constant bowl diameters gave all pistons a constant squish area.

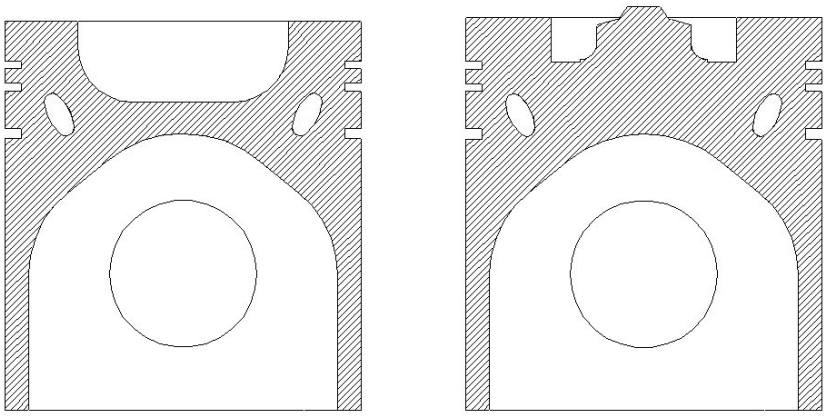

Figure C3-2. Cross-Sectional Drawings of Stock and Blank Pistons

C3.3.4 Camshaft Design – Compression Ratio

To achieve the effective compression ratios given in Table C3-1, new camshafts were designed and procured. Variable valve timing (VVT) systems were initially investigated, but were deemed too expensive with too long of a lead-time for use on this project. Caterpillar provided dimensional drawings of the G3501 camshaft upon which new designs were based. All dimensions and specifications of the original design were maintained, except for the intake valve closing (IVC) timing. Calculations of the intake closing angle for each of the expansion ratios were performed.

C3.3.5 High-BMEP Engine Concepts

Various engine concepts were evaluated for the ability to achieve high engine power densities or BMEP. These concepts were micro-pilot ignition with different combustion chamber designs, multiple-site spark ignition, lean burn and stoichiometric with exhaust gas recirculation.

C3.4 Experimental Procedures

C3.4.1 Knock Determination

Knock can be measured with accelerometers mounted on the engine block or determined via a filtered cylinder pressure signal. A knock sensor was not practical on the Caterpillar G3501 engine due to excessive mechanical noise that caused false signals in an accelerometer. The excessive mechanical noise was generated through unloaded gears, the counterbalance shaft, and various attachments on this engine. Therefore, knock was measured via the cylinder pressure signal. The DSP features two knock indicators based on a filtered cylinder pressure waveform. These two knock indicators were configured for the G3501 engine and monitored in the real-time calculation mode when operating the engine. A threshold value of 1.5 bar Knock Peak was set after several empirical tests performed on the engine. This value represented a mild but consistent knocking condition.

C3.4.2 Determination of Knock Limited Spark Timing and Knock Limited BMEP

The experimental procedure involved sweeps of the spark timing and fuel-air equivalence ratio at given load steps to determine the knock-limited BMEP for each engine configuration. Since the engine controller performed speed control, the dynamometer controller maintained a constant load and tests were performed over constant load steps. Closed loop control of the air-fuel ratio was not a feature of the engine control system, therefore MAP was altered to change the fuel-air equivalence ratio. As a result, the test procedure involved sweeps of spark timing from a timing retarded from MBT to a knocking condition in 4° intervals at given MAP and engine load. The MAP was then changed and spark timing sweeps were repeated. These sweeps occurred between approximately 0.60 and 0.70 equivalence ratios. Spark advance was limited to 40° BTDC by the ignition control software.

Upon completion of each test at a specific load, a linear knock-limit curve was then fit to the knocking test points. Efficiency at each test point was then compared to the knock-limit curve. Engine load was increased until the maximum efficiency corresponded with the knock-limit curve thus defining the knock-limited BMEP. Testing at successively higher load points, until reaching the knock-limited BMEP, was performed with each engine configuration.

C4.0 RESULTS AND DISCUSSION

The first test performed was a repeat of conditions tested by Caterpillar to allow comparison of the data obtained by each entity. The second test was an evaluation of the Miller cycle for increased knock-limited BMEP and efficiency.

C4.1 Comparison Testing

Data provided by Caterpillar on the G3501 engine included performance and emissions data at an engine speed of 1500 rpm. After completing the installation and debugging of the G3501 engine in a test cell at SwRI, several data points were repeated to ensure the engine, engine controls, and data acquisition systems were operating properly. The data agreed well with that provided by Caterpillar.

C4.2 Miller Cycle Evaluation

Evaluation of the Miller cycle began with detailed testing of the original engine configuration described in the first row of Table C3-1 (expansion ratio of 12:1 and expansion factor of 1.0). The configurations given in Table C3-1 with a 10:1 effective compression ratio were all subsequently tested. The configuration with a 9:1 effective compression ratio was not evaluated due to schedule constraints. Testing of the various configurations involved sweeps of inlet manifold pressure and ignition (spark) timing at increasing loads until knock-limited BMEP was achieved. The knock-limited BMEP was defined as the load where peak BTE occurred at the knock-limit.

Several variables were held constant throughout testing to minimize the number of test points, while still allowing direct comparison of the various configurations. These variables included the following:

- Engine speed = 1800 rpm
- Inlet air temperature = 54.5°C (130°F)
- Simulated turbocharger efficiency = 64 percent
- Inlet air relative humidity ~5-percent

The simulated turbocharger efficiency value was used to determine the exhaust back pressure at each test point based on measured inlet manifold pressure, air-fuel ratio, and exhaust temperature. Engine operating limits were dictated by the average peak cylinder pressure and exhaust temperature.

C4.2.1 Comparison of Motoring P-V Diagrams

At the beginning of tests for each configuration of expansion ratio and expansion factor, motoring tests were performed. The maximum engine speed for which the G3501 engine could be motored was 950 rpm. These motoring tests were performed to check the actual effective compression ratios and were performed with a constant boost pressure and temperature, but with zero exhaust back pressure.

The G3501 engine could not be motored at the test speed of 1800 rpm, so data from several firing runs with similar MAP were compared. As the engine speed was increased from 950 to 1800 rpm, the peak compression pressure became higher for the Miller cycle compared to the conventional cycle. Less air was displaced between BDC and IVC at the higher engine speed, causing pressure to build in this portion of the stroke at a faster rate and creating the higher peak compression pressures. Thus, peak compression temperatures were expected to be even higher for the Miller cycle at the higher engine speed and the tendency to knock greater as a result.

C4.2.2 Knock-Limited Spark Timing

As mentioned previously, knock was determined in testing when an average knock peak value of 1.5 bar occurred. An average knock peak value of 1.5 bar corresponded to a mild but consistent knocking condition. Obtaining an exact value of 1.5 bar for the knock peak was difficult due to the quick response of the engine control system in adjusting the fueling rate to maintain an engine speed of 1800 rpm. The modulation of the fueling rate became worse under lean air-fuel ratio conditions at the knock-limit due to significant differences in the instantaneous engine speed between a knocking cycle and a non-knocking cycle. Therefore, a knock peak range of 1.3 to 1.7 bar was accepted for the knocking condition.

Linear interpolation, or extrapolation, was used to account for deviations in the recorded knock peak values at each MAP setting. Efficiency was recorded at each test point and compared to the knock-limit curve. Testing was repeated at successively higher loads until the maximum BTE corresponded with the knock-limit curve for that particular load. Similar data were recorded for all engine configurations at all loads tested.

C4.2.3 Knock-Limited BMEP and Efficiency

The maximum observed efficiency for each configuration at each load tested was compared to evaluate benefits of the Miller cycle. With each configuration, the efficiency increased as the BMEP was increased due to improved mechanical efficiency. However, the decreased knock-limited spark timing with increasing expansion factor, correlated with a decreased knock-limited BMEP. A graph of the maximum observed efficiency points for this evaluation is shown in Figure C4-1. The curves of BTE versus BMEP for each configuration show the expected trend of increasing efficiency with increasing load. For the conventional cycle (solid symbols), lowering the compression ratio from 12:1 to 10:1 allowed an increase in knock-limited BMEP, but at a reduced efficiency. The Miller cycle configurations (open symbols) exhibited successively reduced knock-limited BMEP with increasing expansion factor. In Figure C4-1, a dashed line has been drawn through the knock-limited BMEP points of the three configurations with an effective compression ratio of 10:1 to illustrate the Miller cycle trend. Although the knock-limited BMEP was reduced with the Miller cycle at constant effective compression ratio, the efficiency was increased with increasing expansion factor. An increased efficiency with increasing expansion factor at a given BMEP indicates the

benefit of increasing the expansion ratio. Pumping losses also decreased with increased expansion factor adding to the improved efficiency.

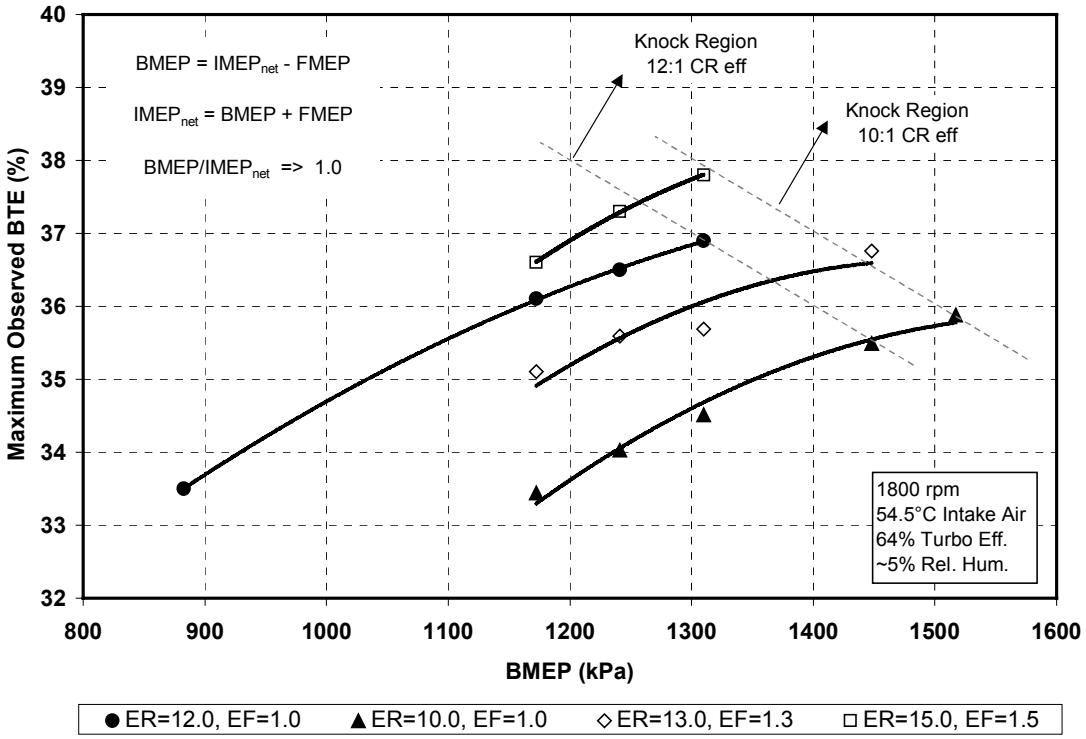

Figure C4-1. Maximum Efficiency Versus BMEP for all Engine Configurations

Peak efficiency data for each configuration at 1310 kPa BMEP is plotted versus expansion factor in Figure C4-2. The efficiency is improved with the Miller cycle when compared to a conventional cycle with the same effective compression ratio and at the same engine load. The efficiency improvement by going from a 1.0 to a 1.5 expansion factor, with a constant effective compression ratio of 10:1 at 1310 kPa BMEP, is approximately 9.5 percent (~3.3 BTE percentage points). The increase in the knock-limited BTE is slightly less.

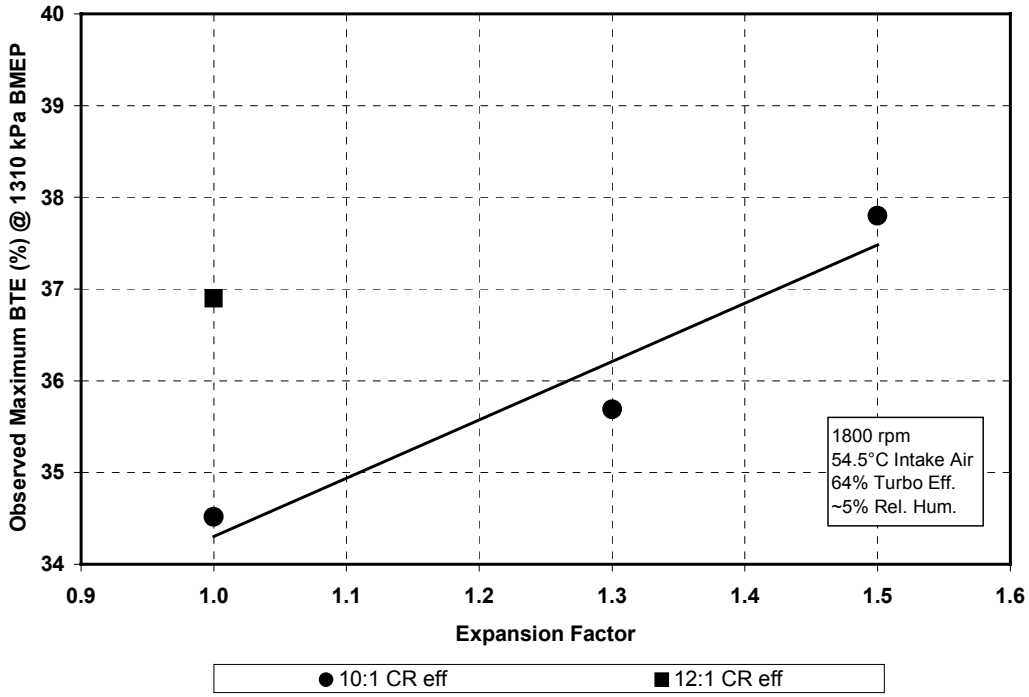

Figure C4-2. Efficiency at 1310 kPa BMEP Versus Expansion Factor for all Engine Configurations

C4.2.4 Comparison of Other Performance Indicators

As mentioned previously, the peak cylinder pressure increased with the Miller cycle, despite maintaining a constant effective compression ratio. The peak cylinder pressure for all configurations increased with load due to the increased trapped gas mass in-cylinder. The increase in pressure, as expansion factor was increased, is inversely related to the volume of the combustion chamber. As discussed in the piston design section, the Miller cycle was implemented by maintaining the same effective CR and increasing the ER. In order to maintain CR at higher ER, the combustion bowl depth was decreased, reducing the combustion chamber volume at TDC.

In addition to the combustion chamber volume, the piston modifications resulted in a reduction in the maximum squish velocity. The change in squish velocity was a result of reduced piston bowl volume and not piston-to-head clearance or squish area, which were the same for all designs. The squish velocity is an indication of in-cylinder piston-induced turbulence and changes in squish velocity would be expected to effect combustion rates. The high squish velocities increased the burn rate and reduced the combustion duration. Combustion duration increases at leaner equivalence ratios. It should be noted that typically, an increase in the combustion duration would result in a decrease in efficiency. However, the efficiency benefit resulting from the increase in expansion ratio of the Miller cycle was sufficient to offset any penalty imposed by increased combustion duration for a net gain in efficiency, as noted previously.

One of the anticipated problems with the Miller cycle is the penalty in volumetric efficiency resulting from changes to intake valve closing, effectively reducing the engine displacement. The observed penalty was not as severe as the estimated penalty indicating that either the effective intake valve closing was substantially different or a charge-filling benefit was obtained. This can be an important effect since effective implementation of the Miller cycle requires higher boost levels to maintain engine power. A charge filling benefit can reduce the boost level requirement.

C4.2.5 Comparison of NO_X Emissions

Exhaust emissions were measured during the majority of Miller cycle testing to look at trends and provide data for which the fuel-air equivalence ratio could be calculated. However, the focus of this testing was not to find the conditions for lowest emissions, but to define the knock-limited BMEP and efficiency. A majority of the test points were at conditions with spark timing more advanced than MBT to find the knock-limit. As expected, the measured NO_x concentrations for these very advanced conditions were very high. However, these data sets did allow the relative trends in NO_x concentrations with the Miller cycle to be evaluated. Figure C4-3 depicts the NO_x-BTE trade-off for the 10:1 effective compression ratio configurations at a constant load of 1310 kPa BMEP. While a reduction in brake specific NO_x was not realized with the Miller cycle, an improvement in efficiency with equivalent NO_x emissions was achieved. An approximate 5 to 6 percent increase in efficiency can be obtained at the same NO_x level with the 1.5 expansion factor.

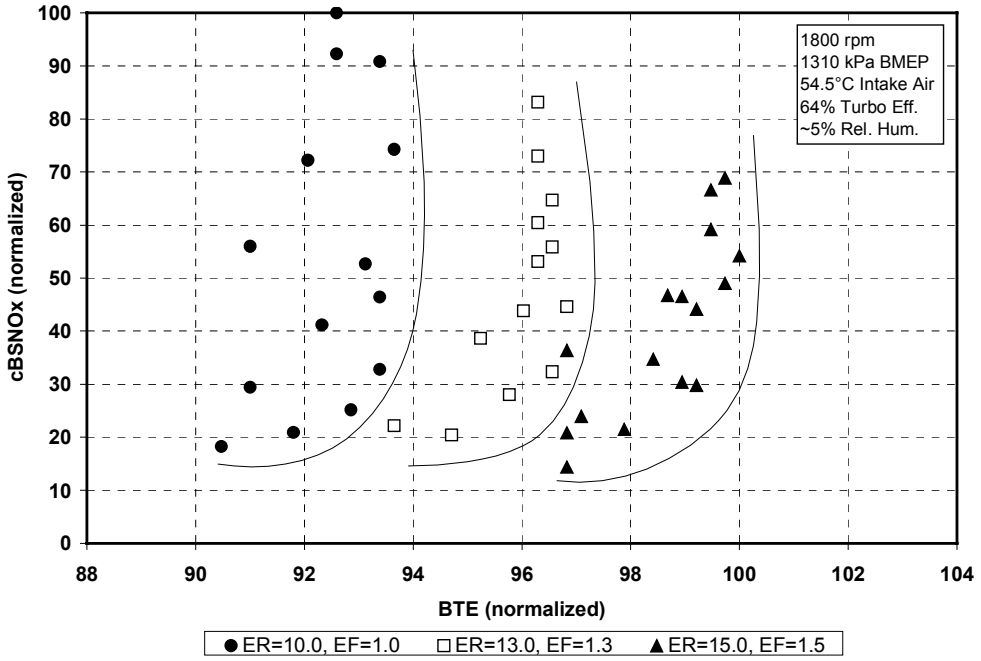

Figure C4-3. Normalized NO_x – BTE Tradeoff at 1310 kPa BMEP for 10:1 Effective Compression Ratio and 1.0, 1.3, and 1.5 Expansion Factors

C4.3 High BMEP Engine Concepts Evaluation

Brake Mean Effective Pressure or BMEP represents the work per cycle divided by the cylinder volume displaced per cycle[3]. BMEP is often conceptualized as the average cylinder pressure acting on the piston over the cycle. BMEP is interrelated with other performance parameters such as peak cylinder pressure and combustion phasing. In a natural gas engine, there are several limits on BMEP. First, based on the design of the engine structural members (piston, cylinder head, bearings, etc), there is a peak cylinder pressure limit. Second, for a given BMEP level, as timing or combustion phasing is advanced, not only is the peak cylinder pressure limit approached, but the possibility of knock also increases. Third, since the BMEP represents an average cylinder pressure, there is a minimum peak cylinder pressure required to produce a given BMEP level. These limits are illustrated in Figure C4-4.

It is important to note the operational limits, in particular, the peak cylinder pressure limit, that for the test pistons were 1900 psi and 2300 psi for the aluminum and steel piston designs, respectively. These limits were well below the 3200 psi peak cylinder pressure target for the ARES engine (Table A4-3), thus limiting the testing. The peak pressure and knock limitations were most severe at the higher expansion ratios and for lean conditions in which the in-cylinder mass and pressure were increased due to the presence of excess air. When these limits were reached, higher BMEP could still be obtained by increasing boost and retarding timing or combustion phasing. Retarding combustion phasing however decreases the engine efficiency counteracting the benefit of raising the BMEP level. There would still be a benefit perhaps in capital cost associated with higher BMEP levels.

Due to the limitations discussed above, analysis and presentation of this data is difficult. Some combustion configurations were knock limited and some were peak cylinder pressure limited with a different limit for different pistons. Figure C4-5 illustrates the maximum IMEP levels associated with various combustion concepts. (Recall that the IMEP = BMEP + FMEP + PMEP). This chart presents dilution strategy concepts using stoichiometric combustion with EGR as the diluent and lean burn combustion where excess air is used as the diluent. Also presented are the ignition system concepts, micro-pilot (MPI), multiple-site spark ignition (MS_1), and single source spark ignition (SI). The lean burn micro-pilot concepts were characterized by very rapid heat release early in the cycle resulting in IMEP levels that were limited at a low level by the peak cylinder pressure. The micro-pilot concepts were able to run leaner than corresponding spark ignition concepts which also resulted in higher peak pressures relative to the SI cases. In contrast the micro-pilot stoichiometric with EGR concepts were able to obtain high levels of IMEP prior to reaching the peak cylinder pressure limit. For the spark-ignited concepts, the reverse trend was observed. The lean burn cases were able to achieve higher IMEP levels than the stoichiometric with EGR. The spark-ignited EGR cases were limited by knock. While the interpretation of this data is difficult due to interaction of timing and expansion ratio with MEP and peak cylinder pressure, qualitatively, one can see that achieving the high levels of BMEP required for the ARES engine are possible.

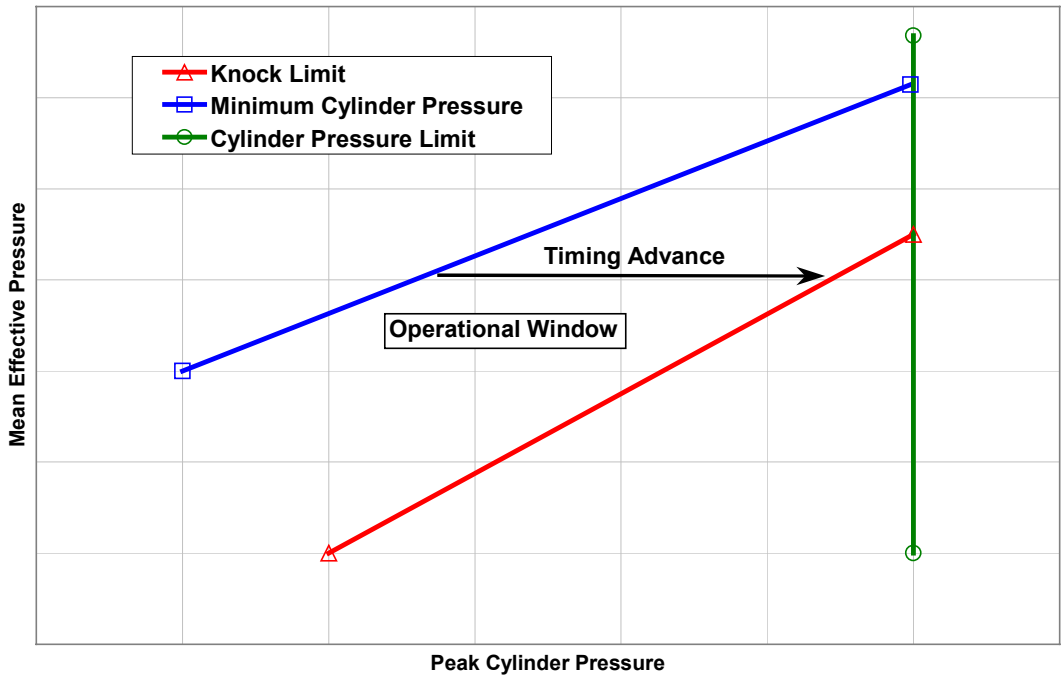

Figure C4-4. Engine Operational Window in Terms of MEP and Peak Cylinder Pressure

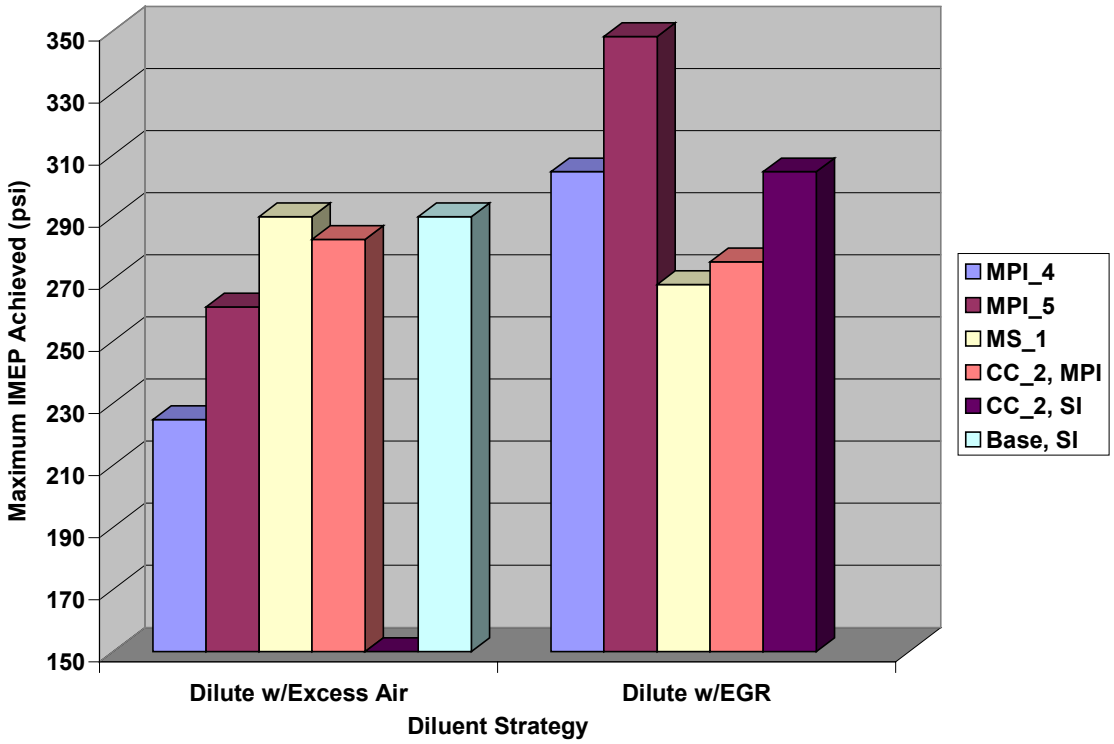

Figure C4-5. IMEP Levels Achieved with Combustion Concepts

C5.0 SUMMARY

A Caterpillar G3501, a single-cylinder research engine loaned to SwRI by Caterpillar, was installed and used as a test engine for this project. Various combustion concepts were evaluated to obtain knock free operation at high BMEP levels.

Testing on the G3501 engine initially involved a comparison test to data previously acquired on this engine by Caterpillar. The data acquired at SwRI compared well with Caterpillar's data, indicating the engine was operating properly.

The Miller cycle was utilized to reduce the effective compression ratio and in-cylinder temperatures reducing the knock tendency and NO_x formation. Special camshafts were designed to achieve the desired effective compression ratios. Pistons with different bowl volumes were designed and procured to achieve the desired expansion ratios. Evaluation of the Miller cycle involved the testing of combinations of compression ratio and expansion ratio. These configurations allowed a comparison of the effects of increasing expansion factor (expansion ratio) with constant compression ratio.

Testing was performed at 1800 rpm with a constant inlet air temperature of 54.5°C, pseudo turbocharger efficiency of 64 percent, and inlet relative humidity of approximately 5 percent. Sweeps of spark timing and inlet manifold pressure were performed with each configuration at various load steps to determine the knock-limited spark timing. The load step was increased until the knock-limited BMEP was achieved. Knock-limited BMEP was defined as the occurrence of peak BTE at the knock-limited spark timing for a given load.

Implementation of the Miller cycle resulted in an increase in BTE at a constant NO_x level. Increasing the expansion ratio also resulted in an increase in BTE. However, due to higher in-cylinder pressures, the level of BMEP that could be obtained without knock or exceeding the peak cylinder pressure was reduced. Various combustion concepts were evaluated for high BMEP operation. This testing was limited by the peak cylinder pressure limitations of the test pistons. Interrelationships between peak cylinder pressure, BMEP, combustion phasing, and expansion ratio make it difficult to analyze the acquired data. Lean burn and stoichiometric with EGR concepts were evaluated with single-site spark ignition and multiple-site ignition concepts. One Micro-pilot, stoichiometric-EGR concept was able to achieve 350 psi IMEP.

C6.0 REFERENCES

1. Okamoto, K. et al, "Study on Miller Cycle Gas Engine for Co-Generation Systems," SAE Paper 960949.
2. Diesel & Gas Turbine Worldwide Catalog - Product Directory and Buyers Guide, 1998 Edition, Volume 63.
3. Heywood, J.B., Internal Combustion Engine Fundamentals McGraw-Hill, 1988.

D. MICROFINE WATER SPRAY INJECTION FOR KNOCK AND NO_x CONTROL IN LARGE-BORE NATURAL-GAS ENGINES

EXECUTIVE SUMMARY

The use of direct in-cylinder injection of a microfine water spray to reduce in-cylinder temperatures and inhibit knock or autoignition of unburned gas was evaluated. By properly tailoring spray characteristics and injection timing, the water will evaporate in the charge air, cooling the charge. The cooled charge should reduce the tendency of the engine to knock, and should also reduce the formation of nitric oxides. The excess dilution effect of the water vapor will be avoided by operating the engine at a lower (richer) air-fuel ratio (AFR), and simply replacing some of the excess air with water vapor.

Calculations with the ALAMO_ENGINE code have shown that the water must be evaporated efficiently in the charge air. Further, the optimum time for the water injection is just after intake valve closing, if the water can be efficiently evaporated with such early injection. Efficiency gains at equivalent knock-margin brake mean effective pressures (BMEP's) were about 11-percent. These efficiency gains were accompanied by dramatic increases in knock-limited BMEP and reductions in NO_x, with a trade-off in the amount of BMEP increase and NO_x reduction.

Modifications were made to a Caterpillar G3501 single-cylinder engine to test the concept of water injection. The central spark plug location was modified for installation of a water injector. Two spark plugs were mounted near the outside edges of the combustion chamber. Although the atomization quality was not as good as desired, and the injection duration longer, it was possible to test the injector without a major head redesign. The results indicated a reduction in NO_x by about 37 percent at a water/fuel mass ratio of 0.24, and a reduction by about 50 percent at a water/fuel ratio of 0.80. The measured BTE was essentially unchanged, as was the BMEP.

D1.0 BACKGROUND

Water injection has been used in spark-ignition engines to increase power and reduce knock for some specialized applications in the past. However, these applications have involved engines operating with stoichiometric mixtures, and the addition of water vapor acts like a diluent that inhibits knock in a similar fashion to the way excess air inhibits knock at lean AFR's. That is, the diluent, either water vapor or excess air, reduces knock for three reasons: (1) the diluent lowers flame temperatures, reducing compressional heating of the end gases; (2) the turbulent flame speed is reduced since the laminar flame speed is reduced for lean or diluted mixtures, delaying the compressional heating of the end gas and (3) the reaction chemistry in the end gases is slowed in lean or diluted mixtures.

However, in a lean-burn natural gas engine, the combustion is typically operating near the lean limit. Therefore, the addition of water will add further diluent that could cause the engine to misfire. Thus, the above three mechanisms are not applicable for reducing knock by water injection in lean-burn engines. Rather than adding water vapor as a diluent, the objective of this project was to inject water in-cylinder as a liquid spray, and to cool the charge by evaporative cooling when the water evaporates. The diluent effect was removed from consideration by operating the engine at the same fuel mole fraction after accounting for the additional water vapor as the fuel mole fraction in the baseline, lean-burn engine. Thus, it is hypothesized that the knock mitigation will result due to cooling the initial charge, resulting in lower temperatures for both the burned gases and the end gases.

D2.0 OBJECTIVE

The objective of this test was to evaluate the direct injection of water as a microfine spray for reducing knock and NO_x in natural gas engines. The use of a microfine spray was intended to allow for significant water droplet evaporation before the drops reach the walls of the combustion chamber.

D3.0 APPROACH

The project consisted of the following tasks:

- Computational analysis of direct, in-cylinder water injection
- Design (or selection) of water injectors, and testing for spray quality
- Engine testing of direct, in-cylinder injection of microfine water spray

The computational study was performed to determine the improvements in knock, NO_x, and BMEP that could be achieved with water injection, assuming the water efficiently cools the air charge. It also assumed that the flammability of the mixture was relatively unaffected by the water vapor if the fuel mole fraction was maintained near that for lean-limit combustion. A cycle simulation code developed at SwRI, the ALAMO_ENGINE code, was used in this analysis.

The injection of water in a very fine spray allows for evaporation of the water in the charge air rather than at the walls of the combustion chamber. This approach should efficiently cool the air charge, rather than simply reducing heat rejection to the coolant. Injectors were selected to produce a very fine spray. The spray quality was verified using a Malvern Model 2600 Laser-Based Particle Size Analyzer. The spray evaporation rate was estimated with another code developed at SwRI, the TESS (Trajectory and Evaporation of Spray Systems) code.

Tests of the effect of water injection on engine performance and emissions were conducted with a Caterpillar G3501 single-cylinder, lean-burn natural gas engine. The water injector was placed in the central head location currently used for the spark plug in the natural gas version of this engine, and two spark plugs on opposite edges of the combustion chamber were used.

D4.0 COMPUTATIONAL ANALYSIS OF WATER INJECTION

Calculations of engine performance and emissions with direct, in-cylinder water injection were conducted using a cycle simulation code developed at SwRI called ALAMO_ENGINE. This code consists of a conventional cycle-simulation model coupled with a chemical equilibrium code that computes flame products and temperatures. Two scenarios for injecting water were considered. The first scenario considered was injecting water before the spark, in which case the dilution effect of water vapor on the gas mixture had to be considered. The second scenario considered was injecting water after the spark, in which case the dilution effect on the early flame propagation could be ignored.

D4.1 Water Injection Prior to the Spark Event

The effect of direct in-cylinder water injection was examined computationally. These calculations showed very favorable results for water injection. Efficiency gains at equivalent knock margin brake mean effective pressures (BMEP's) were about 11-percent. These efficiency gains were accompanied by dramatic increases in knock-limited BMEP with approximately constant NO_x. The increase in BMEP could be traded off with a decrease in NO_x.

The baseline case was chosen as a 170 psi (1172 kPa) BMEP, 6-cylinder engine with a bore of 170 mm, stroke of 180 mm, mechanical compression ratio of 12.0:1, operating at an $(A/F)_{dry}$ of 26:1 and 1200 rpm, without Miller cycle type valve timings. The valve timings were intake valve opening at 10 degrees before top dead center (BTDC), intake valve closing at 10 degrees after bottom dead center (ABDC), exhaust valve opening at 60 degrees before bottom dead center (BBDC), and exhaust valve closing at 10 degrees after top dead center (ATDC). The intake manifold air temperature was assumed to be 54.4°C or 130°F. Spark timing was set to provide a NO_x emissions level of 0.99 g/Hhp-hr. Burn rates were set at 23 crank angle degrees (CAD) for 10 to 90-percent burn duration at 1200 rpm, the same as measured at a typical condition for the Caterpillar G3501 at SwRI. Burn rates were maintained constant with water injection, although the actual burn rates might be lower. Initial computations of knock for the water injection studies assumed a natural gas octane number of 135. The assumed octane number was reassessed based on a typical natural gas. The final calculations reported here were performed for an "average" natural gas with an octane number assumed to be 124. Calculations at the baseline conditions were also performed for a low-octane natural gas with an assumed octane number of 119. Natural gas octane numbers were assumed to be as follows: 90^{th} percentile (good) natural gas, 128; average natural gas, 124; approximately 10^{th} percentile (bad) natural gas, 119.

Direct in-cylinder water injection was simulated by assuming a fine spray with a 95-percent air cooling efficiency. That is, 95-percent of the heat required to vaporize the water spray was assumed to come from the in-cylinder air charge, and only 5-percent from the coolant. A high efficiency can be achieved by using a microfine spray that

evaporates in the air rather than on the combustion chamber walls. For this analysis, the water was assumed to be injected over 30 crank angle degrees (CAD), with the beginning of injection varying from 30 to 170 CAD before top dead center (BTDC) firing. The 170 CAD BTDC firing was the time of intake valve closing, and water injected before that time would displace the air charge, degrading volumetric efficiency.

The effect of water injection timing on BMEP is shown in Figure D4-1. As indicated in the figure, the highest BMEP was achieved with a start of water injection at 150 CAD BTDC. The effect of water injection timing on brake thermal efficiency (BTE) is shown in Figure D4-2, which also shows the most efficient performance at 150 CAD BTDC. Figure D4-3 shows the effect of water injection timing on the integrated knock parameter, with the best (lowest) knock parameter occurring for injection timings of 150 CAD BTDC or earlier. The very low knock parameters with water injection shown in Figure D4-3 indicate that the engine BMEP can be increased dramatically from the baseline level without knocking. An increase in BMEP increases both the power density and the efficiency of the engine. Keeping the baseline spark timing, the effect of water injection timing on NO_x is shown in Figure D4-4. The very low NO_x values with water injection show that the spark timing could be advanced to increase the efficiency while still keeping NO_x below the baseline 1.0 g/bhp-hr value.

Interestingly, all four of the important performance variables, BMEP, BTE, knock, and NO_x appeared to be optimized with the same water injection timing, 150 CAD BTDC. For that reason, the 150 CAD BTDC timing was used for the calculations discussed below that were conducted at constant integrated knock parameter value. Increasing the water injection duration from 30 CAD to 60 CAD reduced the predicted BTE from 39.46 to 39.16-percent, and further increasing the duration to 90 CAD reduced the BTE to 38.77-percent. Therefore, shorter injection durations are desirable, and the 30 CAD duration was assumed for the constant-knock calculations.

The above calculations showed that water injection reduces both knock and NO_x so that various changes can be made to improve efficiency. All of these calculations were performed with a relatively low A/F ratio of 24.3:1, which should reduce the chances for flammability problems with water injection. Keeping the same A/F ratio and water injection characteristics, but adding turbocompounding (80 percent turbine efficiency, and 98 percent mechanical efficiency in coupling the shaft energy to the engine shaft), reducing exhaust system heat losses by 50-percent, increasing the primary turbocharger turbine and compressor efficiencies from 76 and 78-percent respectively to 80-percent, increasing the speed from 1200 rpm to 1800 rpm, and advancing the timing results in a predicted BTE of approximately 46.0-percent with a BMEP of 2607 kPa, a knock parameter of 0.821, and NO_x emissions of 0.66 g/bhp-hr.

In conclusion, the water injection appears to be a favorable approach for increasing efficiency and BMEP by reducing knock tendency, with an added bonus of significantly reduced NO_x.

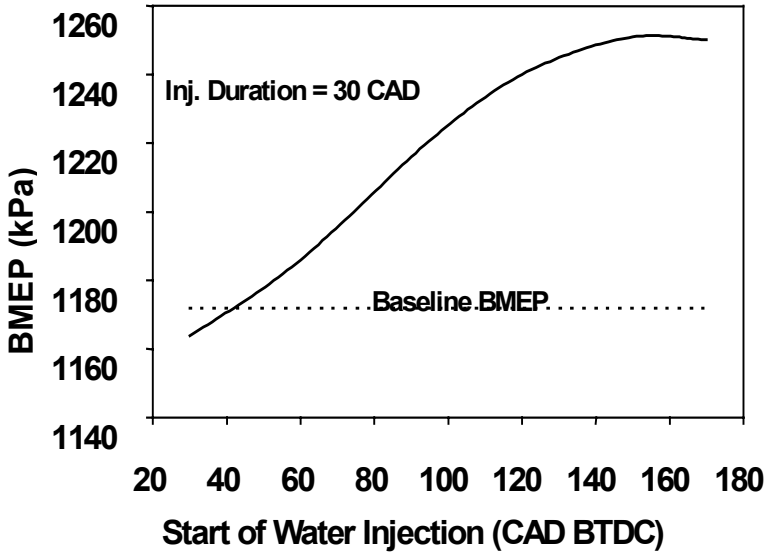

Figure D4-1. Effect of Water Injection Timing on Brake Mean Effective Pressure (BMEP) at Constant MAP

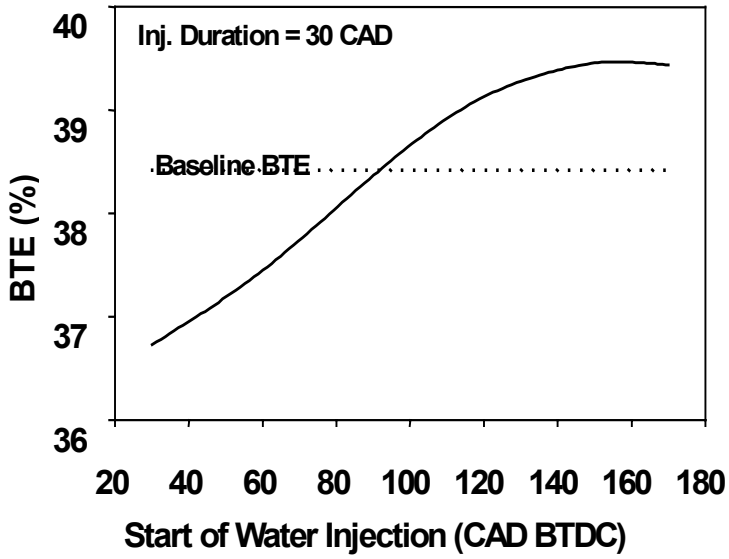

Figure D4-2. Effect of Water Injection Timing on Brake Thermal Efficiency (BTE) at Constant MAP

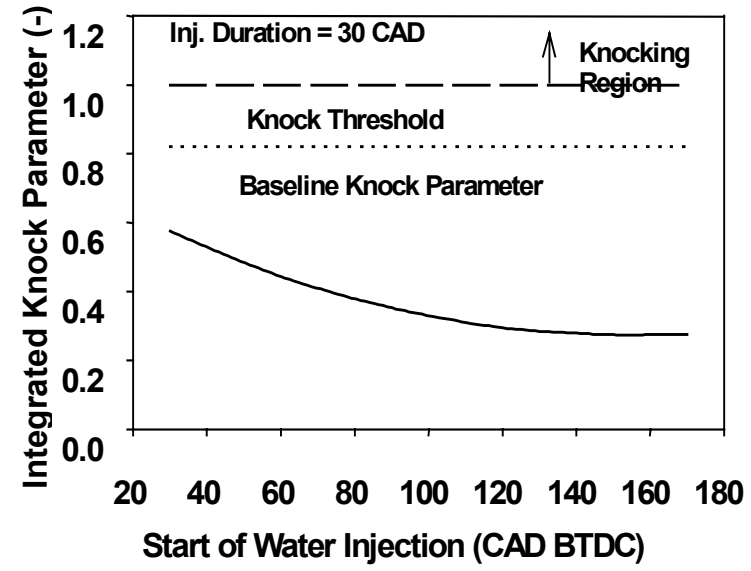

Figure D4-3. Effect of Water Injection Timing on Integrated Knock Parameter at Constant MAP

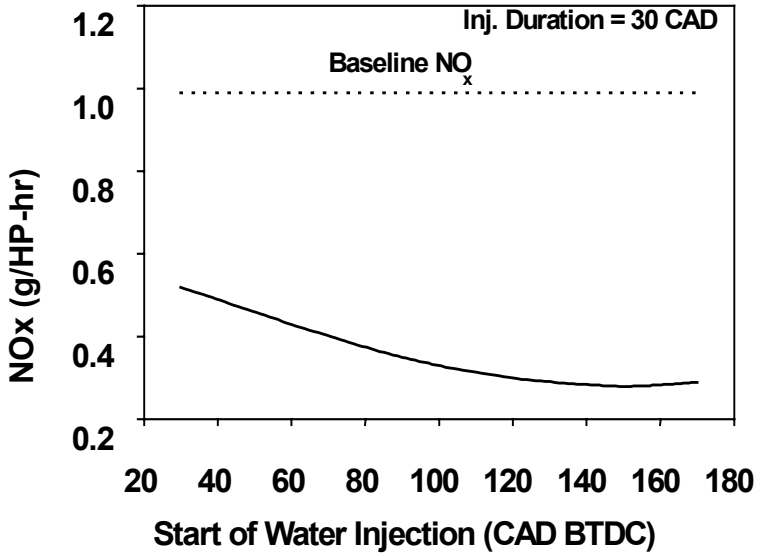

Figure D4-4. Effect of Water Injection Timing on NO_x at Constant MAP

D4.2 Water Injection After the Spark Event

An alternative approach to injecting water before the spark plug fires is to inject after the ignition event. In this case, it might be possible to operate the engine at the same air-fuel ratio as in the lean condition, since water vapor would not be present to inhibit flame propagation at the time of the spark. However, the dilution of the air charge by the water vapor later in the combustion process might cause a partial burn. Calculations were performed to investigate water injection near TDC.

In conclusion, the injection of water near TDC may be effective in reducing NO_x, but it was predicted to be relatively ineffective in increasing BTE. Thus, as discussed above, injection of water just after intake valve closing still appears to be the most attractive strategy for improving BTE, assuming the water could be evaporated efficiently before hitting the combustion chamber walls.

D5.0 SELECTION OF INJECTORS FOR DI WATER INJECTION

SwRI obtained two prototype DI gasoline fuel injectors from two different companies. One was modified for testing on the G3501 engine. It was a static flow of 10.2 g/s. Rather than being able to inject water over 60 CAD, the injection event was over 200 CAD at the high load conditions. Thus, the DI gasoline fuel injectors were very limited in flow rate compared to the desired value. Further, the DI gasoline injectors were not designed to flow water, or to operate at the high cylinder pressures that will be encountered in the Caterpillar engine. These injectors atomize water very well, but there were corrosion problems with the water. Therefore, the atomizers were flushed with gasoline or diesel fuel after testing with water.

D6.0 ENGINE TESTING OF DIRECT, IN-CYLINDER WATER INJECTION

Various ways of injecting water into the Caterpillar G3501 single-cylinder engine were investigated. The Caterpillar G3501 cylinder head was modified to replace the central spark plug with the DI gasoline injector. Modifications were made to the head for inserting the two spark plugs on opposite sides of the outer part of the combustion chamber. The location for the two spark plugs is shown in Figure D6-1. A photograph of the overall push tube with injector is shown in Figure D6-2.

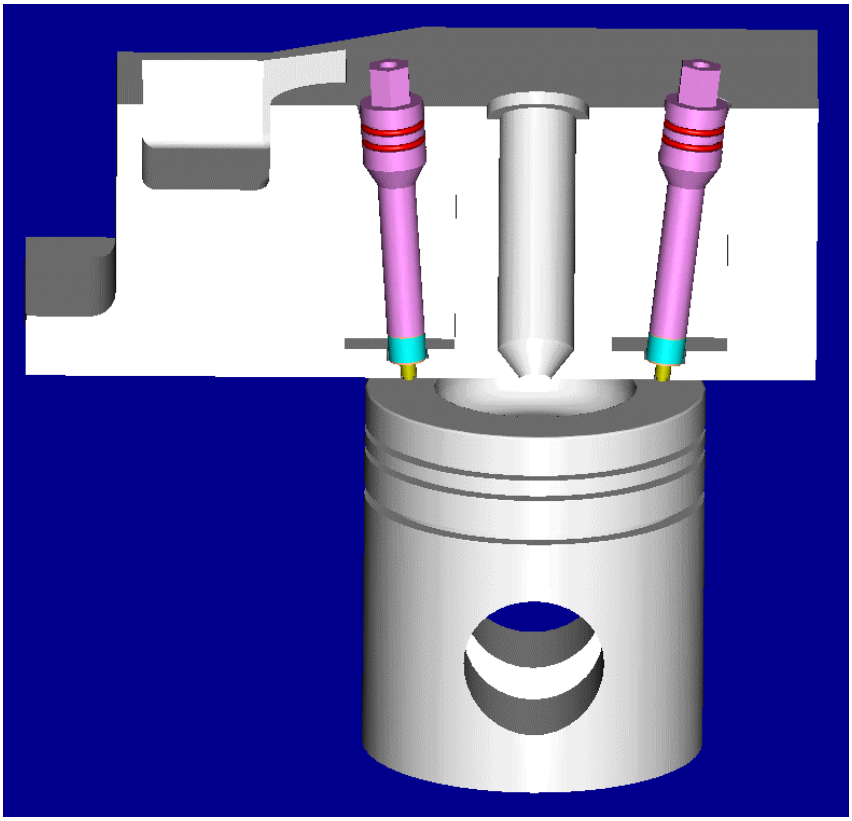

Figure D6-1. Spark Plug Locations in Outer Part of Combustion Chamber

Figure D6-2. DI Gasoline Injector and Push Tube

Testing was conducted at 1200 rpm at 105 psi (724 kPa) BMEP. Two water injection rates were tested. Water was injected at 1450 psig (10 MPa gage) with pulse widths of 3.5 milliseconds (ms) (25.2 CAD) and 11.8 ms (85 CAD), with the start of injection beginning at 125 deg. BTDC. The corresponding water/fuel mass ratios for these two pulse widths were 0.24 and 0.80 ms. The desired water/fuel mass ratios were in the range of 1.0 to 2.0, but it was not possible to inject that amount of water in the time available and still close the injector at 40 deg. BTDC to avoid back-flow of combustion gases into

the injector. During these tests, the A/F ratio was not adjusted to a richer condition to account for the water vapor dilution effect. Therefore, the water injection both cooled and diluted the gases to be burned.

As shown in Figure D6-3, the water injection appeared to reduce the NO_x emissions from about 4000 ppm with no water injection to about 2500 ppm with a water/fuel mass ratio of 0.24, and to about 1900 ppm at a water/fuel mass ratio of about 0.80. These reductions were reasonably close to the predicted NO_x reductions.

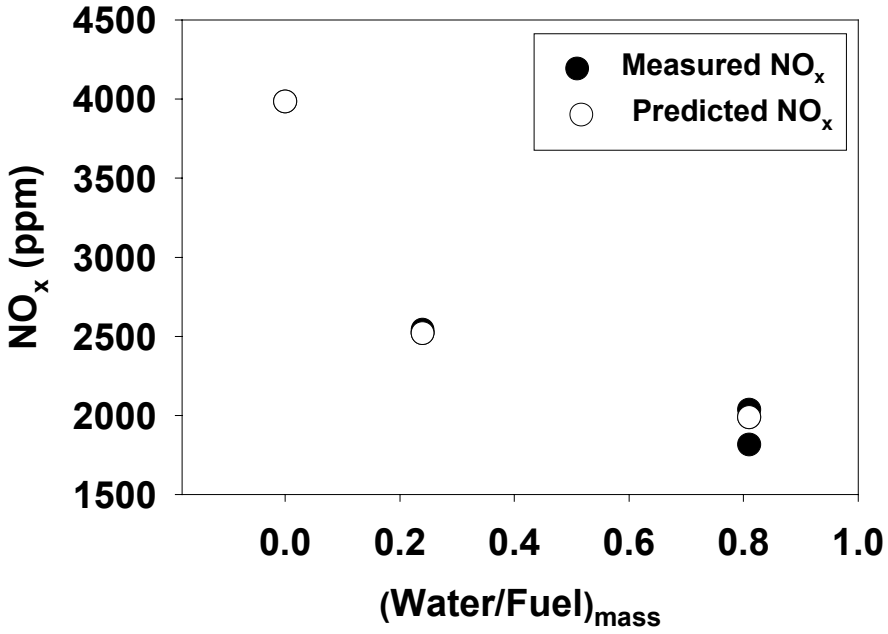

Figure D6-3. Effect of Water/Fuel Mass Ratio on NO_x Emissions

Figure D6-4 shows that the brake thermal efficiency (BTE) does not significantly change with the change in water injection. It had been predicted that the BTE might increase with water injection if the water could be injected at about 150 deg. BTDC with an injection duration of about 30 CAD. However, the actual injection duration for the longer pulse width was about 85 CAD, and the model indicated that such a long injection duration would cancel out any BTE gain. There was concern that water injection might decrease the combustion efficiency, but Figure D6-5 shows that the combustion efficiency stayed reasonably high, about 96.3 percent, independent of the water injection rate. The water injection was predicted to decrease the propensity to knock, but at this low BMEP, the knock tendency was too low to measure. Appropriate injector design for proper spray characteristics and durability is paramount to successful application of this technology.

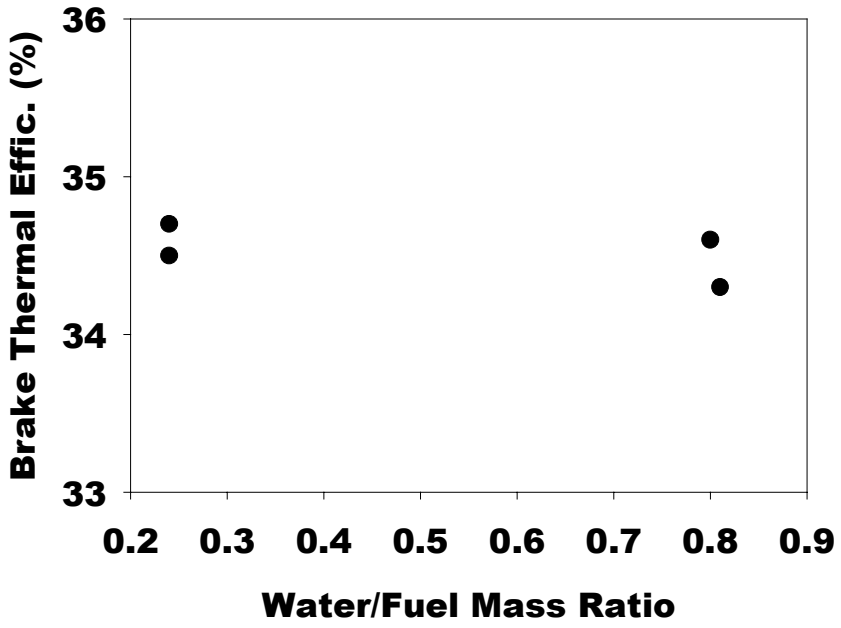

Figure D6-4. Effect of Water/Fuel Mass Ratio on Brake Thermal Efficiency.

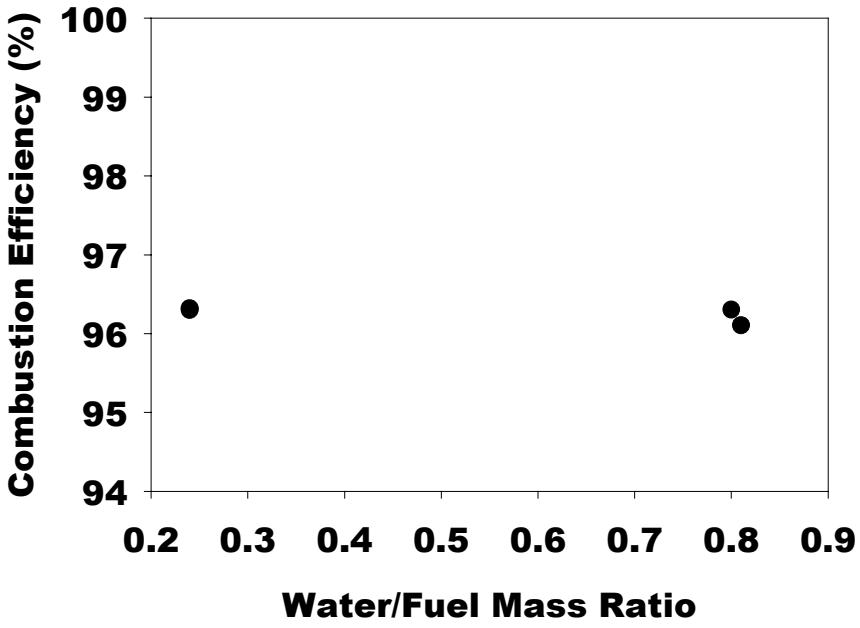

Figure D6-5. Effect of Water Fuel Mass Ratio on Combustion Efficiency

D7.0 SUMMARY

The computational analysis showed that direct-injection of a microfine water spray can be used to reduce the tendency of a lean-burn engine to knock, and to reduce the NO_x emissions. The reduced knock tendency allows increases in spark timing and/or BMEP that will increase power and improve efficiency.

A DI gasoline injector was selected for testing on the Caterpillar G3501 engine. The cylinder head was modified so that the water injector was centrally mounted. The cylinder head was also modified for two spark plugs mounted near opposite edges of the combustion chamber.

The engine tests did show significant reductions in NO_x with increases in water injection rates. Increasing the water injection rate from a water/fuel ratio of 0.24 to 0.80 decreased the NO_x by about 24 percent, a significant reduction, but still indicating a poorer charge cooling effect than desired. The selected injector was not optimum, producing larger drop sizes than required for more complete evaporation and charge cooling to occur in the free air stream. Appropriate injector design for proper spray characteristics and durability is paramount to successful application of this technology.

Although no combustion effects were noted at the conditions tested, a critical question to be answered is whether the water vapor from the water spray would degrade the combustion performance. This question was not answered during the conduct of this project, and remains an open question.

E. MICRO-PILOT IGNITION TECHNOLOGY EVALUATION

EXECUTIVE SUMMARY

The results of the technical path evaluation indicated that short combustion duration and lean air-fuel ratio are required for obtaining high efficiencies without knock. Currently, spark-ignited, prechamber (SIPC) combustion systems are used to provide a fast burn rate and extend the lean misfire limit. SIPC combustion systems have limitations and challenges that are well known throughout the industry. These include: (1) manufacturing complexity, (2) high heat loss, (3) spark plug durability, and (4) durability of gas fuel valves. Another potential technology for obtaining high burn rates for lean mixtures is the use of a pilot amount of diesel fuel to ignite the natural gas and air mixture. This concept is not new, since dual-fuel engines have been and are widely used. What is new is the development of high-pressure, diesel injection systems that have the potential of delivering small quantities of diesel fuel in a manner that provides spray penetration to the periphery of the combustion chamber. In the past, pilot-ignited engines have been limited to about 5 percent pilot fuel due to inadequate turn-down of existing diesel injection systems and poor fuel delivery characteristics at low pilot flow. Current state-of-the-art injection systems can overcome these prior limitations.

The objective of this task was to evaluate the potential of using a diesel micro-pilot for igniting a lean premixed gas and air mixture, increasing combustion rates, and improving knock tolerance. Additional objectives included definition of optimum injection system parameters for good performance and development of a more comprehensive understanding of pilot ignition process.

The literature was reviewed for information on pilot-ignited natural gas engines and for technical details on the injection system hardware used in these applications. SwRI diesel spray penetration models were used to evaluate current injection system technology for micro-pilot applications and to assess current systems for features required of micro-pilot systems. A common rail, diesel injection system was adapted to the CAT 3501 single cylinder test engine. Various combustion chamber concepts were evaluated with respect to misfire, knock and combustion efficiency.

The results indicated that nozzle parameters, hole diameter, number of hole, and spray angle, had little effect on the ignition and combustion of dilute fuel-air mixtures. High injection pressure produced faster combustion rates. Results were obtained at pilot quantities below 0.5-percent. Higher pilot quantity was found to produce higher NO_x, while not necessary for ignition of the fuel-air mixture. Combustion chamber design was shown to be more important for combustion stability and combustion rate. Complete

combustion of lean mixtures was found to be problematic. Although the pilot was able to ignite extremely lean mixtures, the combustion efficiency for these mixtures was low. High levels of in-cylinder turbulence were found to be beneficial for flame propagation and combustion stability.

Additional work should focus on combustion chamber designs that minimize in-cylinder crevice regions that contribute to low combustion efficiency, and designs that promote in-cylinder turbulence to enhance flame propagation and combustion stability. The single-cylinder work should be extended to a multi-cylinder engine. Also, cold starting, transient response, part-load operation, and durability that were not investigated on this project should be addressed.

E1.0 BACKGROUND

The results of the technical path evaluation have indicated that short combustion duration and lean air-fuel ratio are required for obtaining high efficiencies without knock. Currently, spark-ignited, pre-chamber (SIPC) combustion systems are used to provide fast burn rate and extend the lean misfire limit. SIPC combustion systems have limitations and challenges that are well known throughout the industry. These include: (1) manufacturing complexity, (2) high heat loss, (3) spark plug durability, and (4) durability of gas fuel valves. Another potential technology for obtaining high burn rates for lean mixtures is the use of a pilot amount of diesel fuel to ignite the natural gas and air mixture. This concept is not new, since dual-fuel engines have been and are widely used. What is new is the development of high-pressure, diesel injection systems that have the potential of delivering small quantities of diesel fuel in a manner that provides spray penetration to the periphery of the combustion chamber. In the past, pilot-ignited engines have been limited to about 5-percent pilot fuel due to inadequate turn-down of existing diesel injection systems and poor fuel delivery characteristics at low pilot flow. Current state-of-the-art injection systems can overcome these prior limitations.

The advantages of open chamber pilot ignition compared to SIPC potentially include: (1) lower in-cylinder heat losses due to omission of pre-chamber, (2) improved reliability by replacing spark plugs with proven diesel injection equipment, (3) lower hydrocarbon emissions due to less wall quenching, and (4) easier manufacturing due to simpler combustion chamber design.

E2.0 OBJECTIVE

The objective of this task was to evaluate the potential of using a diesel micro-pilot for igniting a lean premixed gas and air mixture, increasing combustion rates, and improving knock tolerance. Additional objectives included definition of optimum injection system parameters for good performance and development of a more comprehensive understanding of the pilot ignition process.

E3.0 APPROACH

This task consisted of a literature review, a state-of-the-art survey of micro-pilot technology and diesel pilot injection systems, and experimental evaluation of various micro-pilot combustion concepts. The literature was reviewed to locate specific information on the effect of pilot ignition on knock limited BMEP, lean misfire limit, combustion rate, and NO_x-efficiency tradeoff. Of particular interest was a direct comparison between various combustion system types: spark-ignited open-chamber, spark-ignited prechamber, conventional dual-fuel, micro-pilot open-chamber (MPOC), and micro-pilot prechamber (MPPC) for engines with a bore size of approximately 170 mm. The dual-fuel literature was also reviewed for injection system details, specifically, injection pressure, pilot quantity, and injection nozzle geometry.

SwRI diesel spray penetration models were used to evaluate current injection system technology for micro-pilot applications and to assess current systems for features required of micro-pilot systems. Spray penetration, spray mixing, and accurate control of small fuel quantities were the parameters of interest.

A common rail, diesel injection system was adapted to the CAT 3501 single cylinder test engine. Various combustion chamber concepts were evaluated with respect to misfire, knock and combustion efficiency.

E4.0 MICRO-PILOT TECHNOLOGY SURVEY

A wide variety of technical publications on dual-fuel engine technology were reviewed. The topics ranged from fundamental discussions of the effects of natural gas on diesel pilot ignition delay and knock, to more applied presentations of specific engine designs, or dual-fuel implementation. There were two review papers of note in the literature. O'Neal (1982) summarized the state-of-the-art of dual-fuel engines, and presented the first graphical representation of dual-fuel knock limited BMEP as a function of compression ratio. Weaver and Turner (1994) provided a very good review of dual-fuel engine technology, performance, and emissions covering the period of time since 1982. During this period of time, the concept of using a pilot-ignited pre-chamber was implemented in production engines and patented by Cooper Energy Services. The first implementation was by Cooper on a LSB engine with subsequent implementations by Coltec, MAN, Fincantieri, and by Cooper on Superior and Enterprise engines.

There were six noteworthy references that provided detail on comparison of various combustion systems: Blizzard, et al. (1991), Blythe (1994), Chrisman, et al. (1998), Hupperich and Durnholtz (1997), MAN B&W Technical Brochure, and Meyers, et al. (1997). In summary, each of the references indicated that pilot ignition improved performance and lowered NO_x emission levels relative to spark-ignited combustion systems. Pilot ignition was most successfully implemented in the pre-chamber configuration.

It should be noted that in each instance, the pilot quantity was on the order of 1 to 3 percent of the total energy input and required an injection system capable of injecting a small quantity of diesel fuel in a precise and controllable manner. Using a customized injection system represents an improvement over conventional dual-fuel systems that can operate on 100 percent diesel or in dual-fuel mode with one injection system. SwRI suspects that even though custom injection systems were used, the open-chamber implementations of pilot ignition were limited by inadequate injection system hardware. This subject is discussed in more detail in the section related to injection system requirements.

E5.0 ASSESSMENT OF INJECTION SYSTEM REQUIREMENTS

Comparison of combustion systems in the literature have clearly indicated that implementation of pilot ignition in a pre-chamber provides a better NO_x-efficiency tradeoff than an open-chamber implementation. The question is why? SwRI believes that pre-chamber designs overcome injection system limitations that inhibit open-chamber performance. Many of the injection systems capable of injecting small (micro) quantities of diesel fuel in a precise and repeatable manner were designed for automotive applications, engines with bore diameters typically below 100 mm. These systems are not capable of providing satisfactory injection spray penetration and mixing for large-bore engines. A pre-chamber design, with much smaller dimensions, does not require extraordinary injection characteristics for good penetration and mixing. The main limitation of pre-chamber designs appears to be cold starting. Provided a satisfactory injection system can be developed, open-chamber designs do not appear to be afflicted with cold starting problems nor the complexity of pre-chamber designs.

SwRI performed a brief analysis to determine the requirements of an open-chamber injection system for micro-pilot applications. Assumptions for the analysis included a 170 mm bore engine, combustion bowl diameter of 120 mm, and BMEP of 1600 kPa (~230 psi). Based on results found in the literature, minimum NO_x emissions were found with minimum pilot resulting in an optimum approaching 1 percent of the total energy input. The pilot quantity, typically expressed in mm^3 per injection, will ultimately depend on the engine power level, efficiency, and pilot-to-total energy ratio.

Another parameter of interest is the time available for injection. Typical diesel ignition delay times are on the order of 0.5 msec. Adding natural gas to the mixture will reduce the oxygen mole fraction and extend the ignition delay time of the diesel fuel. Also, it is anticipated that the compression ratio for this engine will be lower than typical diesel compression ratios, which will also increase the ignition delay time. For this analysis, it was assumed that the ignition delay time would be on the order of 1 msec. To maximize ignition energy, all fuel should be injected prior to ignition. Thus, the ignition delay time defines the maximum injection duration.

In addition to defining the injection duration, the ignition delay time also defines the spray tip penetration rate since an optimum ignition location would likely be at the periphery of the combustion chamber. Thus, the spray must penetrate to the edge of the combustion chamber, defined by the bowl diameter, during the 1 msec ignition delay time. Figure E5-1 depicts the direction of flame propagation if ignition occurs close to the center of the combustion chamber. Shown in the figure is a generic combustion chamber diameter with a centrally located 4-hole pilot injection nozzle. As indicated, ignition of the pilot close to the center would be similar to conventional single spark plug ignition and the flame would propagate in a generally outward direction. This ignition scenario would be prone to auto-ignition of the end gases and knock. While increasing the penetration distance does not guarantee ignition at the periphery of the chamber, it increases the likelihood of a flame propagation that begins at the edge of the chamber and

propagates inward and radially, increasing the combustion rate and lessening the knock tendency. This mode of flame propagation is depicted in Figure E5-2.

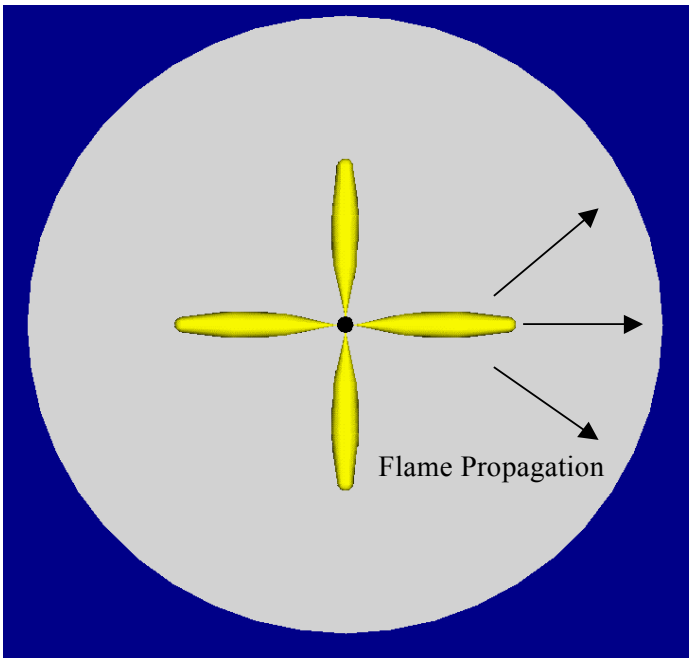

Figure E5-1. Illustration of Flame Propagation Direction for Pilot Injection Using Low Injection Pressure and Providing Poor Jet Tip Penetration

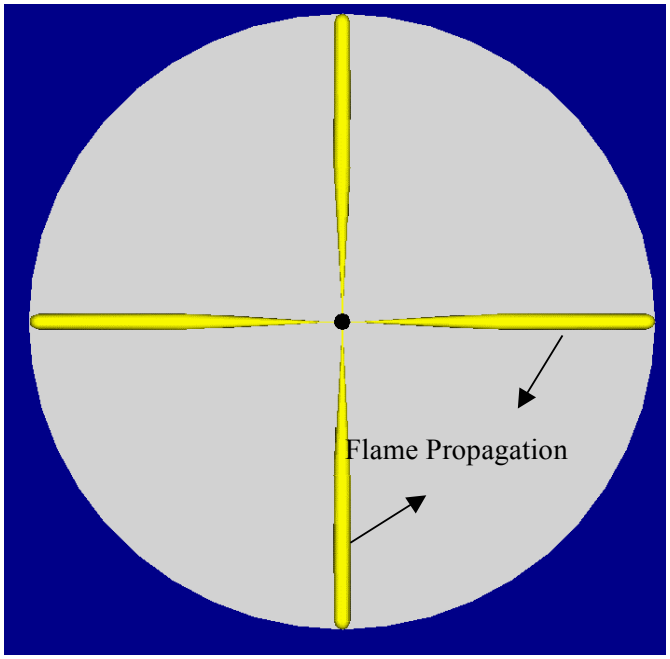

Figure E5-2. Illustration of Flame Propagation Direction for Pilot Injection Using High Injection Pressure and Providing Good Jet Tip Penetration

Based on this rather elementary analysis, the following injection system characteristics were defined:

- Injection duration < 1 msec (7.2^o CA at 1200 rpm)
- Penetration rate > 60 mm / msec
- Nozzle tip geometry ~ 4-6-hole nozzle for multiple ignition sites.

The next step in the analysis was to determine the range of nozzle hole diameter and injection pressure that would provide the above injection characteristics. A SwRI computational code (JETMIX) for predicting diesel jet penetration and mixing was used for this analysis. Various combinations of injection pressure and nozzle tip geometry were evaluated.

In addition to the jet penetration, JETMIX provides an estimate of the fuel-air mixing by defining a mixing parameter (MP_1). MP_1 computes the ratio of the mass of fuel richer than stoichiometric to the total mass of fuel for times greater than 0.6 msec. For diesel applications, a smaller MP_1 (approaching 0) is desirable as this indicates that the fuel is well mixed with the air. High values (approaching 1) for MP_1 indicate poor mixing and a tendency for combustion in fuel rich zones with subsequent production of soot. Although soot is not particularly a problem for dual-fuel engines, the mixing parameter can still provide an indication of jet mixing. The optimum value for MP_1 and the degree of mixing for this application is unknown at this time.

Nevertheless, the penetration rate and mixing parameter can provide guidance for the selection of the proper injection pressure and nozzle diameter. Figure E5-3 illustrates the mixing parameter and penetration distance at 1 msec for a range of injection pressures and nozzle hole diameters. As shown, high injection pressures and small hole diameters provide good mixing (small MP_1) and good penetration.

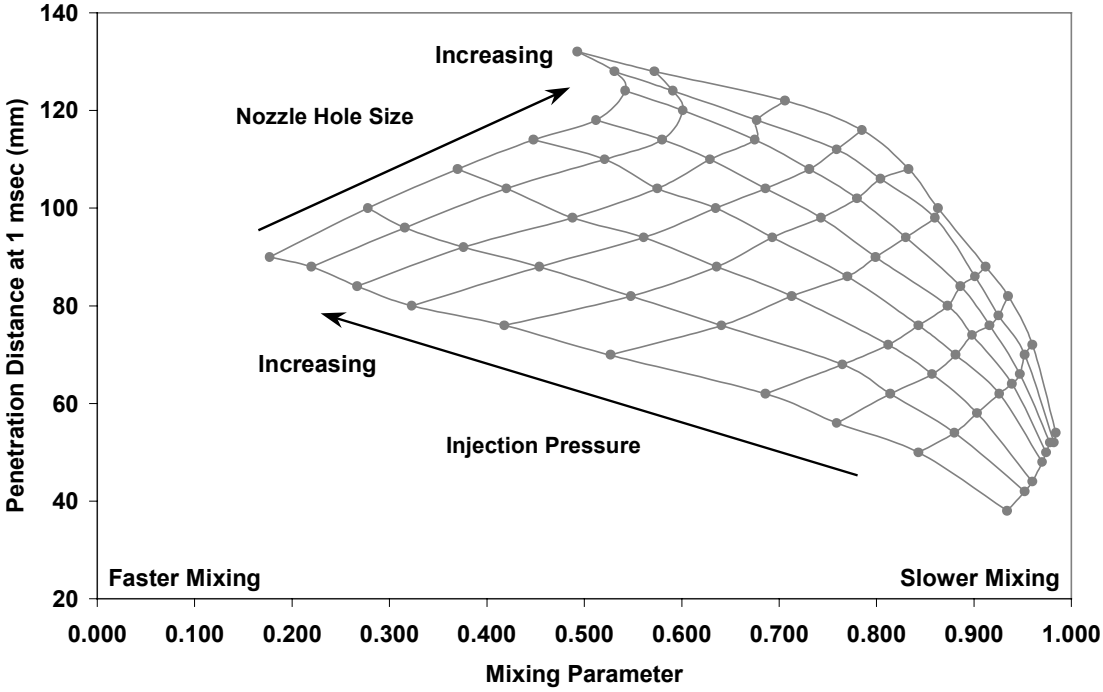

Figure E5-3. Jet Penetration and Mixing for Matrix of Injection Pressures and Nozzle Hole Diameters (JETMIX Results)

E6.0 REVIEW OF INJECTION SYSTEM HARDWARE

The dual-fuel and micro-pilot literature was surveyed for information on injection system designs. As previously noted, in cases where the literature compared the performance of open-chamber and pre-chamber micro-pilot combustion systems, the pre-chamber implementation of the micro-pilot concept provided better performance. It was theorized that the open-chamber configurations presented in the literature were limited by the injection system design. This conclusion naturally led to an investigation of the injection system designs for dual-fuel engines.

Injection parameters of interest were the injection pressure and the nozzle configurations (number of holes and hole diameter). The analysis discussed in the previous section concluded that small holes and high injection pressures were required to achieve the jet penetration and mixing required for micro-pilot ignition.

The literature was surveyed for injection system details for micro-pilot systems. Although there are numerous dual-fuel engine papers published, many contained insufficient details of the injection system to be included in this review. Generally lacking were details of the injection nozzle, specifically nozzle hole diameter. In some cases, injection pressure was presented as nozzle opening pressure or peak injection pressure. The JETMIX code, as used here, assumes a steady-state jet and requires an average or mean injection pressure. Where possible, estimates of mean injection pressure and nozzle hole diameter were made for this study.

The literature review located six publications with sufficient detail for analysis: Blizzard, et al. (1991), Beck (1995), Chrisman, et al. (1997), Gerbert, et al. (1996), Johnson, et al. (1990), and SwRI (1996). The estimated nozzle hole diameters and injection pressure for each case were used to compute the penetration distance of the fuel spray at 1 millisecond and the mixing parameter using the JETMIX model. These data were added to Figure E5-3 and are presented as Figure E6-1, which illustrates the jet penetration and mixing for a matrix of injection pressures and nozzle hole sizes. There are several key features to this figure. First, a line representing an injection pressure limit of 165 MPa has been imposed on the injection pressure – nozzle hole size matrix. Second, a line representing a minimum penetration distance at 1 millisecond of 60 mm has been placed on the graph. This minimum distance is proportional to the diameter of the combustion chamber, a larger diameter chamber requires a greater penetration distance. The third line, represented with open symbols, represents a combination of injection pressures and nozzle hole diameters that would provide one percent pilot of diesel fuel per injection within 2 crank angle degrees for a 4-hole nozzle. Finally, the data for injection pressure and nozzle hole diameter for systems found in the literature are represented on the graph by solid symbols. As shown, the injection systems typically found in micro-pilot or dual-fuel applications are relatively low in pressure and do not provide the penetration or mixing characteristics required for proper implementation of this concept.

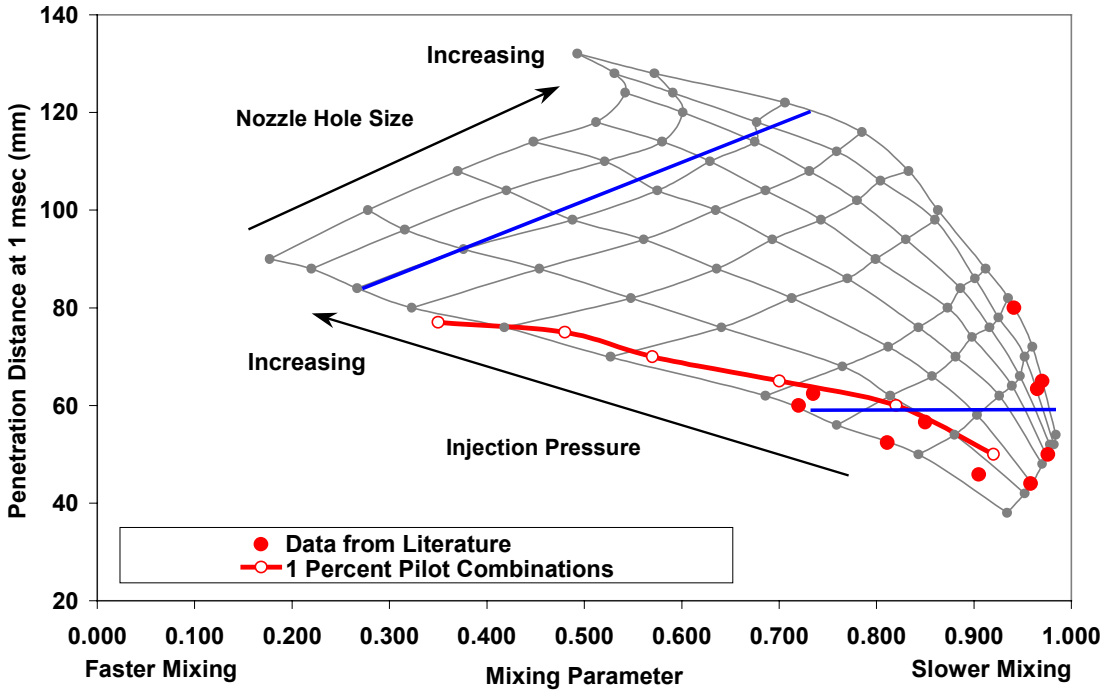

Figure E6-1. Comparison of Injection System Data from the Literature with the Target Penetration and Mixing Parameter Range from the Micro-Pilot Analysis

Of the literature surveyed, typical injection systems for micro-pilot ignition ranged from unit injectors (SwRI, 1996), pump-line-nozzle systems (Blizzard, 1991), rotary distributor pumps (Chrisman, et al., 1997), or accumulator type common rail systems (Beck, 1995). Many of these systems were adapted from high-speed diesel injection systems that were available at the time. Recently, common rail injection systems with flexible timing and high injection pressures have been developed for high-speed diesel engines. These systems appear to have the right characteristics for micro-pilot injection systems. Short injection durations with relatively high injection pressures can be achieved with a great deal of flexibility in injection timing. Injection pressure for a common rail system is mainly independent of engine speed. Electronically controlled unit injectors also appear to be well suited for pilot ignition applications.

There are several manufacturers of common rail systems that would be applicable to micro-pilot ignition, including Bosch, LucasVarity, and Siemens. The injector designs are relatively simplistic on the outside and can be easily adapted to a large bore engine.

E7.0 EVALUATION OF MICRO-PILOT IGNITION ON CAT 3501 SINGLE CYLINDER ENGINE

E7.1 Injection System

A common rail injection system was selected for evaluation on this project. This injection system was found to have the desired characteristics discussed in the prior section. A photograph of the common rail unit, the injection pump, and the injector is shown in Figure E7.1. The injection event was electronically controlled via pulse width modulated signal. The common rail pressure was controlled via a pressure relief valve on the end of the rail. The opposite end of the rail contained the pressure-sensing unit. A photograph of the common rail system installed on the CAT 3501 engine is shown in Figure E7.2. Prototype injection nozzles were procured from Duap, a company based in Switzerland.

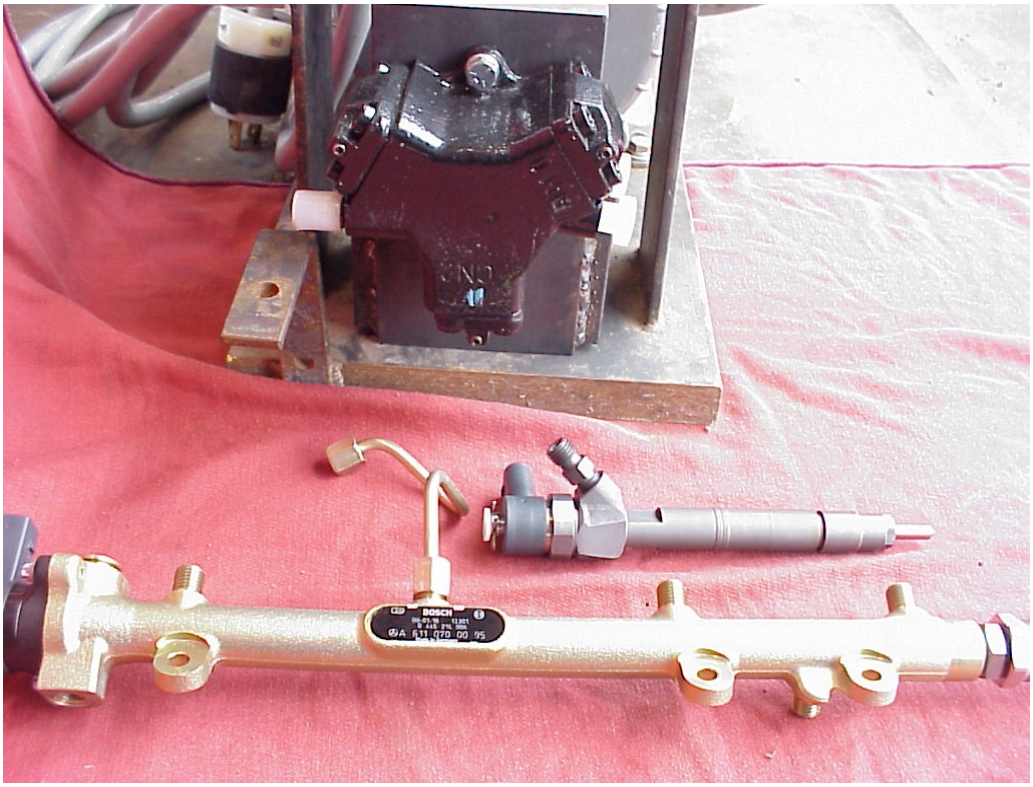

Figure E7-1. Photograph of Bosch Common Rail Injection System

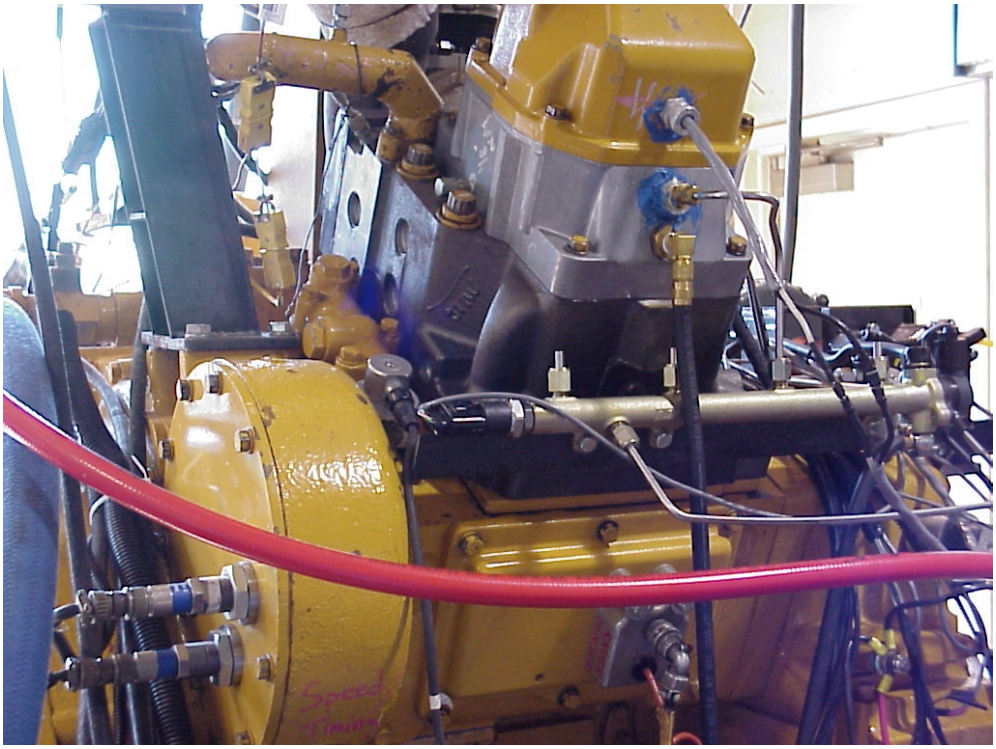

Figure E7-2. Photograph of CAT3501 with Common Rail System Installed

A stock gas engine cylinder head was procured and modified to accept the Bosch injector. An adapter was designed and machined to retain the injector in the cylinder head. Figure E7-3 illustrates the injector adapted to the CAT 3501 cylinder head. An oil cooling tube was directed into the well containing the injector. Oil was pumped into the well and allowed to flow out of the top to provide cooling to the injector. This system worked well as no injector failures occurred. The controller for the engine was modified to include drivers and algorithms for controlling the common rail injection system. The engine control unit provided fuel flow control of both the diesel pilot and the natural gas while also controlling the injection pressure, injection timing, and injection quantity. Closed-loop air-fuel ratio control was achieved using a wide-range exhaust oxygen sensor and modulation of the natural gas fuel flow.

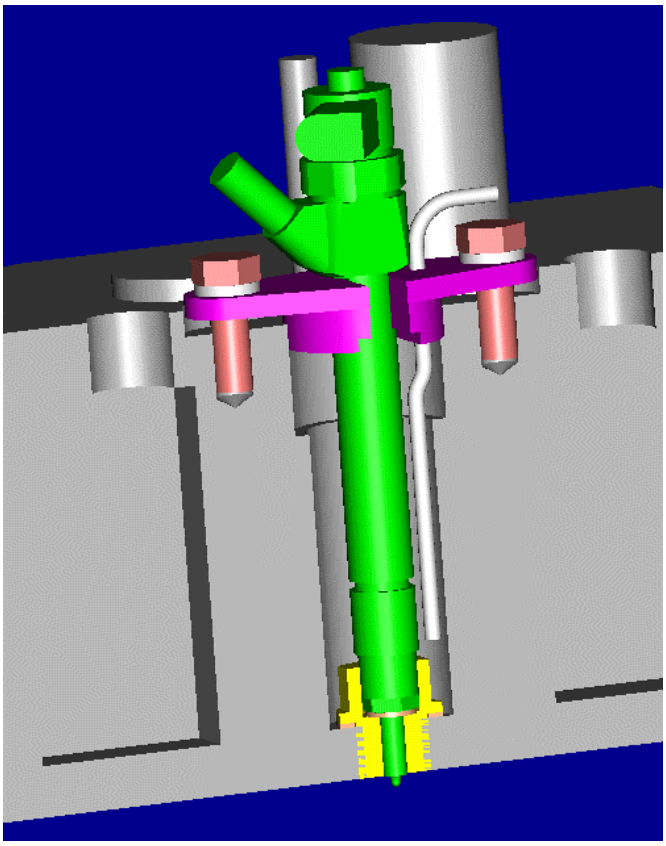

Figure E7-3. Bosch Injector Adapted to CAT 3501 Cylinder Head

E7.2 Test Pistons

A total of six pistons were designed for evaluation with the pilot ignition system. It should be noted that three of the pistons were machined from blank aluminum pistons typically used in the gas engine. These pistons are shown in Figure E7-4. Piston CC_2 was a piston used on spark ignition testing associated with other aspects of the ARES project. CC_2 was designed to provide a high level of turbulence to speed flame propagation and combustion. MPI_1 and MPI_2 were designed to offer a more open combustion chamber allowing spray penetration. For the purposes of this program, the peak cylinder pressure limit for the aluminum pistons was 130 bar. The remaining pistons were machined from blank steel pistons with a peak cylinder pressure limit of 160 bar. The steel pistons were designed to have an open combustion chamber with minimal squish. The steel piston designs are shown in Figure E7-4. The combustion chamber features were machined into the piston such that they aligned with the fuel spray from the six-hole injection nozzle.

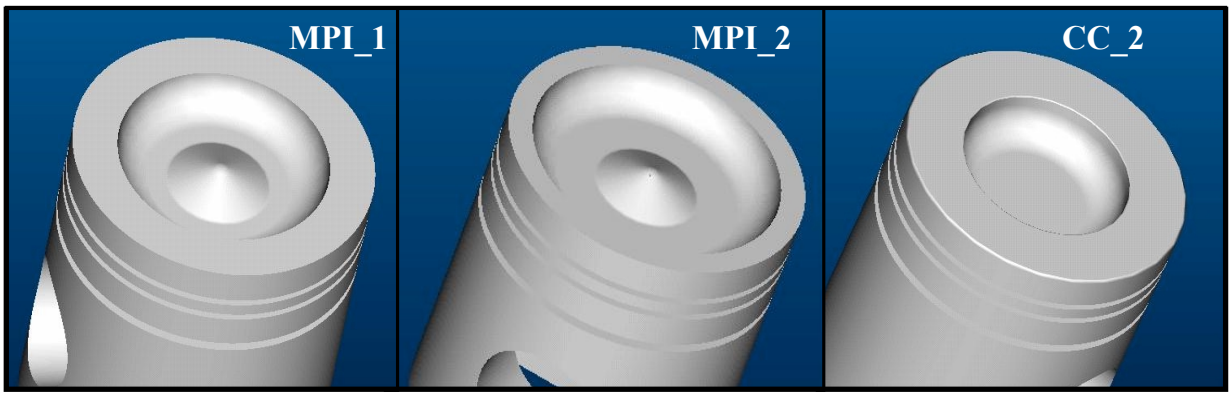

Figure E7-4. Images of Aluminum Pistons MPI_1, MPI_2, and CC_2

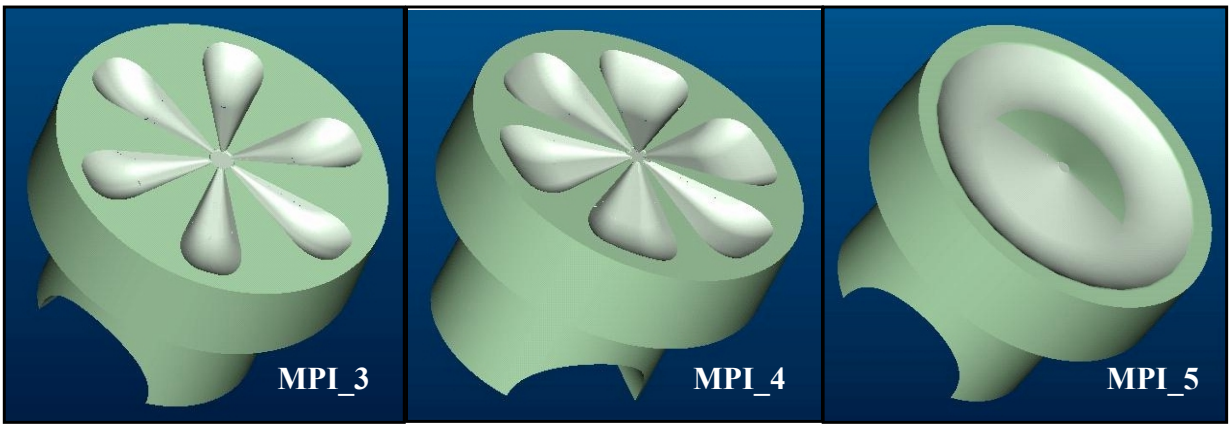

Figure E7-5. Images of Steel Pistons MPI_3, MPI_4, and MPI_5

E7.3 Test Matrix

The test variables with a micro-pilot combustion system are numerous. Design parameters include the combustion bowl shape, compression ratio, expansion factor, injector nozzle geometry, including the number of holes, the hole diameter, and the spray angle. Operational parameters include pilot quantity, injection timing, and injection pressure along with the main chamber equivalence ratio. Table E7-1 lists the range of dependent variables evaluated on this project. Although the main focus of the micro-pilot work was on lean combustion, stoichiometric combustion was also tested using exhaust gas as a diluent in place of excess air. This added another dimension to the testing. The dependent parameters of interest included misfire tolerance, knock limit, combustion rate, engine thermal efficiency, and emissions levels.

Table E7-1. Range of Operational Variables

Operational Variable	Variable Range
Injection Pressure	48-117 MPa (7 – 17 ksi)
Injection Timing	7 to 30°BTDC
Pilot Quantity	0.25-3 % total energy
Equivalence Ratio	Lean limit to Stoichiometric
Exhaust Gas Recirculation	15 – 25 %
Engine Load (BMEP)	1100 – 2000 kPa 170 – 300 psi
Engine Speed	1200 and 1800 rpm

The engine was instrumented for cylinder pressure, natural gas flow rate, exhaust emissions, assorted pressures, and critical temperatures. Instrumentation for measuring diesel fuel flow was also installed. Testing was conducted to determine the lean misfire limit, combustion rate, knock-limited BMEP, and efficiency of the various combinations of injection parameters and combustion bowl geometries. Cold start was problematic for some configurations, but was not addressed, since the primary focus was at rated power. Various scenarios can be conceived to overcome the cold start problem including the use of a spark plug, glow plug, or variable valve timing to raise the compression ratio during starting and at light loads.

E7.4 Test Results

The data collected, while not covering every possible combination of variables, allows for some interesting comparisons. Specifically, micro-pilot ignition can be directly compared to open-chamber spark ignition data, stoichiometric-EGR can be compared with lean burn, and the effects of various injection system parameters can be compared. These comparisons are discussed in the following sections.

Micro-pilot versus SI open chamber

Both micro-pilot and spark-ignited open chamber configurations were evaluated. The spark-ignited configuration was tested with a Miller Cycle camshaft with a 1.5 expansion factor providing an effective compression ratio of 10:1. The micro-pilot case required higher compression ratio for ignition and was tested with the stock camshaft. The data presented below were taken at 1800 rpm and 170 psi (1170 kPa) BMEP. Figure E7-6 illustrates the combustion efficiency (computed via exhaust emissions) for the micro-pilot and spark ignition configurations. As shown the pilot ignited data had higher combustion efficiency for a given equivalence ratio. The micro-pilot extended the lean limit of the

engine although the combustion efficiency dropped off rapidly for mixtures leaner than 0.56 equivalence ratio. The combustion efficiency for the micro-pilot case was sensitive to combustion phasing at the lean conditions with higher combustion efficiency obtained at more advanced timings. The micro-pilot data also exhibited faster combustion rates at leaner equivalence ratios as indicated by the 10 to 90 percent burn duration plotted in Figure E7-7. Shorter burn durations were obtained at more advanced combustion phasing.

The corresponding NO_x-BTE tradeoff is shown in Figure E7-8. With higher combustion efficiency, leaner combustion, and faster burn rates, it was expected that the micro-pilot would have higher thermal efficiency. As shown, the SI data had higher efficiency for a given NO_x level. This result is somewhat surprising until the testing constraints are considered. Each configuration had a peak cylinder pressure limit of 130 bar peak pressure, the maximum peak pressure limit of the test piston. The timing was advanced for each configuration until the cylinder pressure limit was reached. The relationship between peak cylinder pressure and the combustion phasing is shown in Figure E7-9. The micro-pilot combustion had higher peak cylinder pressures for a given combustion phasing due to higher in-cylinder mass at the leaner conditions and also due to faster burn rates. Thus the combustion phasing of the micro-pilot data was retarded relative to the SI data. Since efficiency is strongly related to combustion phasing or timing, the retarded combustion phasing of the micro-pilot contributed to lower efficiencies. If cylinder pressures were not limited, higher thermal efficiencies would be obtained with micro-pilot ignition. In addition, recall that the micro-pilot tests utilized the stock camshaft, while the SI case used a Miller camshaft. Prior testing has shown that one advantage of the Miller cycle is that part of the compression work is shifted to the turbocharger allowing intercooling of the charge prior to introduction into the combustion chamber part way through the compression stroke. Thus everything being equal, the SI data would be expected to have lower NO_x than the corresponding micro-pilot data. Confounding this rational is an expectation of higher NO_x for micro-pilot ignition. Prior results have also shown that NO_x is directly proportional to the pilot quantity.

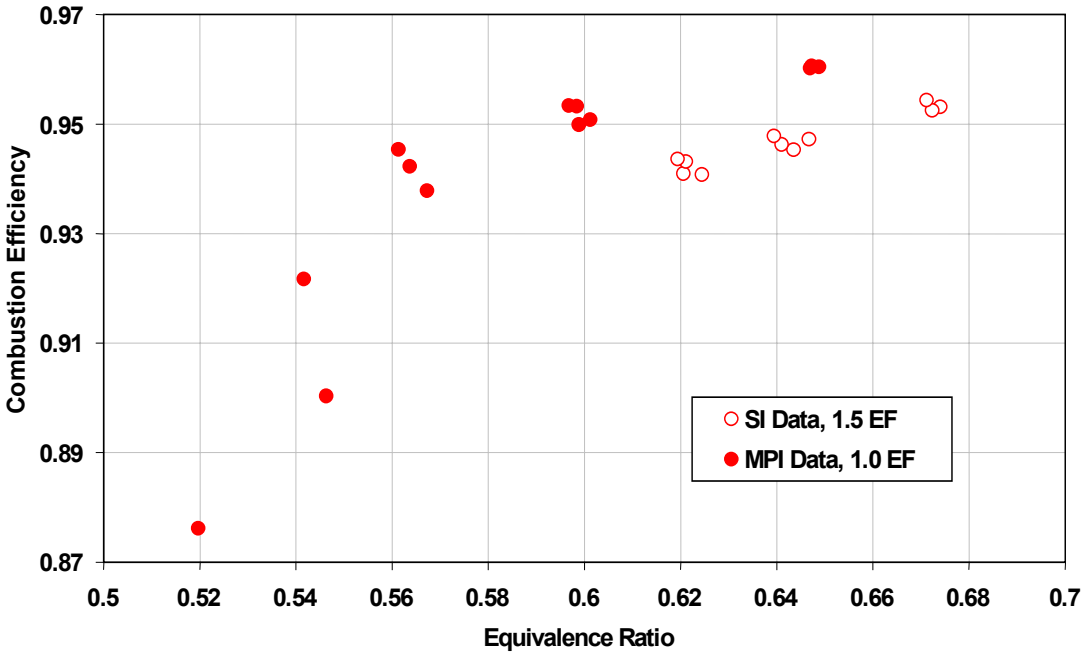

Figure E7-6. Combustion Efficiency for SI and MPI Configurations

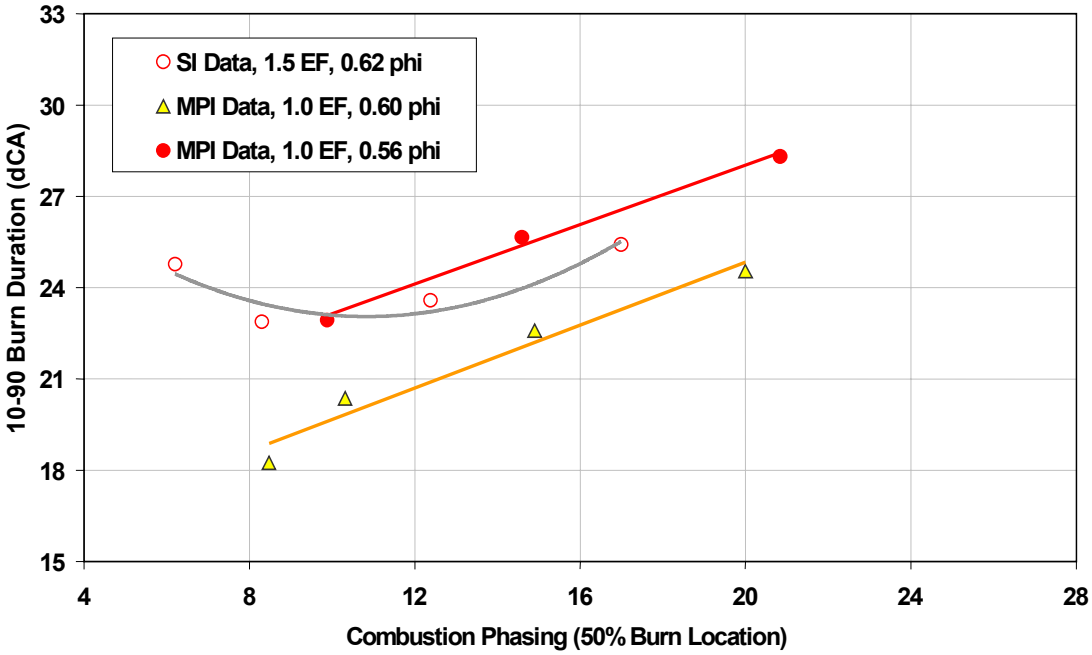

Figure E7-7. Combustion Duration for SI and MPI Configurations

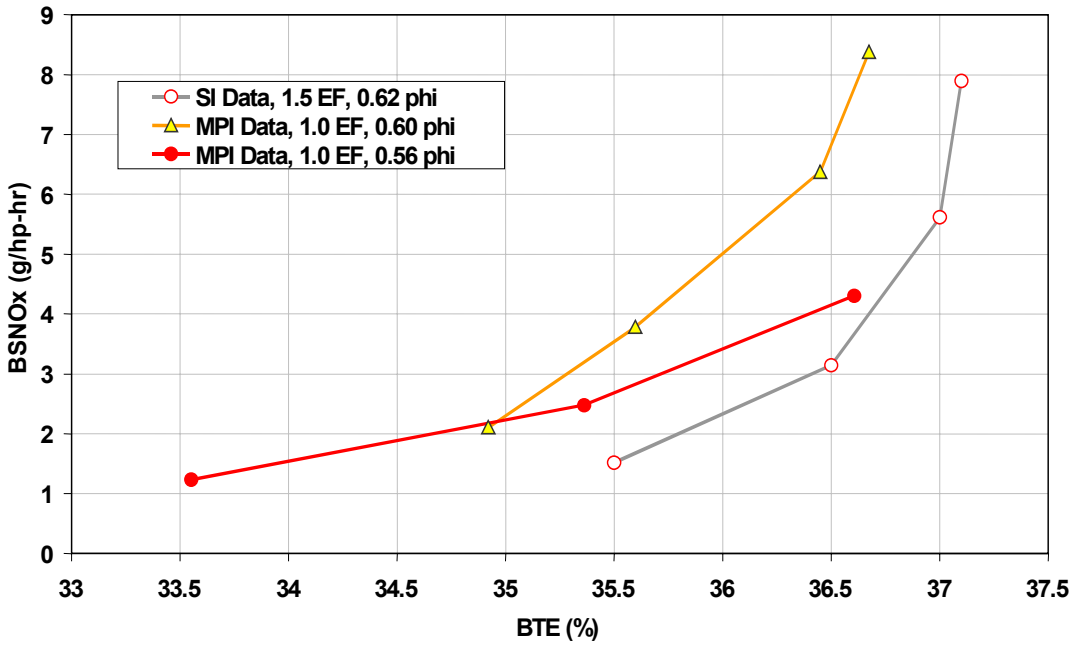

Figure E7-8. NOx-Efficiency Tradeoff for SI and MPI Configurations for Lean Combustion

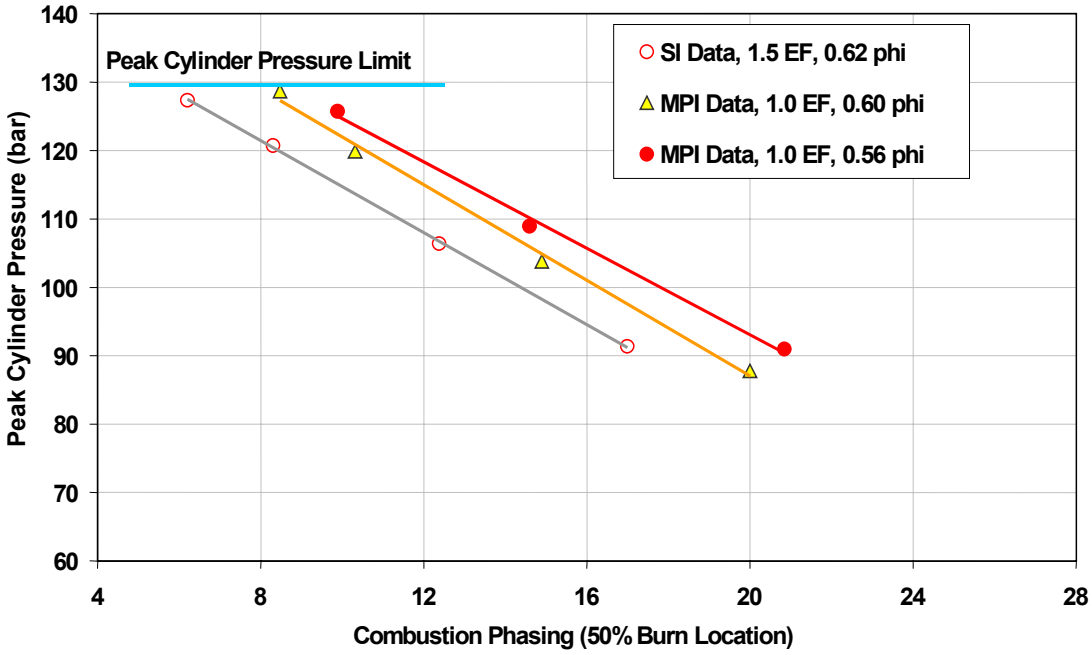

Figure E7-9. Peak Cylinder Pressure for SI and MPI Configurations

Effect of Nozzle Geometry on Engine Performance

As described in the Injection System section, four injection nozzles were obtained. These nozzles enabled testing to be conducted with two levels of three nozzle parameters, nozzle hole diameter, nozzle included spray angle, and number of holes. In addition, injection pressure, injection timing, and injection quantity could be varied to determine the effect of each parameter. These nozzles were tested with two of the micro-pilot pistons, MPI_1 and MPI_2. The results presented in this section represent data at 1170 kPa (170 psi) BMEP and 1800 rpm. The combustion efficiency, combustion rate, and the NO_x-BTE tradeoff were the dependent parameters of most interest.

Combustion efficiency in lean-burn gas engines is primarily a function of equivalence ratio. Leaner mixtures result in lower in-cylinder temperatures, increased unburned hydrocarbons, and lower combustion efficiency. Quench and crevice regions contribute to the unburned hydrocarbons and to some extent are independent of injection system parameters but highly dependent on combustion chamber design and compression ratio. However, if by selection of injection nozzle geometry, one could enable the flame to propagate into the quench regions, then combustion efficiency and thermal efficiency could be improved. Figure E7-10 illustrates the effect of equivalence ratio on combustion efficiency for the two pistons of interest, MPI_1 and MPI_2. As shown, MPI_1 had lower combustion efficiency. The lower combustion efficiency could be attributed, in part, to the higher expansion ratio of MPI_1, which means that the crevice region is a larger fraction of the combustion chamber volume at TDC. Additionally, the higher expansion ratio leads to lower in-cylinder temperatures at the end of combustion. The quench region volume will be effected by the in-cylinder temperature late in the cycle. If the exhaust port temperature is used as an indicator of the in-cylinder temperature at the end of the cycle, there is a fair correlation between the exhaust port temperature and the combustion efficiency as shown in Figure E7-11. These effects are discussed as preface to the discussion of the injection system parameters. As shown in Figure E7-10, there was not much difference in combustion efficiency at equivalence ratios above 0.60. So for these conditions, injection system parameters had little effect. Of more interest perhaps is the effect of injection system parameters at leaner equivalence ratios, since one objective would be to operate the engine as lean as possible to obtain low NO_x. Improving the combustion efficiency at lean equivalence ratios would improve thermal efficiency since BTE is directly proportional to combustion efficiency as well as expansion ratio as shown in Figure E7-12.

Ignition delay and combustion duration was of interest. The ignition delay estimated by the 0- to 10-percent burned duration correlated well with the jet mixing parameter as shown in Figure E7-13. Combustion duration was correlated with the jet penetration parameter as shown in Figure E7-14, and also injection pressure, upon which penetration is strongly dependent.

An overall summary of this work was that the injection system parameters could be selected to provide a small benefit in terms of combustion improvements. Higher injection pressures increased penetration and combustion rate and appeared to improve

combustion efficiency. Hole size and the number of holes had little effect on the combustion. Selection of the nozzle hole size and number of holes should be based on the desired injection quantity, penetration, and fueling rate.

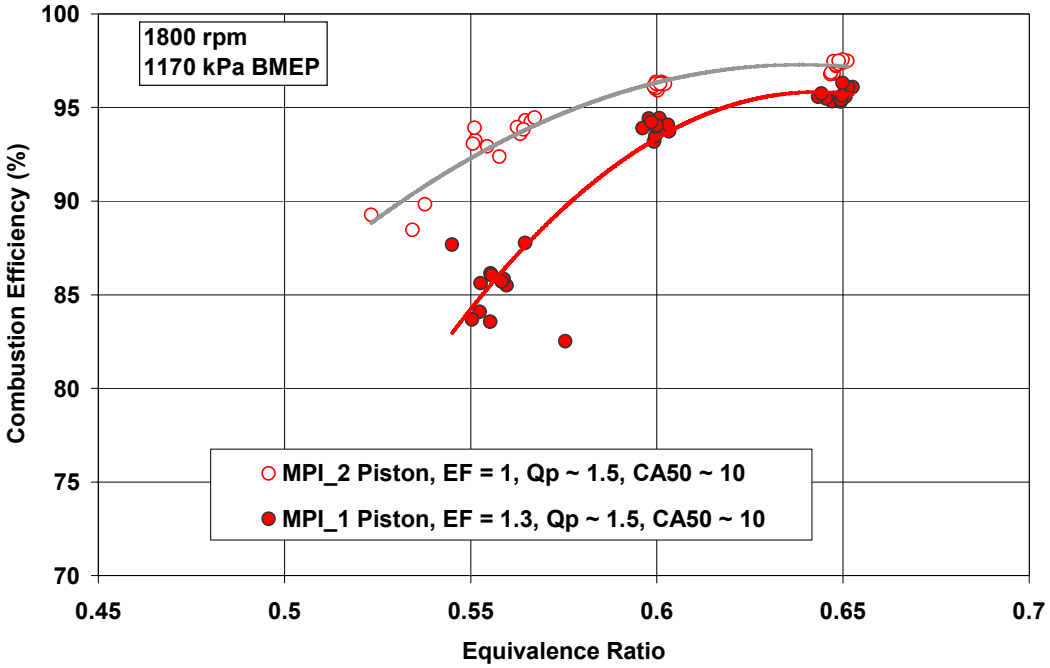

Figure E7-10. Combustion Efficiency vs. Equivalence Ratio for Pistons MPI_1 and MPI_2

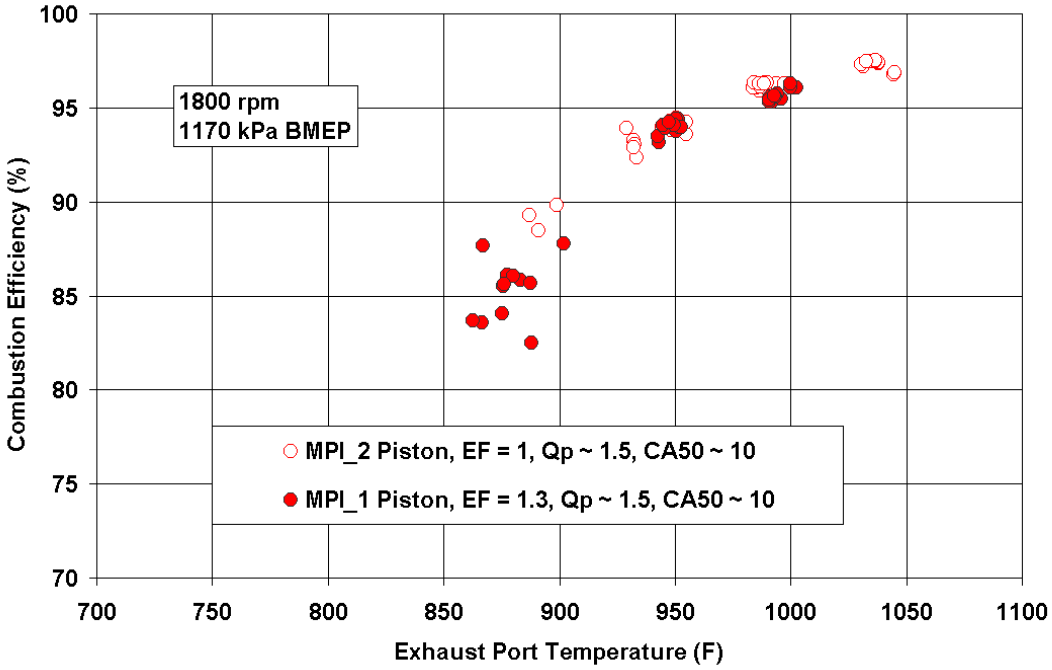

Figure E7-11. Combustion Efficiency vs. Exhaust Port Temperature for Pistons MPI_1 and MPI_2

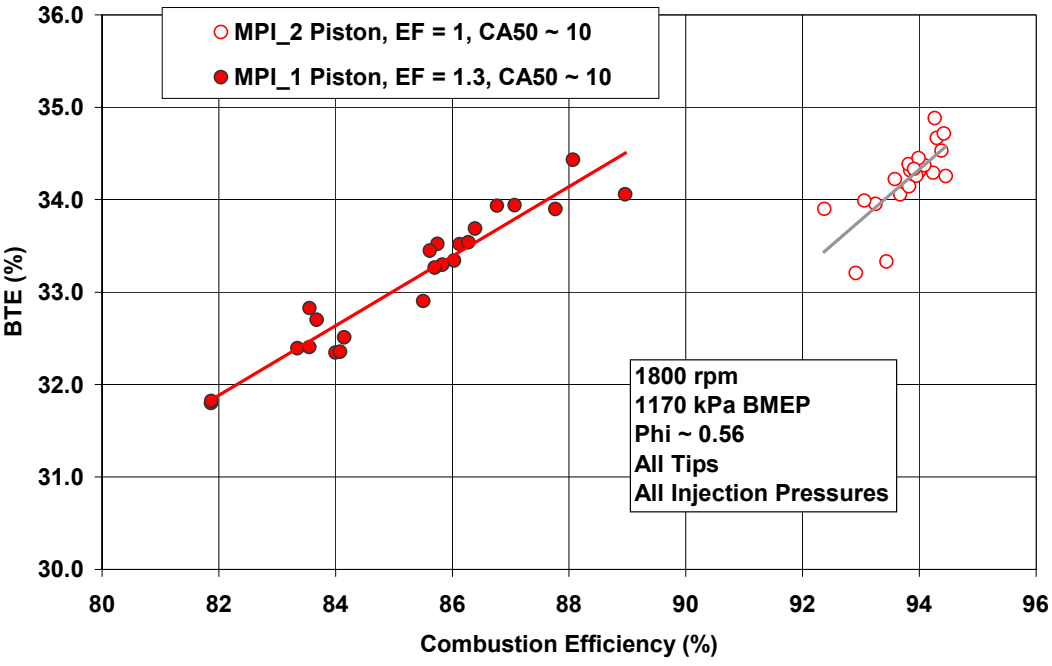

Figure E7-12. Effect of Combustion Efficiency on BTE

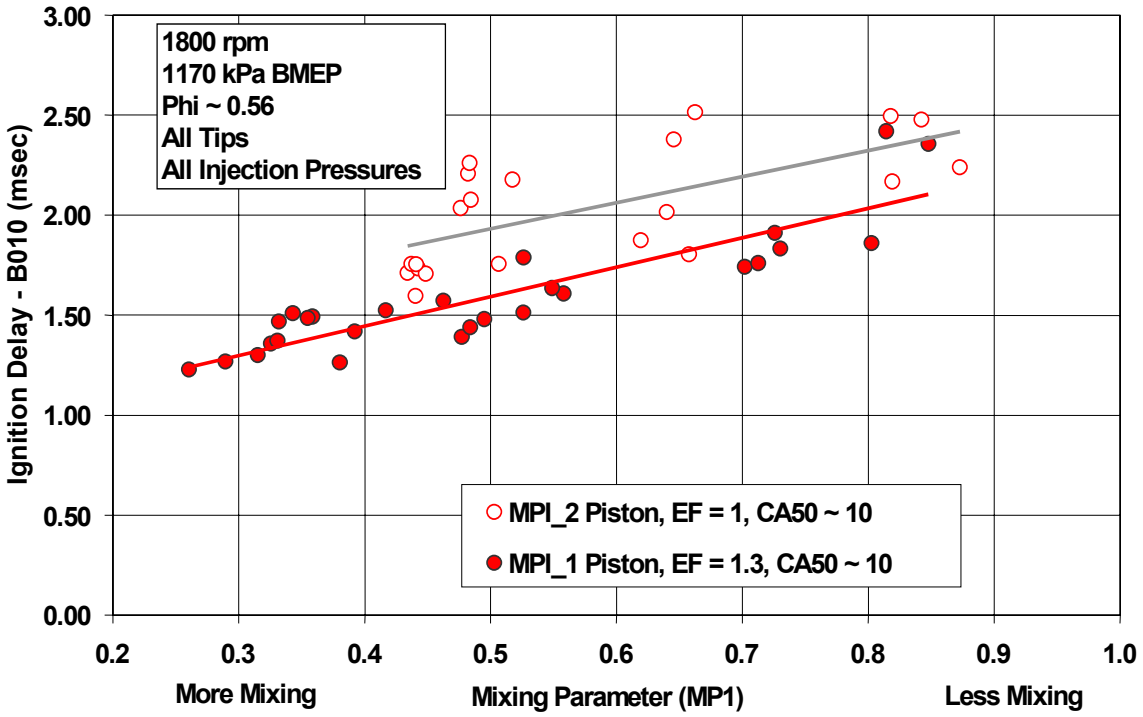

Figure E7-13. Correlation of Ignition Delay with the Jet Mixing Parameter

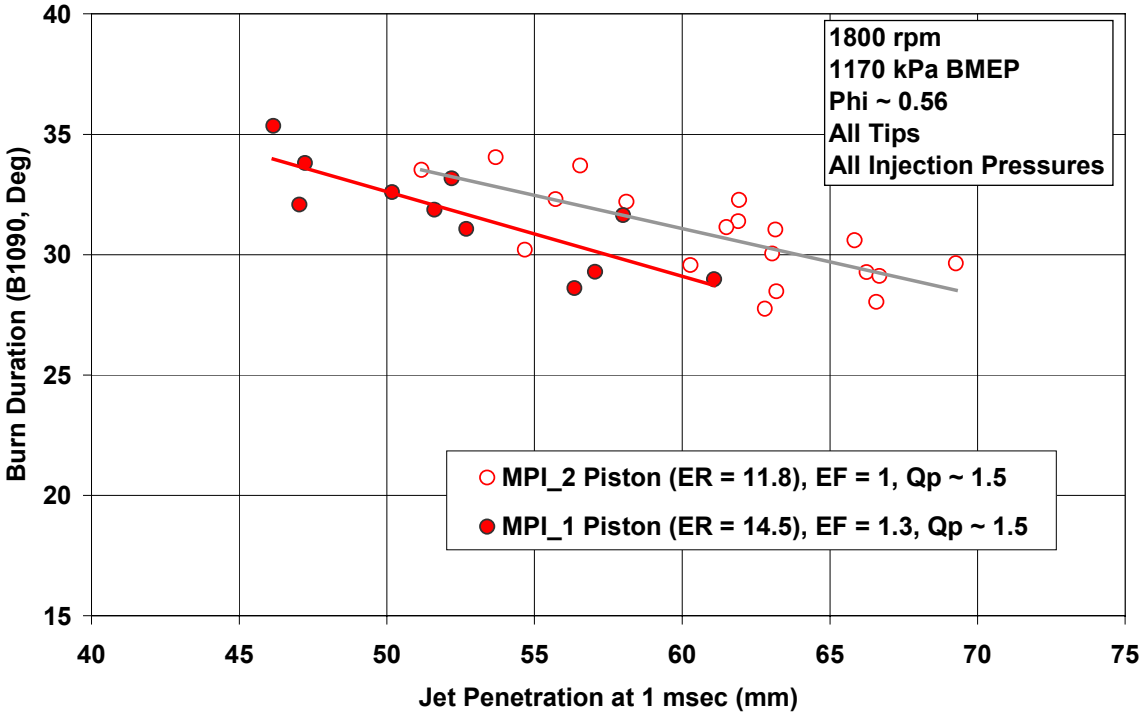

Figure E7-14. Correlation of Combustion Duration (B1090) with Jet Penetration

Effects of Combustion Chamber Design on Engine Performance

With thermal efficiency closely tied to combustion efficiency, combustion chamber design for complete combustion is a necessity. Minimizing crevice volume by raising the top ring and other measures are well-known unburned hydrocarbon reduction techniques. However, for micro-pilot combustion, bowl design may also be important. Micro-pilot is essentially a multi-site ignition technology, and as such may have different requirements for in-cylinder turbulence. Ideally, the pilot fuel spray would penetrate to the edge of the combustion chamber and ignite the mixture at the periphery. The flame would then propagate inward and radially similar to the concept that places spark plugs at the periphery of the combustion chamber. Various concepts were considered. First, open chamber designs that in theory would allow the spray to propagate to the edge of the cylinder. In reality, it is known that the ignition of the diesel fuel spray does not occur at the tip of the spray but at some intermediate distance. Thus the ideal situation in which the gas-air mixture is ignited at the edge of the chamber is never fully realized. Second, a traditional high squish piston concept that would provide high turbulence levels is required to speed flame propagation. The piston concepts have been shown previously in Figures E7-3 and E7-4.

The design concepts were evaluated in the engine at various conditions involving changes in equivalence ratio, injection timing, pilot quantity, engine speed and load. Figure E7-15 illustrates the combustion duration as a function of jet penetration distance for four of the pistons. Figure E7-15 indicates that piston CC_2, a high squish piston, had the fastest combustion of the designs tested and that in-cylinder turbulence is still desirable and important in flame propagation. It should be noted that since the injection pressure was held constant for the data plotted in Figure E7-15, that the variation in penetration was a result of variation in cylinder pressure as the timing of injection was changed. Thus combustion duration could also be correlated with the injection timing or combustion phasing. The NO_x – efficiency tradeoff, shown in Figure E7-16, also favors the highly turbulent CC_2 piston.

The higher compression ratio pistons, MPI_3 and MPI_4, were also tested however, this testing was limited due to detonation, peak cylinder pressure limitation, and combustion stability. As shown previously, combustion efficiency was not only dependent on equivalence ratio but also on the phasing of the combustion event. With open chamber piston designs, advanced timing was required to obtain reasonable combustion efficiency particularly with lean mixtures. At the high compression ratios of the MPI_3 and MPI_4 pistons, advanced timings lead to detonation and high peak cylinder pressures. With these constraints, these piston designs were not appropriate.

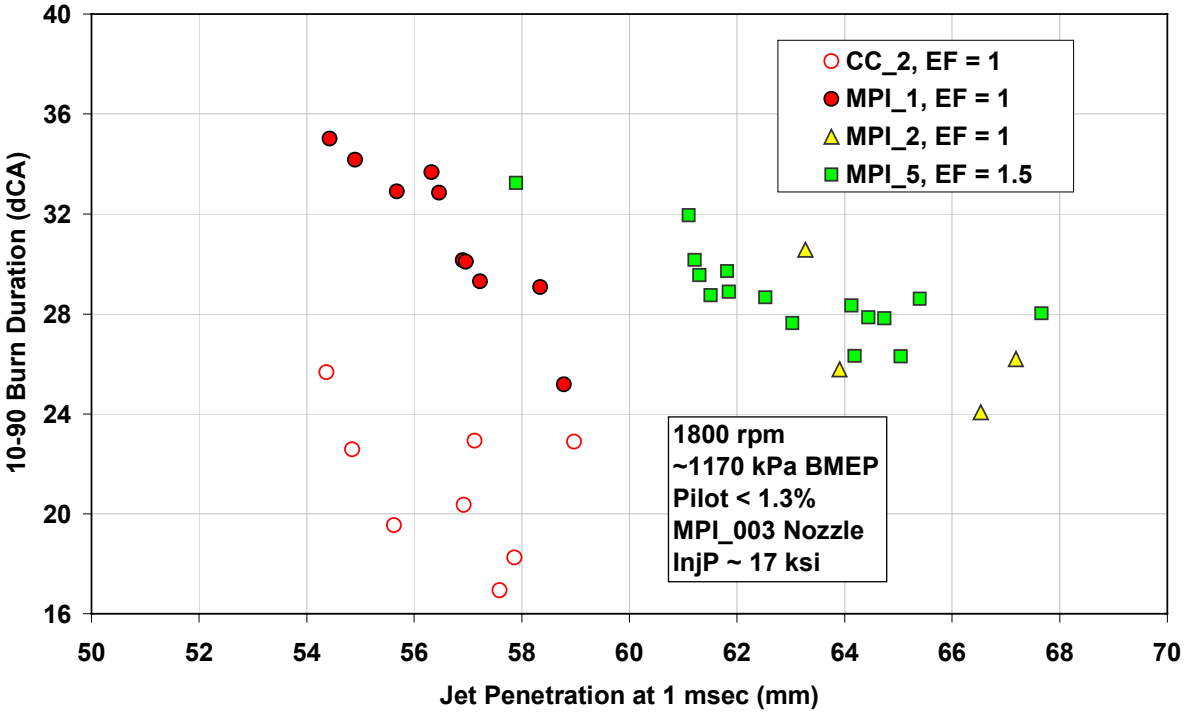

Figure E7-15. Combustion Duration versus Jet Penetration for Four MPI Pistons

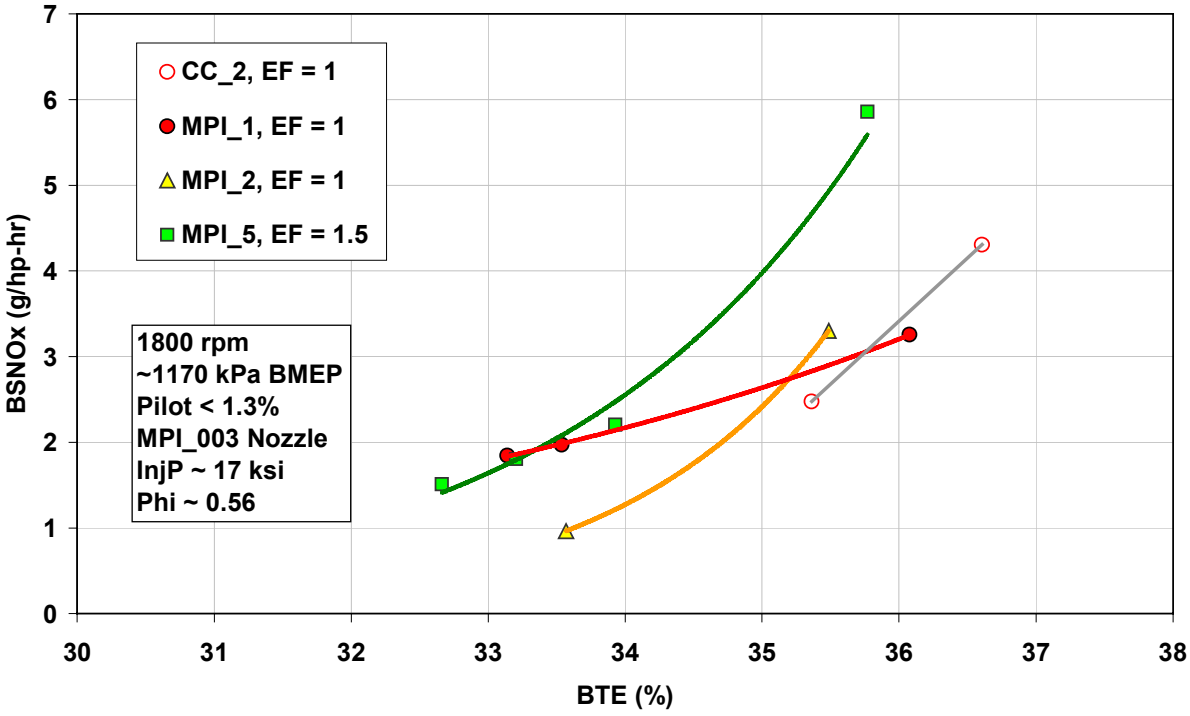

Figure E7-16. NO_x – BTE Tradeoff for Four MPI Pistons at 0.56 Equivalence Ratio

E8.0 SUMMARY

The literature was reviewed for information on pilot-ignited natural gas engines and for technical details on the injection system hardware used in these applications. In each reference cited, the implementation of pilot ignition in a prechamber provided a better NO_x-efficiency tradeoff than the open-chamber implementation. Lack of adequate injection systems appeared to be the limiting factor for open-chamber designs. Although injection system details were lacking in many references, where sufficient detail was reported, the injection system was relatively low in injection pressure and was unlikely to provide the required injection characteristics. An analysis was performed to define characteristics required for an optimum open-chamber injection system.

Current injection system hardware was evaluated relative to the above characteristics. Due to the size of the engines and the desire for flexible injection timing, a common rail injection system appears to be best suited for this application. Common rail systems can also provide injection pressure independent of engine speed, a feature that may be required for starting and low speed operation.

A common rail injection system was obtained and installed on the CAT 3501 single-cylinder engine. Micro-pilot ignition was evaluated with a variety of piston designs, nozzle geometries, and combinations of pilot quantity, injection pressure, and main chamber equivalence ratio. The results indicated that nozzle parameters, hole diameter, number of hole, and spray angle, had little effect on the ignition and combustion of dilute fuel-air mixtures. High injection pressures produced faster combustion rates. Results were obtained at pilot quantities below 0.5-percent. Higher pilot quantity was found to produce higher NO_x, while not necessary for ignition of the fuel-air mixture. Combustion chamber design was shown to be more important for combustion stability and combustion rate. Complete combustion of lean mixtures was found to be problematic. Although the pilot was able to ignite extremely lean mixtures, the combustion efficiency for these mixtures was low. High levels of in-cylinder turbulence were found to be beneficial for flame propagation and combustion stability.

E9.0 RECOMMENDATIONS

Thermal efficiency of natural gas engines has been shown to be proportional to the combustion efficiency for dilute mixtures. So while micro-pilot ignition successfully ignited extremely dilute mixtures, complete combustion was not obtained. Additional work should focus on combustion chamber designs that minimize in-cylinder crevice regions that contribute to low combustion efficiency, and designs that promote in-cylinder turbulence to enhance flame propagation and combustion stability. The single-cylinder work should be extended to a multi-cylinder engine. Also, cold starting, transient response, part-load operation, and durability that were not investigated on this project should be addressed.

E10.0 REFERENCES

1. Beck, N. J., "Optimized Performance and Emissions for Dual-fuel Gas/Diesel Engines", USDOE Diesel Engine Emissions Reduction Workshop, 1995.
2. Blizzard, D.T., et al., "Development of the Cooper-Bessemer Clean Burn Gas-Diesel (Dual-Fuel) Engine", ICE-Vol. 15, ASME, 1991.
3. Blythe, N., "Development of the Fairbanks Morse Enviro-Design Opposed Piston Dual-fuel Engine", ICE-Vol. 22, ASME 1994.
4. Chrisman, B.M., et al., "Investigation of Micro-Pilot Combustion in a Stationary Gas Engine", ICE-Vol., ASME 1998.
5. Gebert, K., et al., "Development of Pilot Fuel Injection System for CNG Engine", SAE Paper 961100, 1996.
6. Johnson, W. P., et al., "All Electronic Dual-fuel Injection System for Belarus D-144 Diesel Engine" SAE Paper 901502, 1990.
7. MAN B&W Technical Brochure, "Gas and Dual-Fuel Engines from MAN B&W – Economic, Reliable, and Ecologically Compatible".
8. Meyers, D. P., et al., "Evaluation of Six Natural Gas Combustion Systems for LNG Locomotive Applications", SAE Paper 972967, 1997.
9. O'Neal, G. B., "The Diesel-Gas Dual-Fuel Engine," Symposium Paper, Non-petroleum Vehicular Fuels III, Inst. Of Gas Technology, 1982.
10. SwRI Report, "Gas Combustion System Evaluation", SwRI Project 03-7928, April 1996.
11. Weaver, C.S. and Turner, S.H., "Dual-fuel Natural Gas/Diesel Engines: Technology, Performance, and Emissions," GRI report no. GRI-94/0094

F. EVALUATION OF NO_x CATALYST FOR LEAN-BURN NATURAL GAS ENGINES

EXECUTIVE SUMMARY

The objective of the work was to evaluate aftertreatment technology for NO_x reduction in an oxidizing exhaust stream typical of a lean burn stationary, natural gas engine. Two approaches were explored, the use of a lean NO_x catalysts and the use of selective catalytic reduction (SCR).

A comprehensive literature/patent search was performed that identified three types of lean NO_x catalysts. These were methane-SCR catalysts, methane-coupling catalysts, and activated carbon catalysts. A total of 22 formulations were identified for testing. Several suppliers were contacted for the preparation of the candidate catalyst samples. A total of 15 different catalysts were finally evaluated.

The SwRI synthetic gas reactor was set up to perform the lean NO_x catalyst testing and a suitable test protocol was developed. Most of the tests were performed with a water concentration level of 10 percent, oxygen level of 10 percent, and a gas hourly space velocity of 25,000 hr^{-1}. A few catalysts were also tested at less severe conditions, i.e. with zero water, 2.5 percent oxygen, and at a gas hourly space velocity of 7,500 hr^{-1}. No activated carbon catalysts were evaluated due to major difficulties in getting samples coated onto ceramic monoliths.

The highest NO conversion to N_2 measured was only about 15-percent. This was the Ce-Ag-H ZSM5 catalyst tested at the least severe conditions, i.e. with zero water, 2.5-percent oxygen, and at a gas hourly space velocity of 7,500 hr^{-1}. From these results, it was clear that lean NO_x catalysis has not advanced sufficiently to provide the > 90-percent NO_x reduction to N_2 required for the ARES engine.

A paper study was initiated of the selective catalytic reduction technology to determine if it warranted consideration and experimentation. The paper study on SCR systems disclosed that this technology was quite promising in conjunction with ammonia or urea used as reductant but estimated conversion efficiency could still be improved.

A limited evaluation of an SCR system was initiated on exhaust produced by a natural gas-powered heavy-duty 12L engine. An SCR system was obtained from Siemens at no cost to the ARES program for purposes of this evaluation. The results indicated that indeed the urea SCR technology was capable of NO_x conversion efficiencies greater than 90-percent. At the stoichiometric urea to NO_x ratios, it was demonstrated that measured NO_x concentrations were less than 5 ppm with no appreciable ammonia slip detected.

F1.0 INTRODUCTION

Aftertreatment of exhaust gas from lean burn natural gas engines poses a great challenge. With oxygen in the exhaust stream, reduction of NO_x becomes difficult. However, to achieve low emission levels aftertreatment will be required. Three possible areas for exhaust aftertreatment were identified as Selective Catalytic Reduction (SCR), lean NO_x catalysis, and plasma NO_x control. Lean NO_x catalysts were an emerging technology for diesel and gasoline applications, with some promising advances reported for natural gas applications. This program evaluated the effectiveness of lean NO_x catalyst and SCR technology.

F2.0 OBJECTIVE

The objective was to identify, obtain, and evaluate state-of-the-art lean NO_x catalysts and SCR systems to reduce the NO_x emissions from a stationary, natural gas engine.

F3.0 TECHNICAL APPROACH

F3.1 Lean NO_x Catalysts

Initially, SwRI performed a literature and patent search to obtain the latest available information on lean NO_x catalysts, with special attention given to the effectiveness of methane (CH_4) as the reducing agent. The search focused mostly on catalysts that were reported to work well when CH_4 was used as the reductant.

A SwRI representative visited with the DOE scientists who were currently working on lean NO_x catalysis to determine if there was any useful information that could be incorporated into the project. At the same time, OEM catalyst manufacturers (Engelhard, Degussa, Allied Signal, Johnson Matthey, etc.) were approached to determine if they were willing to supply samples of their lean NO_x catalyst technologies. The OEM's were provided with the expected exhaust conditions, and asked to submit suitable catalyst samples. In return for their participation, they were each offered an abbreviated report of the test results from their catalysts.

A synthetic gas reactor (SGR) was used to evaluate the various lean NO_x catalyst technologies. A test procedure was developed that consisted of exposing the lean NO_x catalyst to a synthetic exhaust gas mixture similar to that expected from a lean-burn, natural gas engine. The ability of the catalyst to convert the NO_x was measured at different temperatures (250, 300, 350, 400, 450, 500, 550, and 600°C) and secondary CH_4 reductant concentrations (500, 1000, and 2000 ppm). Hence, a complete test on a single catalyst required approximately 24 individual data points. From these data, a conversion efficiency profile of the catalyst was generated.

F3.2 SCR Systems

A state-of-the-art SCR system was obtained from Siemens for evaluation. The evaluation of the system was conducted on exhaust produced by a natural gas-powered heavy-duty 12L engine. Testing was conducted over several speed-load conditions at two ignition timing levels to simulate expected NO_x levels from an ARES engine.

F4.0 LITERATURE/REVIEW

F 4.1 Lean NO_X Catalysts

A literature search was performed using CAplus database. CAplus covers international journals, patents, technical reports, books, conference proceedings, and dissertations from all areas of chemistry, biochemistry, chemical engineering, and related sciences from 1967 to the present. Only references dated from 1996 to the present were searched since most of the work on lean NO_x catalysts, using methane as the reductant, have been generated in the last few years.

A careful review of the references revealed three classes of lean NO_x catalysts using methane as the primary reductant (CH_4-SCR), or no supplemental reductant at all. These can loosely be described as zeolite-based catalysts, methane-coupling catalysts, and activated carbon catalysts.

F4.2 SCR Systems

Selective Catalytic Reduction (SCR) was discovered in 1957[1]. Platinum (Pt) catalysts were found to react ammonia (NH_3) with nitric oxide (NO) and nitrogen dioxide (NO_2) to form nitrogen (N_2) in a lean [excess oxygen (O_2)] environment, as shown in reactions 1 and 2. Since that time various catalyst formulations have been developed and have been shown to have various operating characteristics. Other catalysts that are effective for SCR include vanadia/titania (V_2O_5/TiO_2) and zeolites (naturally occurring or synthetic alumina-silicate materials with well-defined structures and pore size). These catalysts operate best at different temperatures, as shown in Figure F4-1. The catalyst of choice for the ARES engine will be dependent on many variables, one of which will be the operating temperature. At less than 200°C, the Pt catalyst is the most likely choice. From 250 to 350°C, the V_2O_5/TiO_2 would be more suitable, and the zeolite catalyst may be the only option above 400°C.

$$4NH_3 + 4NO + O_2 \rightarrow 4N_2 + 6H_2O \qquad 1$$

$$4NH_3 + 2NO_2 + O_2 \rightarrow 3N_2 + 6H_2O \qquad 2$$

'NH_3 slip' describes NH_3 that exits the system after the catalyst. Typically, NH_3 slip is only permitted up to about 5 volume parts per million (vppm). In order to avoid NH_3 slip, the ratio of NH_3:NO has to be less than 1:1. A ratio less than 1:1 also reduces the possibility of producing ammonium nitrates. However, NO conversion efficiency is reduced at ratios less than 1:1. Hence, tight control of the NH_3:NO ratio is required. The effects of temperature and NH_3:NO ratio on NO_x conversion and NH_3 slip for a V_2O_5/TiO_2 catalyst are shown in Figures F4-2 and F4-3.

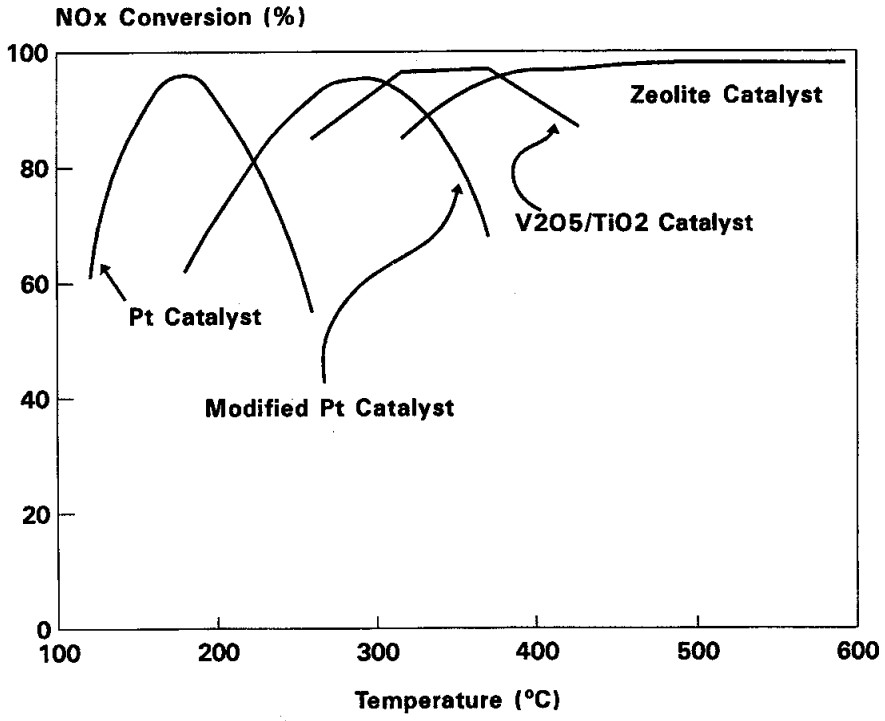

Figure F4-1. Operating Temperature Windows for Different SCR Catalyst Formulations[2]

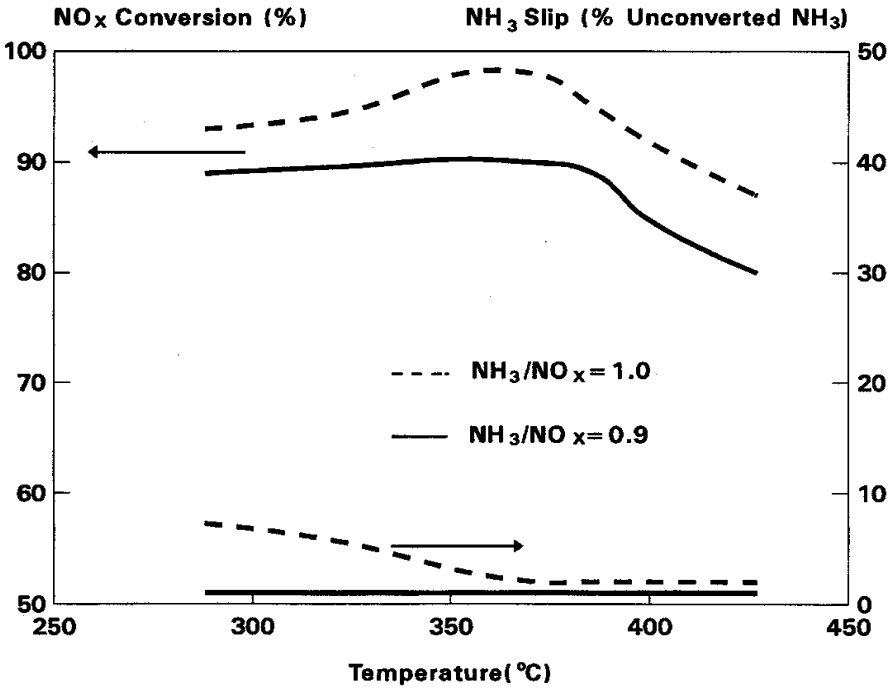

Figure F4-2. Effect of Temperature on NO_x Conversion and NH_3 Slip for a V_2O_5/TiO_2 Catalyst[3]

Figure F4-2 shows how NH_3 slip is effectively zero for all temperatures at an NH_3:NO ratio of 0.9. However, NO_x conversion efficiency is only 90 percent maximum. At an NH_3:NO ratio of 1.0, NO_x conversion efficiency peaks at about 98 percent close to 360°C, but there is some NH_3 slip, and it increases at lower temperatures.

Figure F4-3 shows how NH_3 slip increases with increasing NH_3:NO ratio > 0.9, but decreases with temperature. The non-selective oxidation of NH_3 at higher temperatures (to produce N_2, N_2O, or NO) causes the effective NO_x conversion efficiency to drop. In this example, the ideal operating conditions would be either 360°C, with an NH_3:NO ratio of about 0.9, where the NO_x conversion efficiency is about 90 percent, and the NH_3 slip is zero: or at 427°C, with an NH_3:NO ratio of about 1.2, where the NO_x conversion efficiency is about 96 percent, and the NH_3 slip is zero. The former condition has lower NO_x conversion efficiency, but uses less NH_3 and requires a lower temperature. The latter condition requires higher temperature and more NH_3, but increases the NO_x conversion efficiency. Clearly, the operating conditions must match the emissions requirements, but they must also be held within a tight window of operating conditions to achieve the highest NO_x conversion efficiency without NH_3 slip problems.

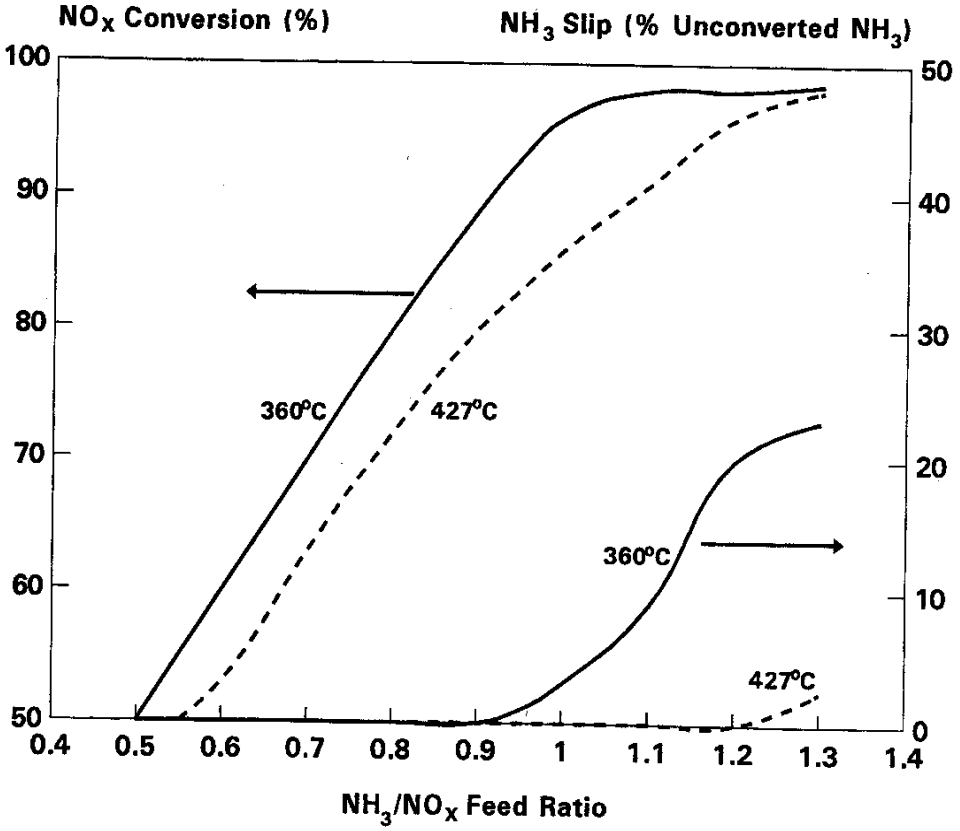

Figure F4-3. Effect of NH_3: NO_x Ratio on NO_x Conversion and NH_3 Slip for V_2O_5/TiO_2 SCR Catalyst[4]

F5.0 LEAN NO_X CATALYST SELECTION AND PREPARATION

The papers reviewed revealed a wide range of catalysts and catalyst classes and after studying the literature, the reviewer identified the possibility for developing a whole range of catalysts that were variants on those in the papers. Even a moderate examination of these options would have resulted in more than 100 different catalyst formulations, which were not considered practical for this project. Therefore, a list of formulations from the literature were chosen with only a very few variants.

F5.1 DOE Lean NO_x Update

At the request of Tom Sebestyen of DOE, SwRI spoke to several members of the DOE National Laboratories that were working on lean NO_x catalysis programs, to supplement the information gathering process with their knowledge and experience. He also attended the DOE Laboratory Catalysis Research Symposium held in Albuquerque. All of the DOE lean NO_x catalyst work focused on diesel and lean-burn gasoline exhaust applications. The contacts reported that little work had been done with natural gas lean NO_x catalysts, but that the types of catalysts identified in the ARES literature/patent search were promising. Although they believed that lean NO_x catalysis using natural gas (mostly methane) as the reductant was potentially the hardest lean NO_x catalyst problem to solve, they mostly indicated that the ARES project was doing the right work.

F5.2 Preparation of Lean NO_X Catalysts

After identifying the most promising lean NO_x catalysts reported in the literature, a list of the 22 candidate formulations was sent to Prototech Company.

Overall, 15 different catalyst formulations were tested. Three catalysts were not prepared because they were intrinsically similar to other catalysts that were tested. The four AC catalysts were not tested because they were never successfully prepared.

F5.3 Solicit Catalyst OEM's

OEM catalyst manufacturers were asked to supply candidate formulations for testing in the ARES program. The samples would be supplied free-of-charge. In return, they would receive the results of testing of the OEM catalysts only, so that they could determine how their technology compares with their competitors. Competitors would not be named to protect their integrity, and to encourage them to submit samples. A letter of solicitation was sent out to Johnson Matthey, Inc., Degussa, Engelhard Corp., ASEC Manufacturing, Catalytic Solutions, Inc., Precision Combustion, Inc., Nippon Shokubai Kagaku Co., Ltd., Prototech Co., and Miratech Corp. Some of the OEM's expressed initial interest, while others declined. After several months, it became clear that none of the catalyst OEM's had technology, which they were willing to submit to the ARES program. It is believed that any catalyst formulations which might have been submitted probably had poor performance under the ARES test conditions, so the OEM's chose not to participate.

F6.0 EXPERIMENTAL SETUP AND PROCEDURES

F6.1 Lean NO_x Catalysts Test Setup and Procedures

SwRI used its Synthetic Gas Reactor (SGR) to setup and run the catalyst testing. The SGR setup is shown in Figure F6-1, and a schematic diagram of the lean NO_x catalyst test setup is shown in Figure F6-2.

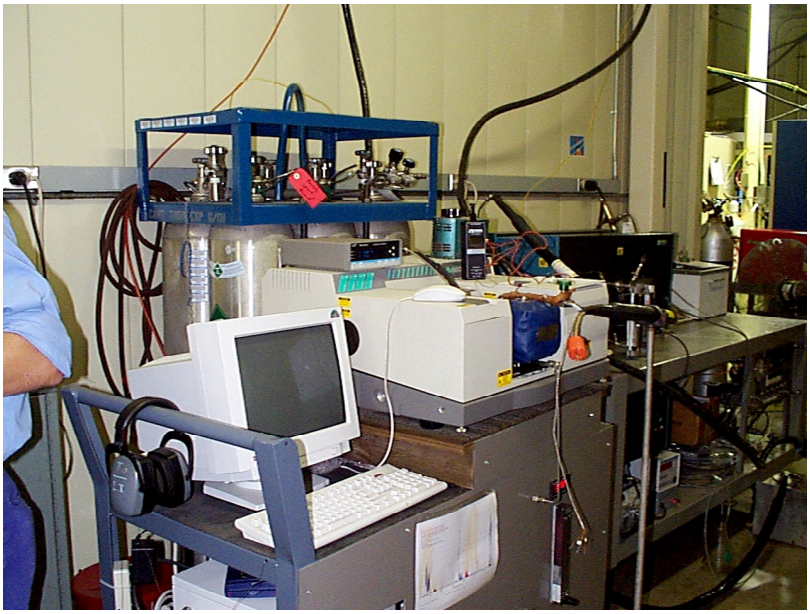

Figure F6-1. SwRI Synthetic Gas Reactor and FTIR Analyzer

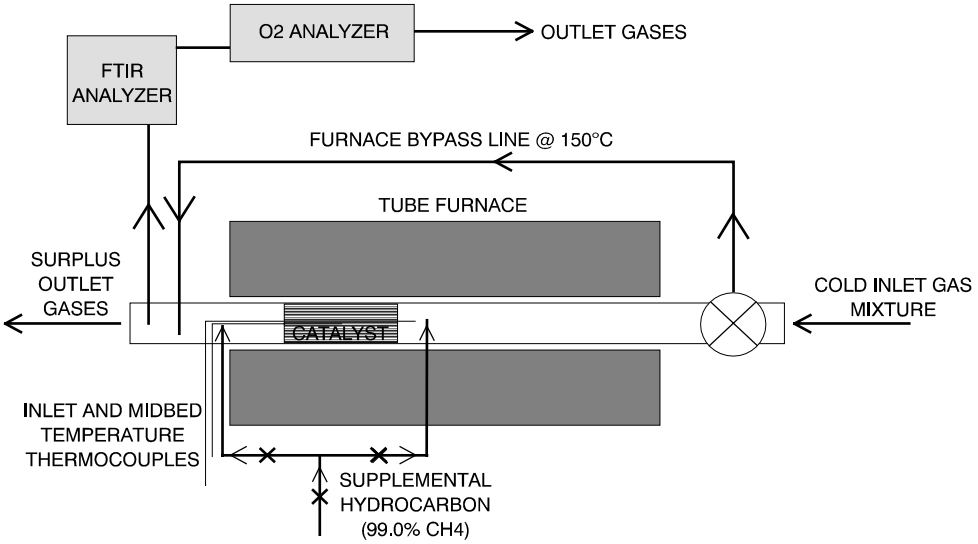

Figure F6-2. Schematic Diagram of Lean NO_x Catalyst Test Setup

For the CH_4 – coupling catalyst, the temperature range was increased to 700°C. Only one test was performed due to gas phase reactions discussed later.

No activated carbon catalysts were successfully formulated. However, if activated carbon catalysts become available at a later date, the temperature range would probably be from 150°C to 350°C. No supplementary hydrocarbon would be required for these catalysts.

F6.2 SCR System Test Setup and Procedures

The test engine for this program was an experimental Mack-E7G engine powered by natural gas. The engine was an in-line 6-cylinder, 4-stroke, having 12.0 L displacement. It was turbocharged, aftercooled, and electronically governed. Mack provided the engine for use in another project.

Emission testing in this project was conducted using pure methane having a controlled composition to ensure comparability of results between the various test configurations. A dedicated tank was filled and placed just outside the test cell to supply the engine needs. Standard SAE 30 W (Texaco URSA) lube oil was provided and used throughout the test activities. The lube oil was coded SwRI EM-2515-EO.

The test was conducted using the 1300 rpm/1055 lb-ft point for its good thermal efficiency based on the work accomplished earlier on this engine. In addition to the performance characterization, regulated emissions were also sampled and analyzed. However, emphasis was placed on NO_x emissions in line with the objective of this project. The same characterization was repeated at a second spark timing, to evaluate the impact of aftertreatment on NO_x emission at different brake thermal efficiency levels.

Two spark timings were tested at several exhaust temperatures to simulate differing degrees of exhaust heat recovery. These temperatures ranged from 180°C to 320°C measured at the inlet of the SCR catalyst.

Emissions measured included hydrocarbons (HC), carbon monoxide (CO), oxides of nitrogen (NO_x), and particulate matter (PM). Hydrocarbons were measured using continuous sampling techniques employing a heated flame ionization detector (HFID). CO and CO_2 were determined with proportional dilute gaseous samples analyzed using non-dispersive infrared (NDIR) instruments. NO_x was measured continuously via a chemiluminescence instrument.

F7.0 LEAN CATALYST TEST MATRIX

As catalyst samples were received, they were tested using the test protocols. The catalysts tested, results, and discussions, are presented here in chronological order. The actual catalysts tested and test details are given in Table F7-1.

Table F7-1. Lean NO_x Test Details

Catalyst I.D.	Formulation	Test Conditions
9	0.3%Pd/HZSM5	Full gas mix, 350-750°C
18	40%La_2O_3/Al_2O_3	Full gas mix, 500-800°C
00	Bare Substrate	Full gas mix, 450-800°C
02	1.24%Co/Al_2O_3(20)//HZSM5(80)	Full gas mix, 200-500°C
10	1.24%Co/Al_2O_3(20)//H-mordenite(80)	Full gas mix, 200-500°C
MH	X%Co/HZSM5a	Full gas mix, 200-550°C
M1	X%Co/HZSM5b	Zero H_2O, 2.5% O_2, 300-600°C
M1	X%Co/HZSM5b	Full gas mix, 300-600°C
3	1.16%Mn/Al_2O_3(20)//HZSM5(80)	Full gas mix, 250-600°C
4	0.49%Pd-HZSM5	Full gas mix, 200-600°C
5	3.0%In-HZSM5	Full gas mix, 300-600°C
6	Ce-Ag-HZSM5	Full gas mix, 300-600°C
6	Ce-Ag-HZSM5	Zero H_2O, 2.5% O_2, 7,500hr^{-1}, 300-650°C
11	1.31%Co/Hmordenite	Full gas mix, 300-600°C
13	1.31%Co,0.47%Pd-H-mordenite	Full gas mix, 250-600°C
14	2.27%Co/Vermiculite	Full gas mix, 200-600°C
15	5.00%Co/Montmorillonite	Full gas mix, 300-600°C
16	0.3%$Pd/SO_4/ZrO_2$	Full gas mix, 200-600°C

F8.0 RESULTS

F8.1 Lean NO_x Catalyst Results

The highest NO conversion to N_2 measured was only about 15 percent. This was the Ce-Ag-H ZSM5 catalyst tested at the least severe conditions, i.e. with zero water, 2.5 percent oxygen, and at a gas hourly space velocity of 7,500 hr^{-1}, Figure F8-1 and F8-2. From these results, it was clear that lean NO_x catalysis has not advanced sufficiently to provide the > 90 percent NO_x reduction to N_2 required for the ARES engine.

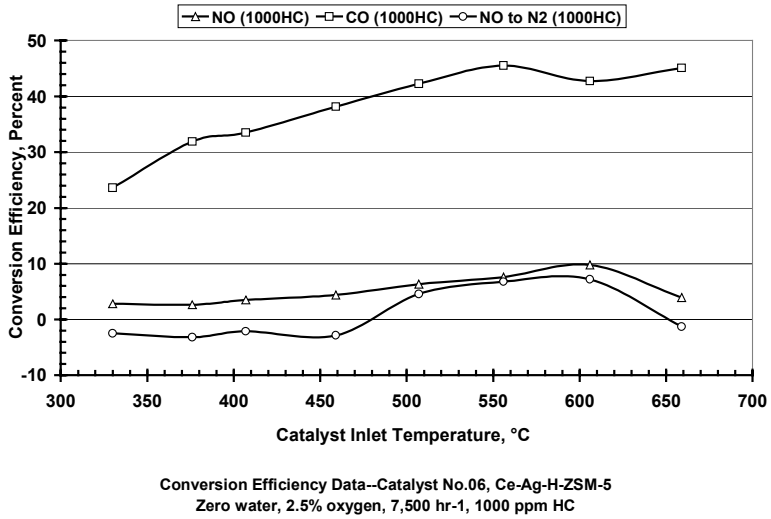

Figure F8-1. Conversion Efficiency vs. Catalyst Inlet Temperature

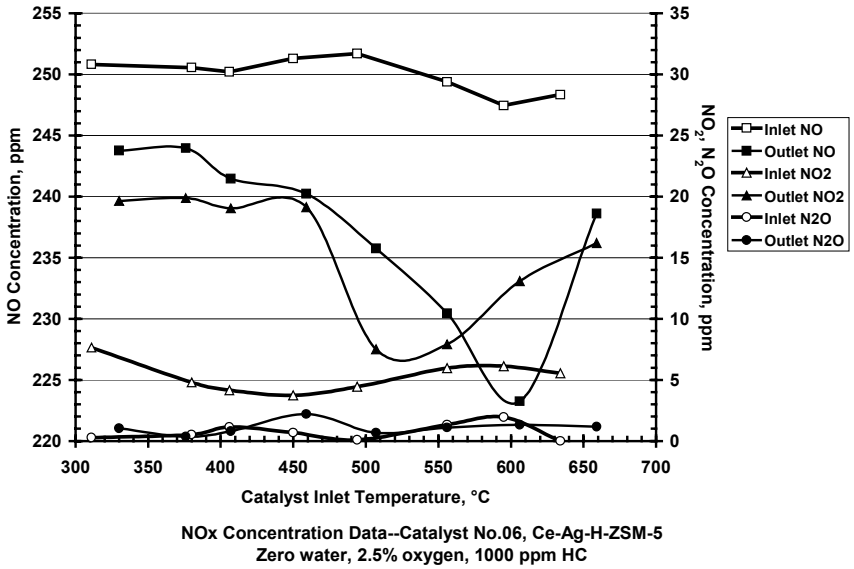

Figure F8-2. NO, NO_2, and N_2O Concentration at Various Locations vs. Catalyst Inlet Temperature

F8.2 SCR System Results

NO_x conversion efficiencies are dependent on exhaust temperature and urea solution injection rate for systems equipped with urea SCR. As exhaust temperature reached above 315°C, conversion efficiencies approached 90 percent in the case of high BTE. The molar NH_3/NO_x ratio in this case was 0.87. A NO_x concentration of 9.75 ppm was measured at an exhaust temperature of 315°C and using a urea injection rate equivalent to 0.87 NH_3/NO_x molar ratio. It is believed that increasing the urea injection rate to the NH_3/NO_x stoichiometric ratio would have yielded greater NO_x conversion efficiency, but our interest was in the low temperature regime. Ammonia slip never exceeded 5 ppm for the advance spark timing condition (high BTE).

The same analysis performed for the low BTE case indicated that it is more likely to meet the objective of the project with the retarded spark timing and a high rate of urea solution. At 315°C catalyst inlet temperature, and 0.94 NH_3/NO_x molar ratio, NO_x was completely reduced with practically no ammonia slip. It is worth noting that since urea SCR technology alone was able to achieve these results, non-thermal plasma was not evaluated at these conditions.

Given these results, it is safe to conclude that if the ARES engine operates at exhaust temperatures of 315°C and a BTE of 38 percent, there will be no need for non-thermal plasma assist for the urea SCR system. This presumes that a NH_3/NO_x molar ratio of 0.94 is used. At about 41 percent BTE, the same conclusion is also valid, but with a higher urea injection rate (equivalent to NH_3/NO_x molar ratio close to stoichiometric).

F9.0 CONCLUSION

The primary conclusion from this work was that the state-of-the-art lean NO_x catalysts developed to convert NO_x to N_2 in a natural gas exhaust have very low activity when exposed to a gas stream containing high levels of water and oxygen. Even in the absence of water and at optimal oxygen concentrations, only minimal activity was seen unless the space velocity was reduced to levels generally considered impractical for engine exhaust aftertreatment. The use of a lean NO_x catalyst with methane as the primary reductant will not achieve the NO_x conversion levels required for the ARES engine with present technology.

SCR catalyst technology, on the other hand, has been demonstrated to achieve about 90 percent reduction in NO_x at NH_3:NO_x ratios near stoichiometry at temperatures representative of natural gas exhaust streams. The requirement for urea to be used as a reductant would impose an additional operation cost and would require on-site storage and complicate control systems. A question that remains is whether 90 percent efficiency will be sufficient for achieving the desired NO_x levels.

F10.0 REFERENCES

1. Cohn, G., Steele, D., and Andersen, H. 1961. U.S. Patent 2,975,025.
2. Heck, R., Chen, J., and Speronello, B. 1994. Operating Characteristics and Commercial Operating Experience with High Temperature SCR NO_x Catalyst. *Environmental Progress*
3. Heck, R., Farrauto, R. Catalytic Air Pollution Control – Commercial Technology, Van Nostrand Reinhold Publishers